Error Estimation for Simplifications of Electrostatic Models

A thesis submitted in partial fulfilment

of the requirements for the degree of Doctor of Philosophy

Navid Rahimi

November 2016

Cardiff University
School of Computer Science & Informatics

Declaration

This work has not previously been accepted in substance for any degree and is not concurrently submitted in candidature for any degree.

Signed . . . . (Navid Rahimi)

Date   . . . .

Statement 1

This thesis is being submitted in partial fulfillment of the requirements for the degree of PhD.

Signed . . . . (Navid Rahimi)

Date   . . . .

Statement 2

This thesis is the result of my own independent work/investigation, except where otherwise stated. Other sources are acknowledged by explicit references.

Signed . . . . (Navid Rahimi)

Date   . . . .

Statement 3

I hereby give consent for my thesis, if accepted, to be available for photocopying and for inter-library loan, and for the title and summary to be made available to outside organisations.

Signed . . . . (Navid Rahimi)

Date   . . . .

To my family and friends
for their patience and support.

Abstract

Based on *a posteriori* error estimation a method to bound the error induced by simplifying the geometry of a model is presented. Error here refers to the solution of a partial differential equation and a specific quantity of interest derived from it. Geometry simplification specifically refers to replacing CAD model features with simpler shapes. The simplification error estimate helps to determine whether a feature can be removed from the model by indicating how much the simplification affects the physical properties of the model as measured by a quantity of interest. The approach in general can also be extended to other problems governed by linear elliptic equations. Strict bounds for the error are proven for errors expressed in the energy norm. The approach relies on the Constitutive Relation Error to enable practically useful and computationally affordable bounds for error measures in the energy error norm.

All methodologies are demonstrated for a second order elliptic partial differential equation for electrostatic problems. Finite element simplification error estimation code is developed to calculate the simplification error numerically. Numerical experiments for some geometric models of capacitors show satisfactory results for the simplification error bounds for a range of different deafeaturing cases and a quantity of interest, linear in the solution of the electrostatic partial differential equation. Overall the numerically calculated bounds are always valid, but are more or less accurate depending on the type of feature and its simplification. In particular larger errors may be overestimated, while good estimates for small errors can be achieved. This makes the bound overall suitable to decide whether simplifying a feature is acceptable or not.

Acknowledgements

I wish to thank my friends and colleagues without whose help I would not have been able to get to this point. First of all, I would like to thanks Professor Timon Rabczuk who opened my horizon to research in structural and computational mechanics and introduced me to the INSIST program to pursue my PhD study. His guidance was instrumental in my decision to go to Cardiff University and enroll at the School of Computer Science and Informatics. He has continued to provide me with advice, and I owe him a great deal of gratitude. I wish to acknowledge the support of the School of Computer Science and Informatics as well as The Institute for Computational Engineering and Sciences, who enabled me to be at the position I am in today; in particular the guidance of my supervisors, Frank Langbein, Pierre Kerfriden and Ralph Martin, through lectures, meetings, and less formal discussions — your instructions and directions have been invaluable at specific times and helped me to complete my studies. Frank Langbein provided consistent support in geometric processing and programming skills throughout all stages. I have to thank Pierre Kerfriden for his help to understand goal-oriented a posteriori error estimation; his insights helped me to gain the knowledge required to link simplification modeling error and a posteriori error estimation.

I must thank Prof. Robert Moser and Prof. Tinsley Oden for providing me with the opportunity to collaborate with their research groups and attend their talks and discussions at ICES at Texas University in Austin. I have gained insights in the subject of uncertainty quantification by participating in the relevant courses in the CSEM program as well as meeting with researchers at the Center for Predictive Engineering and Com-

Contents

List of Figures

List of Tables

List of Acronyms

CAD Computer-Aided Design

CAE Computer-Aided Engineering

CAM Computer-Aided Manufacturing

CAPP Computer-Aided Process Planning

CNC Computer Numerical Control

CRE Constitutive Relation Error

CSG Constructive Solid Geometry

DWR Dual Weighted Residual

FEA Finite Element Analysis

FSA Feature Sensitivity Analysis

IGA Isogeometric Analysis

MAT Medial Axis Transform

PDE Partial Differential Equation

PGD Proper Generalized Decomposition

QoI Quantity of Interest

Chapter 1

Introduction

The engineering design communities have been revolutionized by the advent of Finite Element Analysis (FEA), with the ability to analyze designs and consequently improve them. However, since then they also face the well-known challenge of high computational costs of FEA and much effort has been spent on reducing these costs. The complexity of a designed model determines the computational cost of calculating the FEA solution. The complexity can be classified into geometry configurations and constituent material properties of the model. Inhomogeneous materials often cause the high computational costs of analysis processes. Inhomogeneous materials consisting of many constituent materials create complex structures for analysis. The mathematical equations of such materials are notoriously expensive to solve computationally. Therefore, simplifying complex, inhomogeneous materials to homogenous materials can help in the analysis of a model. Moreover, the model geometry determines the style and type of the generated mesh in the preparation for FEA. The involved meshing process is another part that increases computational analysis cost. Meshing is one of the more specific issues that is both expensive to carry out automatically and, for complex models, requires manual intervention. Good meshes can decrease the computational costs by reducing the number of elements produced. There are also usually inaccuracies in meshing the model due to an imperfect representation of the true geometry of the model, which varies depending upon how complex the geometry of the model is. The challenging task is to balance out the computational costs and accuracy. The simulation processes are acceptable when they achieve an adequate level of accur-

acy for the application, whilst at the same time minimize the computational cost of the simulation analysis.

Features form a generic concept in Computer-Aided Design (CAD), where a feature usually refers to a sub-part of a geometric model, often associated with a specific function and always highly context-dependent. The geometry of a model has features of different sizes and shapes. It can be also associated with zones of particular material properties. The feature configuration of the model often dictates the structure of the mesh and how well it represents the actual model. The situation exacerbates if many small features are present in the model geometry. In order to capture small features with mesh elements, the mesh must be refined, and consequently, the overall computational costs are increased. In general, features increase the computational cost of the simulation, and often undermine the robustness and reliability of FEA due to their impact on the mesh. Sometimes complex geometry and topology involved in features lead to inefficient meshes or mesh generation failure. Even given a uniform mesh fully representing a geometric model, the finite element analysis may still produce an inaccurate solution, especially where irregular feature geometries are involved. In order to avoid the problems caused by the number of mesh elements and vertices in the complex geometries, models can be simplified by removing small features which have only a small impact on the solution or quantities derived from the solution.

Therefore, several methods have been proposed to simplify the geometry and topology of the models, in the context of different physical systems. These fall into the realm of shape simplification [14, 102]. The adaptation of the method has been developed for complex system analysis and has been useful for micro [38] as well as macro [61] scale models. As an example, the implementation of FEA for thin plates which have several small features was a very challenging problem, but became feasible by using model simplification techniques [89]. A common method proposed for simplifying the shape of models is based on suppressing or removing irrelevant extra features in the models before executing the FEA, to find a solution to the problem more efficiently.

Despite the fact that these simplification methods are efficient and reliable to reduce geometry complexity, calculating the effect on the simulation results is expensive to compute, depending on the configuration, size and number of features simplified.

Modeling simplification also has an important relation to manufacturing engineering models. Often the manufacturing processes cause differences between the designed and manufactured objects leading to manufacturing uncertainties. These uncertainties can show up as deformations of boundaries and shapes or imperfections in the material components of the models. These deficiencies may cause changes in the primary functions of model output. Thus, the modeling simplification error can estimate the difference in performance between manufactured and designed objects with respect to the quantity of interest.

Overall electromagnetic problems have a wide range of practical applications. Fig. 1.1 illustrates an example of simplifying a geometric model of a shielded coil prior to magnetostatic analysis. The model is an example of shielding the magnetic field of a coil. The gray box is the outer boundary which is a metal box. The inner components consist of the coil and shield. The red and orange parts are features on the coil and shield that may be simplified. Much of the geometry has little effect on the solution, and can be removed before meshing to estimate the effectiveness of the shielding.

In this dissertation, the problem of interest comes from engineering models for the electrostatic partial differential equation and its solution via FEA. This is relevant to a range of industrially important problems. In general term, the proposed simplification modeling error is applicable to the range of physical models that are constructed from second order partial differential equations with divergence free operator. Electrostatics is relevant to problems involving the effects of stationary charges, e.g. damage to electronic components during manufacturing, and build-up of static electricity, especially on plastics and high-voltage components. Electrostatic analysis is important in the design of switchgear, used to control, protect and isolate electrical equipment. Insulation materials such as gas, oil and air are used; flaws in manufacturing processes may
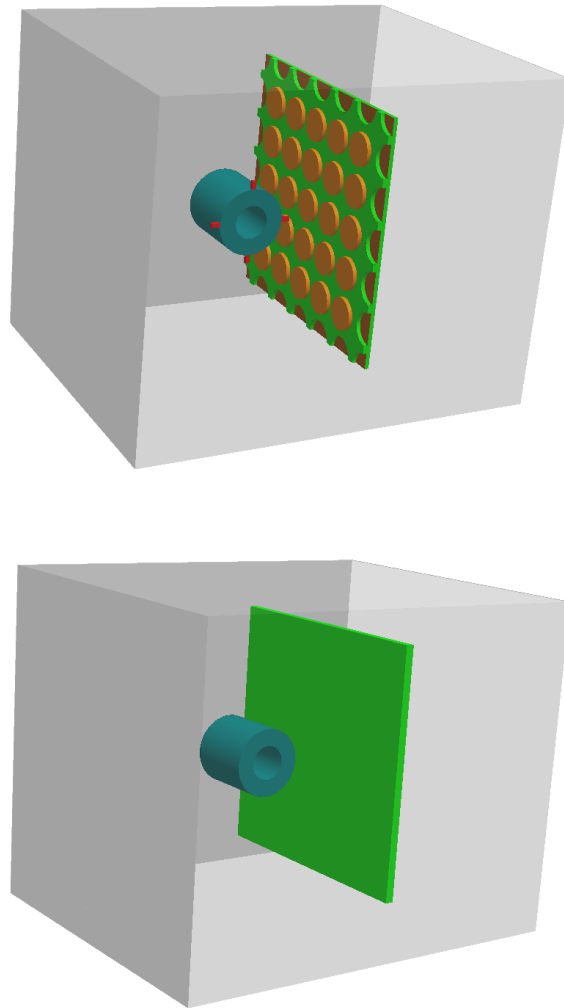
Figure 1.1: Geometric simplification before magnetostatic analysis of a shielded coil. The top model is a full-featured configuration of the shielded coil (before defeaturing process) and the bottom model is the simplified model.

significantly impact its usability. Estimating the manufacturing design error can play a major role in understanding whether the switchgear will operate sufficiently well. For such problems we wish to estimate the effect of simplifying the geometry on the simulation result, specifically represented in a quantity of interest that depends on the solution of an electrostatics problem.

1.1   Motivation and Problem Statement

Computational engineering analysis requires a discretization of a continuous boundary value problem. The discretization quality strongly influences the solution accuracy, which depends mainly on (i) how well the properties of the continuous solution space are preserved in the discretized functional solution space and (ii) how well the discrete geometry (typically a 2D or 3D mesh) represents the continuous geometry. It is well known that generating mesh models from CAD models for engineering analysis is time-consuming and expensive, taking 60% to 70% of the total analysis time [15]. There is a general trend that engineering models are growing in size and complexity of the geometry. For example, presently, a typical automobile consists of about $3,000$ parts, a fighter jet has over $30,000$, the Boeing 777 over $100,000$, and a modern nuclear submarine over $1,000,000$ parts.

Manufacturing a complex model implicates that engineering design and geometry analysis are not separate endeavours. Without accurate representation of CAD geometry and mesh adaptivity, convergence and therefore high-precision results are hard to achieve. Flaws in current engineering analysis procedures also make necessary successful application of important pace-setting technologies, such as design optimization, verification and validation, and uncertainty quantification. Using simplified or idealized CAD model geometries often enables and always speeds up the simulation, based on the idea of removing small or insignificant features which have little effect on the analysis results. However, in the last step of processing the simulation results, the effects of such simplification techniques must be estimated to bound the error they induce on the finite element simulation results. In other words, the simplification error analysis can validate the reasoning for simplifying a set of features and their effect on quantities of interest derived from the FEA solution of the simplified model. This has two advantages: firstly, simpler geometry means that it can be represented by a simpler mesh with fewer, larger elements, making meshing both quicker and more robust. Secondly, as the resulting mesh is simpler, analysis is also quicker. These advantages justify to

investigate estimating the error caused by simplification techniques. Note that the simplification error also indicates the effect or functionality of the simplified features in the original model, if it can be estimated to high accuracy. But this is not the focus of this work.

Various examples of industrial applications of defeaturing are collected in [82], showing how simplification can significantly reduce computational costs in Computer-Aided Engineering (CAE). In the manufacturing process, CAE tools are used for verifying that a planned manufacturing process meets the target cost and speed. With trends of increasing complexity in the geometric representation, the challenge of model preparation for CAE tools is growing drastically. As far as the geometry preparation process for CAE modelling goes, a smooth and quick process saving cost of the simulation is desirable in the manufacturing sectors.

Various approaches for simplifying or defeaturing CAD models have been studied and proposed [17, 71, 87]. Their focus often lies on the defeaturing techniques themselves, aimed at removing small features, rather than on the effects of defeaturing on subsequent model analysis. [87] lists the most common defeaturing techniques applied to industrial designs. The approaches for model simplification are named such as surface entity based, volumetric entity based, explicit feature based and dimension reduction based. These are fully-automatic or semi-automatic simplification techniques for CAD models for a wide variety of applications.

So the key to performing simplification is to know what effect the simplification will have on the solution. Simplifications which make large changes to the solution are likely to be unacceptable. We wish to predict the simplification error arising from replacing complex geometry by simpler geometry, to decide whether the simplified model is sufficient or a more complex and expensive simulation needs to be run instead. Note that this is problem dependent, and features which are important for a solid mechanics analysis may be unimportant for electrostatic analysis, and vice versa.

There are only a few results showing the effect of simplification on the accuracy of

the solution. To study this effect, an error measure indicating the effect of the simpli-fication must be defined. This is not simple, as the difference between the solutions for the original and simplified model are not clearly defined, due to differences in geo-metry and possibly topology, too. However, most engineering analysis tasks are aimed at calculating some specific Quantity of Interest (QoI). Often a QoI can be expressed as an integral of a local quantity, determined by the solution, over a subset of the model [66, 2]. The difference between the estimate for the QoI of the fully-featured and defeatured models is called the *simplification error*. This is the quantity I wish to determine, to decide whether the simplified model is suitable for the analysis task. The aim of analysing the original model is to approximate the behaviour of a real object. Therefore, the analysis of the simplified model should give results approximating the behaviour of the real object within an acceptable range, comparable to the accuracy of the analysis of the original model. The error estimation requires a post-processing algorithm interfaced with the finite element simulation of the defeatured model, which is the problem of interest and the core of the computation here. Previously, most of these algorithms concluded the estimation of error with wide uncertainties with re-spect to the exact value of the simplification error for the studied QoI also known as point-wise error estimation. Therefore, it is necessary to construct tight bounds for the simplification error to estimate the error with more accuracy. These bounds can help to either validate or reject the solution from the simplified model. In this work guaranteed upper and lower bounds for the simplification error are derived, introducing a generic approach, that is specifically refined and applied to electrostatic problems and further numerically validated.

Estimating the simplification error can be done in a similar way to computing other error estimates for finite element and boundary element methods. Approximating a real object with a discretized CAD model causes analysis errors; one aim of error analysis is thus to show that the computation results are close to the exact solution [35]. To deal with either discretization or modelling optimization errors, various strategies are proposed for analytical solutions for finite element methods [42]. Most of the

suggested error estimation techniques do not provide mathematically proven bounds on the error and need to be used with care.

A priori error estimation studies the convergence and stability of numerical solvers, and provides an understanding of the asymptotic behavior of errors for varying mesh parameters. They are not designed to give an actual error estimate for a given mesh [2]. *A posteriori* error estimates are used in computational mechanics to control the error of the solution of ordinary differential equations. They are mostly developed on the global error in the energy norm. Those are typified by predictor-corrector algorithms, where we wish to estimate the differences in errors in solutions obtained by schemes using different orders of error truncation [5]. Recently the theory was extended to estimate the error in particular quantities of interest. To understand the exact error it must be realized that many local and global quantities of interest can be selected with respect to the subject of investigation out of CAE simulation solutions. Every quantity of interest is a function related to the finite element modelling solution. This method is commonly referred to as *goal-oriented* error estimation, since the aim is to provide error estimates and error bounds for a particular quantity of interest. The latter approach also provides the basis for our simplification error estimation. The exact bound method, which has been proposed in [74], can be used to obtain guaranteed upper and lower bounds for a quantity of interest. The basic idea of this approach is to employ the solution of a finite element method and use complementary energy principles to obtain guaranteed upper and lower bounds. By recasting the problem in terms of a dual problem, corresponding to the quantity of interest, guaranteed bounds can be obtained for the quantity of interest using the solutions of local problems. The proposed simplification error estimation approach follows the same principle, but it is developed for the computation of error in the energy norm.

While the approach may be adapted to a wide range of physical problems governed by a second order divergence free partial differential equation, I study it specifically for the case of electrostatic problems. These provide a simple setting in which the

approach can be demonstrated; it is also relevant to the design of capacitors. I apply the proposed method for the estimation of the simplification error for the capacitor, which will be illustrated in three different schemes:

(i) The boundary conditions associated with the electrostatic equation are changed by simplifying the geometry of the capacitor for practical defeaturing reasons. The change in the formation of the boundary conditions will result in a different finite element solution of the electrostatic equation. It consequently influences the QoI expressed as an integral of the electric field over an area of interest. The approach bounds the simplification error in the energy norm of the QoI.

(ii) Due to uncertainties in the manufacturing processes, imperfect boundaries are created in the capacitor that were not considered in the (idealized) design. Upper and lower bounds are constructed for the error in the energy norm showing the effect of manufacturing tolerances on the QoI. So the simplification error estimation technique helps to predict the performance of the manufactured object subject to small manufacturing uncertainties.

(iii) It is studied the error induced in QoIs by the suppression or modification of the dielectric material properties inside the capacitor. The amount of energy that can be stored in a capacitor depends on the dielectric properties of the material between the capacitor plates and their geometry. Therefore, simplifications in the model as well as contamination in the dielectric material in the manufacturing process may have an impact on the capacitance, which is reflected in our choice of QoI.

The error bounds indicate how far the modeling simplification error can grow for the error in QoI of the original model without numerically analyzing it. The approach is able to bound the simplification error using the Constitutive Relation Error (CRE). The CRE is the fundamental part of the construction of bounds. It makes the computation of the bounds affordable and implementable. The CRE manipulates the admissibility conditions and computes the error measure in the energy error norm that enables efficient computation and can be implemented easily within a finite element solver.

The admissibility conditions are the terms to validate the finite element model and its boundary conditions within CRE for the construction of bounds. By expressing the error in terms of a linear QoI and estimating the error in terms of the energy norm, the goal-oriented error approach and the residual error can be applied and combined with the CRE concept to prove strict bounds. The approach is generic and can be applied to any divergence-free elliptic Partial Differential Equation (PDE). It is specifically adapted to different feature locations for electrostatics problems, where the features either lie inside the problem domain or on the boundary. Boundary features are further distinguished by whether they lie on the Neumann or Dirichlet boundary and whether the simplification adds or removes material from the problem domain for negative or positive boundary features. The Dirichlet boundary condition is the type of boundary condition which is imposed on the primary variable like the potential in electrostatic problems and displacements for solid mechanics. The Neumann boundary conditions are imposed on secondary variables like fluxes in electrostatics and traction forces in solid mechanics. Negative and positive boundary features are are either areas added to the domain or removed from the domain respectively where either a Neumann or a Dirichlet boundary condition on the original domain is involved. The different feature cases are elaborated on in Chapter 4.

Specific simplifications it is later considered relate to removing the dielectric material constant in an area and removing small positive or negative features on various boundaries.

1.2   Contributions

The contributions of this thesis are:

- This work proved strict lower and upper bounds on the difference between a QoI calculated from the solution of a Poisson boundary value problem. The bounds

can be calculated solely from solutions of the simplified problem, without know-
ing the solution of the original problem. The error is expressed in terms of QoIs
which are linear in the solution of the Poisson equation. Such QoIs can often
represent useful quantities for evaluating an engineering design. The approach
is generic and can be applied to any divergence-free elliptic partial differential
equation PDE.

- The error bounds are specifically adapted to applications in electrostatics and fea-
tures which either lie inside the problem domain or on the boundary. Boundary
features are further distinguished by whether they lie on the Neumann or Dirich-
let boundary and whether the simplification adds or removes material from the
problem domain for negative or positive boundary features. The QoI is chosen as
the electric energy stored in a region of interest. As this is not linearly dependent
on the electrostatic potential, a suitable linearisation is introduced, which still
indicates the effect of the model simplification on the QoI. The proposed simpli-
fication error estimation is numerically tested for capacitor problems governed
by the electrostatic equation with different simplification scenarios reflecting the
feature types. The analysis is performed on similar mesh structures between sim-
plified and original models to provide insights into the tightness of the bounds
only. The effectivity of the bounds for all the test scenarios, over internal fea-
tures and positive and negative boundary features on the Neumann and Dirichlet
boundary, is used to evaluate the performance of the bounds. For small effects
the bounds perform generally well. For larger effects, the bounds are less tight,
but are still guaranteed to bound the solution and can indicate that the effect of
the simplification may be too large. This makes them useful to decide whether a
simplification creates acceptable simulation results.

These results represent an important step toward practically useful estimations of the
simplification error, demonstrated via two illustrative examples. The application of
bounds are demonstrated for the simplification error for the electrostatic equation on

a capacitor model with a positive feature on the Neumann boundary. This shows that model simplification can reduce the computational costs with respect to meshing and analyzing times, while the error made by the simplification is estimated with the computed bounds. Similarly, the bounds may be applied to estimating uncertainties in the performance of an object due to manufacturing variations and the resulting shape uncertainties. This is illustrated with the help of a capacitor model with a contamination in the dielectric material. The model is evaluated for the homogeneous dielectric material and the simplification error resulting from ignoring the contamination is bounded for a QoI indicating the effect of the contamination on the capacitance. Both examples show the practical relevance of the bounds and how they provide a basis for analysing the simplification error for practical problems in future work .

1.3   Overview

This dissertation is organized as follows. I begin with reviewing the background and related works in Chapter 2. Chapter 3 is devoted to explaining the electrostatic PDE. It is showed how its representation in strong and weak form is derived from Maxwell equations. Then it is discussed the configuration of a capacitor model and its specific application in industry. In Chapter 4, I derive the general form of the simplification error bounds based on the well established framework of goal-oriented error estimation. Section 4.1 introduces various types of simplifications we consider to create simplified models from fully-featured models for different feature types. In Section 4.2, it is described the involved components for the construction of the bounds. The quantity of interest is defined in 4.2.1, where it is also discussed the method for linearizing the quantity of interest. Then the adjoint method is explained and customized for the electrostatic PDE in Section 4.2.2. The CRE and its related conditions are presented in Section 4.2.3, followed by detailed descriptions of the computation of errors for primal and dual models in the energy norms. Chapter 5 apply the general bounds from Chapter 4 to derive specific bounds for electrostatics problems for the different feature

types introduced earlier. How to adapt the general bounds is presented in Section 5.2 for the simplification of an internal feature. Then, in Section 5.3, the general bounds are adapted to simplifying boundary features. Chapter 6 provides numerical results to verify and validate the bounds for the different cases. Conclusions with a discussion of future work are given in Chapter 7.

Chapter 2

Background

In this chapter, it is discussed work and research results related to the ideas and results in this dissertation. I briefly cover related work in CAD, meshing and features and discuss defeaturing techniques, *a posteriori* error estimation and related results in estimating the effect of geometry simplification on engineering analysis results. It is also pointed out how the results of this dissertation relate to and extend other work.

2.1 CAD Models, Meshing and Features

CAD aims to represent physical objects with models for a specific purpose such as manufacturing, analysis, etc [86]. After the first CAD models were introduced decades ago (1960s), CAD technology has evolved, and now is broadly applied in many different industries. In mechanical model design, it is integrated with Computer-Aided Manufacturing (CAM), especially for Computer-Aided Process Planning (CAPP). In order to analyse the physics of a designed CAD model under different external loads and boundary conditions, computational simulations (engineering analysis) are often rendered before constructing a physical realization of the object. Engineering analysis is generally performed using FEA, which solves a discretized boundary problem based on the CAD model. Therefore, the discretization process is essential for the analysis of CAD models, which means CAD technology plays an important role in modern manufacturing processes. It was estimated in 2014 that the overall CAD industry was a

billion dollar business [67].

Different patterns are used to represent 3D geometric information. The first pattern keeps information of the boundary for a solid, referred to as a boundary representation (B-Rep) model [60]. Another pattern records the model constructively as Boolean operations between primitive shapes. This is called a Constructive Solid Geometry (CSG) model [49, 90]. The third pattern stores solids as a sum of simple solids, typically cubes. Solid models explained in this fashion are known as decomposition models. The fourth pattern specifically keeps feature information in addition to the information about the primary shape entities and is known as feature based modeling [30], usually using one of the above underlying representations where features are explicitly identified. Here features form a subset of the model that is linked to some semantic context such as a hole or slot.

Non-Uniform Rational Basis Spline (NURBS) is a family of shape functions used in computer graphics for generating and representing curves and surfaces. The NURBS functions and their extended versions [91, 15] are convenient for free form surface modeling, as they can precisely show all quadric surfaces, such as cylinders, spheres, ellipsoids, etc. The major setbacks of NURBS are that they use a tensor product structure that causes inefficient representation of detailed local features. T-splines are a new breakthrough which generalises NURBS [80, 9] by permitting a row of control points to eliminate unnecessary control points from the NURBS functions. T-splines suggest a better approach than NURBS in that they allow local refinement and coarsening and a solution to the gap/overlap problem. The control grid of T-splines, contrary to NURBS, is permitted to have partial rows of control points.

The discretization of CAD models is often based on a volumetric mesh which is generated directly from a boundary representation (B-rep) model. This conversion can take up a significant part of the analysis, reaching up to 60% to 70% of the total analysis time. One approach to resolving this formidable task in CAD/CAE integration is to use Isogeometric Analysis (IGA) [15]. It takes advantage of using the same basis func-

tions (in most cases NURBS and alternatively T-splines [9]) to represent the discretized geometry and the functional spaces of dependent variables. Recent trends happening in engineering analysis and high-performance computing are also requiring greater precision and tighter integration of the general modeling-analysis process, enabled by IGA.

However, creating an IGA solid mesh for general 3D volumes is much more challenging, even though some recent results enable better conformity of solid volume meshing [94, 97]. As well as mesh generation, CAD/CAE integration also involves a very time consuming and complex process of geometry preparation or idealization, which creates a geometry suitable for analysis by applying different simplification techniques. It takes about 57% of the overall analysis time measured for simulations at Sandia [9], where the mesh generation only accounts for 23% of the overall time. Complex models may produce ill-conditioned matrices and therefore working with non-simplified complex models may generate inaccurate results [73, 54], in the worst case, they may even lead to mesh generation failure [92]. Thus, several geometry simplification or model reduction techniques are introduced to overcome this difficulty. A main task of geometry simplification is *defeaturing*, suppressing geometric details such as holes, fillets, blends, and slots, from a complex CAD model. The work of [87] studied several approaches for fully-automatic or semi-automatic simplification of CAD models for vast applications. It compiled the techniques into the four categories: techniques based on surface entity based operators, volume entity based operators, explicit feature based operators and dimension reduction operators. Model simplifications can be performed manually or automated. The manual simplification takes a deal of human expertise and is time consuming. Recently, some efforts have been made to automate the model simplification process. There are several algorithms, developed to facilitate the feature recognition systems and whether the selected feature should be removed or not [64].

The notion of a feature is in general not defined exactly and often depends on a specific context in which the CAD model is being used. In the context of this dissertation, I consider features imply to be subsets of a CAD model. Features are at an intermediate

level between individual entities representing the model (vertices, edges, faces, etc) and the whole model. Features play a key, and increasing important, role beyond design. In CAD-CAM integration, a typical CAPP system extracts features from a part model and automatically generates computer numerical control code. In CAD-CAE integration, models are simplified by removing small features before meshing for analysis. However, many legacy industrial models exist without explicit feature information, or it is absent for other reasons. Feature recognition is a reverse engineering task to extract meaningful features from history-free models using computer methods. In [64], users can define features in terms of a declarative language based on the individual model entities. Features can be categorized into two main types: (1) primary, volumetric features such as holes, pockets, slots, etc., and (2) secondary, surface features like blends, fillets and rounds. Model simplification operators in this context specify how a feature is being removed from the model (or replaced with simpler geometry), e.g. by closing a hole. Based on type of simplification, model defeaturing techniques are recognized with surface entity based, volumetric entity based, explicit feature based and dimension reduction based. The full wrap of these techniques is illustrated in Fig. 2.1, based on the survey in [87]. The interest of the work in dissertation is not in finding or defining feature types, so further details on that work are omitted.

It is noted that a finite element mesh is only an approximation of the CAD geometry, which can in many situations create error in the simulation results. If the analytical error caused by such approximation is less than an acceptable, low threshold, the results of the discrete simulation are reliable. As here the interest is only in studying the effect of simplifying the model geometry onto the simulation result, it is assumed such approximation errors are negligible in comparison to the simplification error. This assumption means I neglect the discretization error between continuous and discrete model to be (approximately) zero.
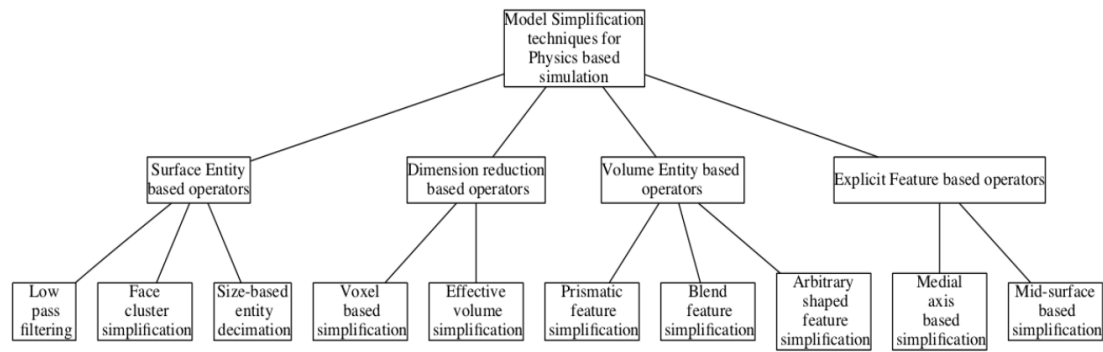
Figure 2.1: **A hierarchical classification of model simplification techniques (see [87]).**

2.2 Defeaturing and Simplification Approaches

This section describes the defeaturing techniques that are well-known both in academia and industry applications. It is divided into four sections below aligned with the different approaches as illustrated in Fig. 2.1.

2.2.1 Surfaced Entity Based Techniques

Features for the surface entity based techniques are simplified by operating on surface entities such as faces, edges and vertices. The surface entity techniques generally fall into three categories: (1) low-pass filtering [50]; (2) face cluster based simplification [81] and (3) size based entity decimation.

The low-pass filter techniques use Discrete Fourier Transform (DFT) and operators performing on surface entities. This model simplification approach is processed mainly in finite element analysis for mesh generation. The mesh is generated from an image. A shape needs to be turned into an image before performing a DFT on it. Then the surface is expressed in the frequency domain. The low frequency ranges constitute the overall shape while the high frequency ranges indicate the detailed features of the surface function of the model. When the high frequency parts are eliminated from

a model, it is known as a low-pass filtered (LPF) model. A threshold for an *a-priori* error was introduced in [50] to evaluate the detailedness or complexity of the respective entity. If the error is below a threshold, the entity is considered a detail, which can be simplified. If the error is greater than the threshold, the feature will belong to the general shape.

The face clustering algorithm is a method to break down the faces in the input model [81]. Sum of faces thus take forms of regions of interest that may be considered for simplification. The method is mainly proposed for simplifying the models for FEA mesh generation application. There are three main steps in this approach: face clustering, finding the suppressible faces and simplification. The model is shown as an adjacency graph with all faces represented as an initial branch of nodes and connecting edges as links. The links are then contracted to form the faces. The face node pairs to be clustered are selected based on the measurements assigned to the links connecting them. The weight depends upon the geometry indices known as the compatibility criteria (calculated heuristically) of non-manifold input. Simplification operators are determined based on virtual topology, where a face is broken up into different faces equal to the number of adjacent neighboring faces having a boundary in common with the original face. Afterwards, the newly generated faces are combined with respective neighboring faces with which they have the same boundary. It can be delineated that only connectivity between the faces changes; however, the geometry stays intact and thus it is named a virtual topology based collapse.

Another face analyzing technique for FEM mesh generation application is reported in [39] to be the same as the virtual topology approach. This approach iteratively merges the model faces to create face cluster regions having an adequately large domain in comparison to the mesh element size with considerably smooth face boundary and flat region. In [83, 20] an *a-priori* error estimation is defined based on aspect ratio and dihedral angle measures. The defeaturing is executed by repeatedly removing faces with low aspect ratio and small measure, followed by remeshing. In this approach, the

validity of a localized mesh refinement is ensured by imposing topology-based constraints.

[51] presents a method to create progressive solid models (PSM) from feature based models utilizing a cellular topology-based technique. A PSM is defined as an overall shape and a set of details. Cellular topology is taken for generating the PSM and surface entity defined operators are developed to simplify the model. The main concept is to start with a feature based model as an input model and construct a sequence of solid models indicating the foundation of object with several aspects of detail. The PSM can operate on the exact NURBS base functions of the underlying models. The Boolean operations for advanced modeling can be changed to the simpler topological entity manipulation at cell level, which is computationally less expensive.

Topology simplification algorithms for finite element mesh generation is introduced in [27]. The model for FEA should be discretized in such a way that the mesh generated for it captures the model details as closely as possible and at the same time minimizes the computation time for analysis. Another requirement of the simplified model is that the mesh should be able to take into account the boundary condition domains, e.g., a point on the part where tractions are applied should be represented by a collapsing node. Also, the mesh edges generated from the simplified model must exactly match the sharp corners of the geometry to minimize the discretization error. Foucault et al. [27] have developed a Mesh Constraints Topology (MCT) based on a model simplification method which enables to represent the sharp corner matching requirement. The MCT method maintains the same topology and generates new geometry adjusted to mesh quality constraints such as size-map, maximum over-density, maximum deviation angle, and boundary condition regions.

Fine et al. [26] developed idealization operators for FEA. The operators are defined in the error concept of vertex removal and spherical region. Mobley [62] reports an object oriented approach to propose surface based defeaturing operators to remove small features for FEA model preparation. A good basis in object-oriented design permits

the programmer of the defeaturing algorithm to hone on the algorithm and not on the data management of the underlying structures. These algorithms need to be developed for near tangencies, coincident edge precision discrepancies, poor intersection curve accuracy, and small geometrical features. Date et al. [18] report a vertex- and edge-collapse based technique for modeling simplification and further refinement. They defined three error measures based on overall geometry error, face size and face shape. The error measures are computed for edges to determine whether they need to be simplified or not.

2.2.2   Volume Entity Based Features

Volume entity based techniques utilise volumetric properties for model simplification. These techniques are categorized into subcategories: voxel based and effective volume based techniques. The work of [3] developed in terms of Trihedral Discretized Ploy-hedra Simplification (TDPS), where it is used on topology reduced surface simplification. The approach consists of three steps: (i)discretization, (ii)reconstruction (iii)face reduction. The effective volume operators are formed on the basis of feature rearrangement given criteria for Level of Detail (LOD). Level of Abstraction (LOA) is also required for detail removal, which will result in the shape different from the original feature shape owing to the non-commutative nature of the union and subtraction Boolean operations. The operators become involved in combination of Boolean operations resulting in geometrically and topologically valid features after rearrangement known as effective volume operators.

A feature-based, non-manifold model is proposed in the works of [52, 51] to focus on the needs of both CAD and CAE applications at the same time for a single model. This system enables the feature based multiresolution and multiabstraction modeling capabilities. Partial entity structure is designed to keep the model information [53]. The detail removal and dimensional reduction at several levels of detail and abstraction make essential process for rearranging features. The detail removal process involves

three steps as follows. The frist step is that all the idealization features specified by their application domains are derived out of the master model. In the second step, the separated idealization features are rearranged according to LOD criteria. If the volume sits below a threshold measurement, the assigned feature is considered for simplification. Thus, the error measure criteria for selection of features is determined by the volume of the feature. Finally, the LOD is set interactively to simplify the model with the features below the specified level. In terms of the multiabstraction of the model is suggested by using LOA criteria to specify the features. LOA criteria depend on applications. In order to generate a mesh model, an automated mesh generation procedure is applied to this model, and this is mapped into a CAE system.

2.2.3   Explicit Entity Based Features

The techniques based on explicit features define a set of explicit features in relation to a particular application such as manufacturing, FEM etc., and evaluate some measurements owing to the simplification decision can be made. The techniques are classified into three subcategories: (i)prismatic feature simplification [19], (ii)blend simplification, (iii)arbitrary shaped feature simplification based on the types of feature covered.

The feature recognition for prismatic feature simplification is performed with a mesh segmentation technique. The angle between two neighbor faces which have a shared edge together determines which feature edge needs to be extracted. These sets of edges are utilized to define regions of interest for the extraction and segment the mesh into regions. The regions with area larger than the threshold assigned as a default under choice of user are categorized as base surfaces. In the next step, the triangles that are not coincident with base surfaces are extracted as Feature Construction Triangles (FCT). In the end, the feature removing triangles (FRT) are substituted with feature FCT to reconfigure the suppressed features. The condition that has to show the satisfactory behavior in order to recover a feature is that the feature boundary vertices (FBV) should be compatible with the boundary nodes of the suppressed feature mesh.

If this condition is not in the place, then the local LOD method is applied to define a set of parent vertices comprising the vertices that are lumped to create the parent node. It creates the binary tree that is traversed to recover adjacent vertex iteratively by vertex splitting [16]. The removed features can be recovered by the information from the LOD tree.

The approach of [103] for blend simplification deals with fillets and round features for B-Rep models. This method characterizes the topological entities that are used to identify the trace faces. Trace faces are there to mark the fillets and rounds in the model to suppress them. The work in [96] executes the simplification method with the delete face technique to eliminate a cluster of faces corresponding to a specific feature. As soon as the feature is disappeared by deleting the faces method, there would be gaps between two faces which are filled by extending or contracting the adjacent faces of the suppressed feature.

2.2.4   CAD Model Dimension Reduction

Dimension reduction of CAD models is a popular defeaturing method in finite element simulation of engineering problems. One of the well established techniques in the literature is Medial Axis Transform (MAT) [55]. The geometry idealization pertaining to dimension reduction used in [22] to simplify a model for analysis and other downstream operations. To determine whether the dimension of the object is to be reduced, aspect ratio is defined and taper criteria are used. This ratio indicates when which part of model needs to be reduced in the dimension. Another noteworthy method is the mid-surface [72]. This approach applications are used in FEA model preparation and feature recognition. The mid-surface is generated by four steps are four steps, namely pairing surfaces, topology based adjacency graph creation, mid-surface patch generation and sewing the patches based on adjacency information.

The recent trend of machine learning techniques [17] can be used as a tool to find reg-

ulations in the preparation of the CAD models. It is used to exploit expert knowledge and to support on the decision making during the defeaturing steps. The concern that machine learning techniques deal with is the definition of the complete data models given as input and output to the learning techniques. The configurations of the model features are learned in several steps. Following the learning step, the analysis of many geometry models will boost identifying the criteria and thresholds that proceed with the definition of the machine learning techniques, of the settings as well as the indicators applied to assign their performance. The method consists of three phases. The initial phase is the construction of the database. The database must contain a massive number of known CAD settings and scenarios. Depending on the learning tasks, the main issue is to learn from the relevant data and to analyze them in order to create a database for machine learning processing. It should include both explanatory variables and also variables to estimate. These variables help to set criteria which estimate the variables from the explanatory one. The data related to the CAD models before simplifications are extracted directly from the initial models or entered by the operator. This data must be as exhaustive as possible and thus the selection of useful data will run in the second phase. The learning phase produces the intermediates that are keys to find results from the input data. This intermediate data points to studied statistical modeling (e.g. characteristics of analyzed features, setting functions) or data clusters (several input data can be grouped into a single intermediate data). The learning model must be able to classify qualitative variables within a tolerance imposed by the user. Results are analyzed for each explanatory variable and each statistical entity. Experiments on the training sets allowed to verify the explanatory variables. In phases three and four, the unknown data are integrated in the initial data and later enriched. The iteration phase facilitates a consistent updating of the knowledge learned to produce a more reliable decision making tool for engineers. The incorporation of two methods is used in [71] for the feature detection. The geometry size field is taken for detecting irrelevant features and a method to suppress the noncorresponding features via facet-based operations on a CAD configurations.
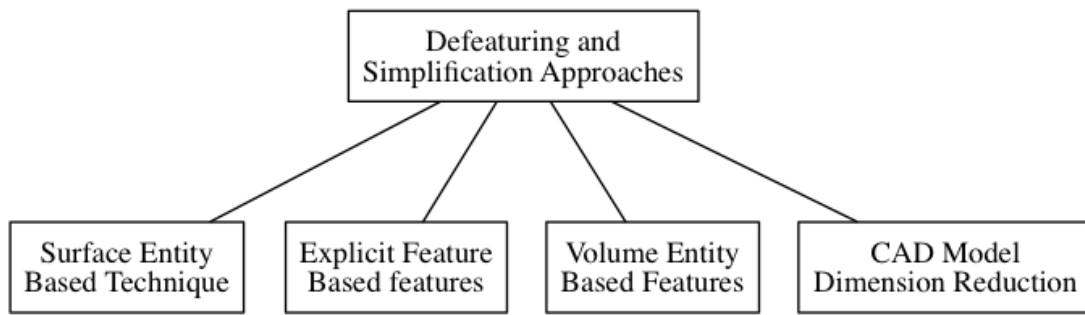
Figure 2.2: The well-known defeaturing techniques in four subsections

Most geometry simplification approaches determine some notion of feature and then use some criteria to decide whether to simplify the model or not. Based on this decision they execute the simplification. The user can decide what features should be removed. However, the simplification needs to be verified to see what the effect of suppressing the feature is on the engineering analysis result. It can be determined by the error in the solution of the model. Some of the simplification methods propose an error estimation techniques that define the threshold on the viability of the simplification. These simplification errors are elaborated next.

The aforementioned defeaturing approaches are illustrated in the Fig. 2.2.

2.3   *A Posteriori* **Error Estimation**

Error estimation has been developed for modeling physical phenomena in engineering and sciences to assess the quality of the solution of partial differential equations in space and time. Numerical error is in nature of such simulations: The discretization process of converting a continuum model of physical phenomena into a computational problem cannot keep track of all the information embodied in continuous models [85, 2]. Since the late 1970s several methodologies have been proposed to estimate the discretization error for finite element analysis. Basically, the error estimation can be classified in two types. One is *a priori* error estimation, which provides information

on the asymptotic behavior of discretization errors. It is not able to give an actual error estimate for a given discretization. In the contrary, *a posteriori* error estimators use the finite element analysis itself to derive estimates of the actual error of a computational solution. They are employed to render schemes in which either the mesh element size (h-refinement) is refined or the polynomial degree is increased (p-method) [21, 7].

The main purpose of any *a posteriori* error estimator is to provide an estimate for the error made by a computational solution in a specified norm. Generally, most *a posteriori* error estimation methods determine the error for the global model without bounds. These should be used with care [35]. At the beginning of 2000, the theory was extended to estimate the error in particular quantities of interest. This extension must be realized with one linear or nonlinear function dependent on the solution of an PDE problem describing a local or global quantity of interest. This approach is called *goal-oriented error estimation* since the aim is to provide error estimates and error bounds for particular quantities of interest. The upper and lower bounds are quantities that are always guaranteed to bound the actual unknown error [66].

The ideal error estimator should meet the following requirements: (i) the error estimator should indicate accuracy in the sense that the estimated error is close to the exact error; (ii) the error estimate should be asymptotically correct in the sense that with refining mesh sizes the error estimate should tend to zero at the same rate as the actual error; (iii) the complete error estimator should guarantee the upper and lower bounds for the exact error; (iv) it should not be expensive to compute; (v) it should be robust regardless of the linear or nonlinearity of the problem; (vi) an implementation of the error estimator should enable to render an adaptive refinement process with the error estimate applied for the optimization of the mesh with respect to the goal of the computation [35]. Indeed, it is rare for such an error estimator to provide a conveniently computable and guaranteed error bounds.

Various global error estimators are introduced for the global error in the energy norm for elliptic problems in [5, 6]. The authors expressed,"Error estimators that are based

directly on the finite element approximation and data of the problem are usually referred to as explicit error estimators. In contrast, implicit error estimators require the solution of auxiliary local boundary value problems. Hence, explicit error estimators in general require less computational effort than implicit schemes, but they make compromises in robustness and accuracy" [5, 6]. Explicit error estimators are developed by a direct computation of the interior error residuals and jumps at the element boundaries to find an estimate for the error in the energy norm [43, 29]. On the other hand, implicit error estimators employ the solution of auxiliary boundary value problems whose solution yields an approximation of the actual error [43]. The advantage of implicit schemes can be stated that in explicit schemes the whole information for the total error is provided only from the approximated solution, when it would be feasible in implicit schemes to obtain more accurate information on the error by solving additional auxiliary problems.

Two common approaches of element residual and subdomain residual methods belonged to the implicit error estimator class. They are developed by [8]. The residual method defines the local error in a single element. It is interpolated for the global error. The method of subdomain residual error estimation is to break down the global residual error into a number of local problems on small element patches.

The recovery-based error estimators are initiated from the implicit error estimator idea. They make use of the fact that the both solution and gradient of the finite element analysis is in general discontinuous at the boundaries between internal elements [66]. The underlying idea is to post-process the gradient and to determine an approximate value for the true error by comparing the postprocessed gradient and non-postprocessed gradient of the approximation. Zienkiewic and Zhu [99] proposed the recovery-based error estimator to postprocess the discontinuous gradient in terms of interpolation functions. [100, 101] show how the first approach of Zienkiewicz and Zhu can improve the better estimates of errors by using the superpatch recovery method if the interpolation is not placed at the nodes but the so-called superconvergent points in element

patches of the domain. However, of course, the Zienkiewicz-Zhu algorithm has an issue to capture full effective values in the presence of material discontinuities since, in a patch-based algorithm, these issues are resolved. Therefore, [28] proposes an element-based error estimator that uses higher-order accuracy points to recover the solution of the constitutive model.

Error in the global energy norm is used to estimate the error in the solution in relation to a particular quantity of interest, or to find at least a high quality mesh to accurately solve for this quantity. Typically an engineer is more interested in a certain quantity derived from the finite element approximation of the solution [66, 36, 68]. The key for estimating the error in such quantities is the equation of a dual model, which is considered in an addition to the primal model. It provides the necessary information for an accurate estimate for the error in the quantity of interest [33]. In fact, it indicates how the information is transfered from the residual error to the error for the specific quantity. The interesting fact of the methodology is that the error estimates are defined in terms of classical energy norm estimates of the errors in the numerical primal solution and numerical dual solution. This method is well-known for its powerful application of adaptivity schemes, where the mesh adaptation is considered to speed up the rate of convergence of the solution with respect to the quantity of interest.

The simplification error algorithm for this dissertation is developed by combining two separate *a posteriori* error estimation methods. As a feature is a subset of a geometry model, the suppression of the feature causes changes in a local subset of the domain of the whole model. Therefore, the simplification error would at its best be localized too. The effect of simplification error is investigated for a particular quantity of interest out of the finite element solution of the model. The goal oriented error estimation executes the algorithm for the estimation of simplification error for a quantity of interest. The constitutive relative error on the other hand enables to localize the computation of the error in the energy norm. I take advantages of these two methods and bound the simplification modeling error in the energy norm. Both methods are described in the

following section.

2.4   Adjoint Model

The adjoint method is defined in [69] as "a general method to compute the gradient of a functional that depends on a set of state variables, which are solutions of FEM models. The adjoint variables are the solutions of an adjoint linear system and can be seen as variables which gather a global measure of the perturbation of the problem with respect to the state variables" [69]. The adjoint method is used in this dissertation to localize the error in the modeling simplification to the specific area under influence of the feature. Numerically the adjoint method is powerful because only one extra linear finite element model needs to be solved. The computational cost is often irrelevant to the number of model unknowns, which is not always the case for pointwise a posteriori error estimation.

The use of an adjoint model for a design optimization in the context of computational fluid dynamics was pioneered in [70], and it was developed for various partial differential equations in aeronautical engineering in works of [34, 41]. In studies of turbulent flow, adjoint equations are used to investigate the active control of turbulent boundary layers to reduce drag through active re-laminarization [45] or to study unstable modes [4]. A long survey of the adjoint model application in meteorology was carried out in [23]. Further the introduction of the adjoint model for PDEs, it became popular for *a priori* error estimation. The complete survey of its application is listed in [1]. The application of duality arguments in the residual based *a posteriori* estimation recently became popular among different areas of computational and applied mathematics, some are highlighted as [66, 33, 10, 37].

The concept of duality modeling also penetrated the areas of geometrical and topological optimization [31]. Their defeaturing error analysis exploits the adjoint formulation of boundary value problems to arrive at strict bounds on the simplified model for

thermal analysis. Their estimator was not able to operate for different feature types and their computation was more expensive rather than defining an auxiliary model in the dual method. Another application of the adjoint model approach for model simplification is presented in [54]. This method builds on a dual weighted residual and topology sensitivity analysis methods. The derivation of the estimator was executed for the simplification of a negative feature for linear elasticity problems. This estimator was extended in [57] by utilizing the dual weighted residual method for a model based on the Poisson equation. It is able to estimate the defeaturing error for removing different feature types. But the estimation is not strict, as the authors did not construct strict upper and lower bounds.

2.5 Simplification Error Estimation

A posteriori error estimation can be applied to most elliptical equations, and it forms an important basis for simplification, modeling and numerical error estimation. For example, [25] analyzes the finite element model for a linear stationary thermal conductivity problem and computes an error estimate for a global quantity of heat conduction related to the solution of the linear heat equation after geometric simplification. It utilizes an approximated format of the energy norm of the difference between the finite element solution on the original and simplified model, and it is able to evaluate the influence on global simulation results caused by removing shape details. It incorporates an adaptive process of geometric simplification with an *a posteriori* FE error estimator. This is achieved by defining an *a posteriori* indicator for an automatic adaptive modeling process. The automation process, however, operates only for one detail, and it is not able to carry out the simplification of several features at once.

In a linear elasticity problem, [89, 88] demonstrate how *a posteriori* error estimation helps in *shape and topological sensitivity analysis* in defeaturing error analysis. Shape sensitivity analysis computes the change in QoIs when the shape of the model is per-

turbed infinitesimally, while topology sensitivity analysis computes the change when an infinitesimal internal feature is added to or removed from a model. Topological sensitivity provides a powerful technique for shape optimization of arbitrary-shaped features. It was introduced in [78]. [89] presents a method which entails a one-time FEA on the base-plate, followed by rapid post-processing to estimate the impact of design changes. Thus, through efficient analysis, the optimal configuration of a feature or cluster of features can be determined rapidly, without relying on FEA. All of the test cases are run over the circular plate membrane model, although it can process the shape optimization technique for the complex geometry within acceptable accuracy. The majority of shape optimization techniques were designed for solid mechanical models. They were not able to render the optimized stiffness FEM matrix analysis for the continuum model with the specific of a plate behavior. The work of [89] developed the optimized version of stiffness matrix for such a domain. [88] tests the idea of topological sensitivity analysis under an additional condition of suppressing several features. It uses *a posteriori* error estimation introduced in [78, 24] and shows how to identify the details in the automated feature suppression while retaining the consistency of the CAD model. Once the solution of the defeatured model is obtained, a confidence interval for the behavior of the full-featured model is derived such that one can be certain that the user-defined quantities of interest are computable, and that is often sufficient making design decisions. The final error indicator, however, is a quite rough estimate and there is no localization of the error.

Li et al [56] extend the work of [89] to determine the defeaturing error, again in an *a posteriori* error estimation framework, when defeaturing CAD models for different feature types. They use *shape idealization* for dimension reduction of a thin model to a 2D plate, and calculate the energy norm of the induced error for specific QoIs arising from the solution of a linear Poisson equation. Therefore, estimating idealization error has to consider possible coupling errors between regions of different dimensions. It selects each thin part in isolation and computes bounds on the idealization error induced by dimension reduction, defeaturing or combination of both. This work is an

example that takes advantage of the feature sensitivity analysis (Feature Sensitivity Analysis (FSA)) in order to handle arbitrary shaped features for linear problems. The use for this method can be seen in the Poisson equation [89], elasticity [32] or plate membrane problem [95]. But none of these methods provide a general approach that can cover all types of feature (positive, negative or internal) and some are only proved for linear problems. Their margin of error in estimating the simplification error is large and there is no guarantee that the technique provides a strict bound for the actual error.

The work of[31] describes removing a negative feature for a thermal conductivity equation where the feature is subject to a Neumann boundary condition. The authors impose a self-equilibrating condition in terms of removing a feature. This type of feature should be far away from the region of interest. Non-self-equilibrating features are of even higher concern. The suppression can theoretically be felt everywhere within the system, and can thus pose a major challenge during analysis. The weakness of this method lies in the requirement of the self-equilibrating condition being fulfilled. The adjoint and primal models are used and combined into a unifying theory to address both, self-equilibrating and non-self-equilibrating, feature types. This work was extended by [54] for negative features with Neumann boundary condition. It uses an approach based on *dual weighted residuals* (DWR) which is based on reformulating the modification sensitivity, originally caused by a geometric difference, as a modeling error, caused by mathematical modeling of PDEs over the same geometric model. The DWR is calculated via sensitivity analysis by integrating over the feature's boundary which can be evaluated using engineering analysis results from the defeatured model. The paper, however, shows the estimator was evaluated when removing negative feature in the boundary and inner feature, and it was not successful to evaluate the error for the suppression of positive features. This technique is closely related to the proposed method, but is not able to handle features on Dirichlet and Neumann boundaries.

The above discussed results can only handle the error caused by simplifying a single feature. [58] shows how to construct a defeaturing error estimator for second-order

shape sensitivity that considers the interaction between different internal or boundary features. The authors used second-order shape sensitivity, based on reformulating defeaturing as a shape transformation process. The error estimator is expressed as a second-order Taylor expansion in multiple variables. This allows the interactions between multiple features. It can handle multiple features to be taken into account, boundary features, and features which may be positive, negative or mixed. They may be subject to either Neumann or Dirichlet BCs. The interesting fact about the shape sensitivity is that the model remains the same for different features, as the defeaturing error is always estimated as the difference between a solution for the fully defeatured model and a partially defeatured model containing the features under study, so analysis solutions only need to be computed once. However, the estimation results are quite inaccurate, and the assumptions made concerning boundary features result in rather wide error estimate ranges with no bounds constructed for the unknown error. While [57] uses goal-oriented *a posteriori* error estimation to improve defeaturing error estimation for Poisson and linear elasticity equations, the approach does not include a strict bound for the error that would prevent over- or underestimation. The authors were not able to constrain the simplification error in the localized domain. This paper only addressed negative features. Thus, in [59] adjoint theory is employed to estimate the simplification error, which improves the error estimation results for internal and negative boundary features with Neumann and Dirichlet boundary conditions. Green's theorem and linearization are used to derive a simplification error formula for a non-linear Poisson equation. All techniques presented have some drawbacks in that only certain types of feature or boundary conditions can be dealt with, the estimates are independent of the feature location in the domain, there is often no guarantee that the estimate will bound or be sufficiently close to the actual error, nor is there a consistent index to indicate the performance of the estimate. Also, none of the previous work takes into consideration the solution and physics governed by the electrostatics equation.

The approach utilizes goal-oriented error analysis using the concept of *constitutive relation error* (CRE) [44, 46]. It is a powerful technique to bound the error associated to

an approximated solution of a finite element model. In particular, it has been applied to the evaluation of discretization errors for the FEM framework based on the concept of the Equilibrated Residual. CRE practically proposes to construct a flux that is statistically admissible and it should meet the condition of being kinematically admissible in the solution variable of the FEM model. Originally, [47] applied CRE to the evaluation of discretization errors in a finite element context, which is similar in terms of practicality and implementation to an equilibrated residual approach [66, 84]. The construction of the CRE method is based upon the satisfaction of the constitutive equation that guarantees the error in the energy norm bound for a linear QoI and increases its sharpness to estimate a more accurate error in the QoI. The finite element solution must be kinematically admissible, and the error is found by minimizing the potential energy in the energy norm. The static admissibility condition is obtained for the flux of the solution of second order divergence PDEs by minimizing the energy norm of the complementary energy equations [46, 48]. Both potential energy and complementary energy theorems are helping to split up the error in the constitutive relation into two different minimization error measures, separately allocated to the field and flux. Both complementary and classical potential energy contribute to the computation of the error in the energy norm for the CRE. CRE has the advantage that it does not require knowing the solution of the original model, and only requires the computation of the energy norms, which is fast, robust and accurate.

The paper [44] focuses on a reliable, accurate and efficient bound for the online error which is the distance between the exact solution and the solution delivered by the reduced model at a particular point of interest of the parameter domain. The auhtors proposed to construct the bounds by constitutive relation error for the parameterized problem of elasticity. The application of CRE in their FEM models is conducted by constructing a recovered stress field that is statically admissible, or equilibrated. Applying the constitutive relation to the kinematically admissible finite element solution that needs to be verified, one obtains a non-equilibrated stress field. The distance in the energy norm between recovered stress field and the finite element stress field is a

bound for the discretization error. The paper [48] implemented the CRE for the numerical simulation performed by means of proper generalized decomposition (Proper Generalized Decomposition (PGD)) approximation. It has been verified in a robust manner via computations performed with PGD by introducing an error estimation procedure based on the constitutive relation error. The resulting error estimator takes all error sources into account, particularly those related to classical discretization and the truncation of decomposition sum.

The idea of goal-oriented error estimation is to link the operator of the PDE with its adjoint operator, giving rise to a dual boundary value problem [33]. The error between the recovered flux and finite element flux (stress in elasticity or electric displacement in electrostatics) for the simplified model in the energy norm bounds the difference between the QoI of the original and simplified problem. It is assumed that the boundary value problem has a unique solution, and that the PDE operator is self-adjoint such as the Laplacian, or the Laplace-Beltrami operator.

Chapter 3

Electrostatic Problems

I begin this chapter by introducing the general Maxwell Equations and customized derivations of the equations for the problem only involving time-independent distributions of charge and fields for electrostatics phenomena. Historically, electrostatics developed as a macroscopic phenomenon. The governing physics of electrostatic problems follows from Maxwell's equations for static fields as any temporal derivatives become zero. The general characteristic of the electrostatic equation and its operator are an appropriate example for the simplification modeling error. Maxwell's equations are differential equations applying locally at each point in space-time (x, t). By means of the divergence theorem and Stokes' theorem, they can be cast in integral form.

Maxwell's equations in their general form are

$$\frac{\partial B}{\partial t} + \nabla \times E = 0 \text{ (Faraday's law)} \tag{3.1}$$

$$\nabla \cdot D = \rho \text{ (Gauss' law)} \tag{3.2}$$

$$\frac{\partial D}{\partial t} - \nabla \times H = -J \text{ (Ampere's circuital law)} \tag{3.3}$$

$$\nabla \cdot B = 0 \text{ (Solenoidal } B) \tag{3.4}$$

where

E : electric field intensity,

D : electric displacement,

J : electric current density,

H : magnetic field intensity,

B : magnetic induction,

ρ : electric charge density

and $D = \varepsilon E$ and $B = \mu H$. This work only considers materials with homogeneous isotropic permittivity for low frequencies, so a frequency dependence does not have to be considered.

For electrostatic theory all materials can be divided into two distinct classes: *conductors*, in which electrical charge can flow easily from one place to another; and *insulators*, in which it cannot move [40]. In the case of solids, all metals and some materials such as carbon are conductors, and their electrical properties can be explained by assuming that a number of electrons are free to wander through the whole volume of the solid. In solid materials of insulators, each electron is bound to a lattice of positive nuclei, and cannot move. When a body rests in equilibrium position, it means no net extra electrical charges exist within the body.

It is noteworthy to mention the roots of all electrostatics, quantitatively described by Coulomb's law giving the force between charged materials at rest relative to each other. Coulomb showed via experiments that the force between two small charged bodies separated in air by a distance that is large when compared to their dimensions (i) varies directly with the magnitude of each charge, (ii) varies inversely with the square of their distance, (iii) is directed along the line joining the charges and, (iv) is attractive if the bodies are oppositely charged and repulsive if the bodies have the same type of charge. If the charges are q_1 and q_2, and r is the distance between them, then the force F on q_2 along the straight line between the charges is

$$F = C\frac{q_1 q_2}{r^2}, \tag{3.5}$$

where the constant C is $1/(4\pi\epsilon_0)$ (in S.I. units). The factor 4π is introduced here to

refer to spherical rather than planar geometry.

This gives rise to introduce the concept of an electric field E, indicating the force acting on a charge. An electric field is given as the force per unit charge acting at a given point in space on a charge in a direction. It, therefore, depends on the distribution of charges, the permittivity of the media and the geometry. This gives

$$F = qE \tag{3.6}$$

where F is the force active on a charge q in the field E. This equation can be expanded to the sum of the forces acting on a charge across multiple locations. However, in a continuous setting, *Gauss's law* uses the notion of charge density instead to lead to a differential equation for E. In order to obtain *Gauss's law*, a point charge q is considered within a closed surface S. Let r be the distance from the charge to a point on the surface, n be the outwardly directed unit normal to the surface at that point, Γ be the boundary of domain Ω. For a continuous charge density $\rho(x)$ over the volume, Gauss's law is stated as "the flux of the electric displacement vector through any surface is equal to the total charge on that surface", which gives

$$\oint_{d\Omega} \mathbf{n} \cdot D \, \mathrm{d}S = \frac{1}{\varepsilon_r} \int_V \rho(x) \, \mathrm{d}V. \tag{3.7}$$

Note that this equation depends on (i) the inverse square law for force between charges, (ii) the magnitude of the force, and (iii) the linear superposition of the effects of different charges (if they existed). This equation gives the partial differential equation form of Gauss' law. By specifying Neumann and Dirichlet boundary conditions, we can derive a variational form to have the equation ready to be rendered via the finite element method. The details of this will be explained later (see Section 3.1).

Gauss' law enables the construction of the electrostatic partial differential equation in Maxwell's equations. The electrostatics problems are the stationary form of electric fields in Maxwell's equations. By assuming that all fields are static, the time derivatives are zero and we get two separate systems for electrostatics and magnetostatics.

Specifically for an electrostatic boundary value problem we obtain

$$\nabla \times E = 0, \tag{3.8}$$

$$\nabla \cdot D = \rho, \tag{3.9}$$

$$D = \varepsilon_r E. \tag{3.10}$$

With the aid of the divergence theorem, Eq. (3.9) becomes

$$\nabla \cdot E = \rho/\varepsilon_r. \tag{3.11}$$

According to Helmholtz's fundamental theorem of vector calculus, any field on a bounded domain in $\mathbb{R}^3$ that is twice continuously differentiable is uniquely determined by the sum of an irrotational (curl-free) vector field and a solenoidal (divergence-free) vector field. According to Eq. (3.8), E for electrostatics is irrotational, so we can introduce a *scalar potential* $\Phi(x)$ from Gauss' law,

$$E = -\nabla\Phi. \tag{3.12}$$

The difference of the scalar potential Φ indicates the work required to transport a charge q from one point (A) to another point (B) in the presence of the electric field E. The negative sign indicates that a positive charge will move from a higher to a lower potential, and work must be done to move it in the opposite direction. By referring to Eq. (3.12) the work is calculated by

$$W = -q \int_A^B E \cdot dl = q \int_A^B \nabla\Phi \cdot dl = q \int_A^B d\Phi = q(\Phi(B) - \Phi(A)). \tag{3.13}$$

So $q\Phi$ can be interpreted as potential energy of a test charge in the electrostatic field. Only the difference between the potential at A and B determines the required work, independent of the path taken. The combination of the Eqs (3.12) and (3.11) gives the partial differential equation for $\Phi(x)$ as a *Poisson equation*:

$$\nabla^2\Phi = -\rho/\varepsilon_r. \tag{3.14}$$

In regions of space where there is no charge density, the scalar potential satisfies a *Laplace equation*:

$$\nabla^2 \Phi = 0. \tag{3.15}$$

Solving a Poisson or Laplace boundary value problem (Eq. (3.14) and Eq. (3.15)) requires Dirichlet or Neumann boundary conditions to ensure a unique solution inside a bounded region. Hence, I can use *Green's identity functions* for electrostatic problems to show that specifying the potential on a closed surface (e.g., conductors at different potentials within a bounded region of space) has a unique solution. This gives rise to Dirichlet boundary conditions. Similarly, it is plausible to define another unique potential problem via the normal derivative of the potential which is the electric field, everywhere on the surface (corresponding to a given surface-charge density) by setting Neumann boundary conditions. This condition defines the Neumann boundary condition to place as a far boundary of the electrostatic media. On this boundary, the norm of flux (derivation of electrostatic potential) is zero to make a stable condition for far side boundaries. The general purpose of this is to obtain a unique solution to the Laplace or Poisson equation in a finite volume V with either Dirichlet or Neumann boundary conditions on the bounding surface S.

3.1   Variational Formulation and Finite Element Analysis for Electrostatics

In order to solve electrostatics problems, the strong form of the electrostatics PDE is converted into a weak form in this section. It can then be solved with finite element analysis. The strong form of an electrostatics boundary value problem is given by

$$\nabla \cdot (\varepsilon_r \nabla \Phi) = \varepsilon_r \nabla^2 \cdot \Phi = -\rho \text{ in } \Omega \tag{3.16}$$

$$\Phi = \Phi_D \text{ on } \Gamma_D \tag{3.17}$$

$$\mathbf{n} \cdot (\varepsilon_r \nabla \Phi) = \rho \text{ on } \Gamma_N \tag{3.18}$$

where Ω is the whole domain and Γ_D, Γ_N make up its boundary for Dirichlet and Neumann boundary conditions respectively. The relative permittivity is presumed to be isotropic for homogeneous materials in the domain Ω. As the potential Φ is smooth, Φ and Ψ are in the Sobolev space $W^{1,p}$, which for $p = 2$ is the Hilbert space $H^1(\Omega) := \{\Phi \in L_2(\Omega) : \nabla\Phi \in L_2(\Omega)\}$ with the inner product $\langle\Phi, \Psi\rangle_{L_2} + \langle\nabla\Phi, \nabla\Psi\rangle_{L_2}$. A Hilbert space is an inner product space that also forms a complete metric space. A Sobolev space is a vector space of functions that are the basis of the theory of weak or variational forms of partial differential equations. It comprises of functions equipped with a norm that is a combination of L^p-norms of the function as well as its derivative of the required order. Sobolev spaces for $p = 2$ form a Hilbert space because of the connection via the Fourier series and hence allow differentiation to be performed, supported by an inner product structure.

Both sides of the governing Eq. (3.18) are multiplied by a test function Ψ and are integrated over the domain Ω, yielding

$$\int_\Omega \nabla \cdot (\varepsilon_r \nabla\Phi)\Psi \; \mathrm{d}\Omega = \int_\Omega \varepsilon_r \nabla^2 \cdot \Phi\Psi \; \mathrm{d}\Omega = \int_\Omega -\rho\Psi \; \mathrm{d}\Omega. \tag{3.19}$$

Integration by parts for the left hand side gives

$$\int_\Omega \nabla \cdot (\varepsilon_r \nabla\Phi\Psi) \; \mathrm{d}\Omega + \int_\Omega \rho\Psi \; \mathrm{d}\Omega = \int_\Omega \varepsilon_r \nabla\Phi \cdot \nabla\Psi \; \mathrm{d}\Omega. \tag{3.20}$$

With the help of the divergence theorem this finally gives

$$\int_\Omega \varepsilon_r \nabla\Phi \cdot \nabla\Psi \; \mathrm{d}\Omega = \int_{l\Gamma_N} \mathbf{n} \cdot \varepsilon_r \nabla\Phi\Psi \; \mathrm{d}\Omega + \int_\Omega \rho\Psi \; \mathrm{d}\Omega. \tag{3.21}$$

Because of the far side boundary conditions, the electrostatic potential is equal to zero on the Neumann boundary condition, the variational formulation simplifies to

$$\int_\Omega \varepsilon_r \nabla\Phi \cdot \nabla\Psi \; \mathrm{d}\Omega = \int_\Omega \rho\Psi \; \mathrm{d}\Omega \tag{3.22}$$

In the case of fulfilling the far side boundary condition (Neumann boundary condition) the weak form simplifies to

$$B(\Phi, \Psi) = \ell(\Psi), \text{ where } B(\Phi, \Psi) = \int_\Omega \varepsilon_r \nabla\Phi \cdot \nabla\Psi \; \mathrm{d}\Omega, \quad \ell(\Psi) = \int_\Omega \rho\Psi \; \mathrm{d}\Omega \tag{3.23}$$

are the bilinear and linear form respectively. B is the continuous bilinear form used to construct the stiffness matrix for the finite element problem. The finite element solution is obtained for homogeneous and inhomogeneous boundary conditions. The purpose for the weak form construction is to convert the original partial differential equation to sets of integrable function over the discretized domain. The test function should exist in the same functional space as the variable function to make the integration possible. The discretized bilinear form B_i is a weak form function for each element that eventually is solved over all elements of the mesh discretization.

It is assumed ε_r is piecewise constant, such that Ω can be partitioned into subdomains Ω_l, $\bigcup_{l=1}^{N} \Omega_l = \Omega$, where ε_r has a constant, scalar permittivity ϵ_l on each Ω_l.

The general electrostatics variational formulation underlies the simulation of the electric capacitors. By using the Galerkin discretization technique and finite element method as well as imposing correct boundary conditions for electrical capacitors, the solution is obtained for the electrostatic partial differential equation, and the finite element solution is used to calculate a particular quantity of interest. In finite element analysis, the electrostatic potential Φ is approximated by

$$\Phi \approx \Phi_h = \sum_{i=1}^{n} \Phi_i N_i(x, y) \tag{3.24}$$

where $N_i(x, y)$ are shape functions. A suitable set of shape functions must be chosen to appropriately discretize electrostatic potentials. Arbitrary order polynomial elements are well suited. These elements should meet the requirements for finite element simulation known as: continuity, consistency and completeness. The discretized test functions are taken from the same shape functions used to discretize the electrostatic potential in accordance with the Galerkin Method. By substituting the discretized functions into the the main governing form, and integrating over each element and then summing over all elements of the domain, it is obtained

$$\sum_{i,j=1}^{n} \Phi_i \underbrace{\int_{\Omega} \varepsilon_r \nabla N_i \cdot \nabla N_j \, d\Omega}_{K_{j,i}} = \underbrace{\int_{\Gamma_N} \mathbf{n} \cdot \varepsilon_r \nabla \Phi N_j \, d\Omega + \int_{\Omega} \rho N_j \, d\Omega}_{l_j}, \tag{3.25}$$

which give the linear equation

$$K\Phi = l. \tag{3.26}$$

The Φ matrix consists of each element Φ_i in the corresponding assembly process that comes along with the respective local stiffness matrix $K_{j,i}$ and l_j placed eventually in the relative positions in the global stiffness matrix K and l.

$$K_{ij} = \int_{\Omega} \varepsilon_r \nabla N_i \cdot \nabla N_j \, \mathrm{d}\Omega \tag{3.27}$$

$$l_j = \int_{\Gamma_N} \mathbf{n} \cdot \varepsilon_r \nabla \Phi N_j \, \mathrm{d}\Omega + \int_{\Omega} \rho N_j \, \mathrm{d}\Omega \tag{3.28}$$

The shape, hp-order and type of refinement of each element may cause noticeable differences in the solution [63]. For the numerical results, I refine the finite element mesh sufficiently and use polynomials of sufficient degree such that the discretization error is negligible for the problems, as verified by testing the convergence of the numerical solutions. The solution is obtained for homogeneous and inhomogeneous boundary conditions. It is important to reconstruct the affine function space in the particular case of inhomogeneous boundary conditions to obtain the solution making use of lifting for the Dirichlet boundary value, $\Phi = \Phi_0 + \Phi_D$ [21, 98]. Φ_0 denotes the finite element solution with repect to the lifting ansatz. This gives the modified linear form and with it a new right hand side, $B(\Phi_0, \Psi) = \ell(\Psi) - B(\Phi_D, \Psi)$. Note that the solution is kinematically admissible, which is an important condition in the derivation of the simplification error estimate. The field is kinematically admissible when it becomes equal to the Dirichlet value on the boundary condition. The set of admissibility conditions require to be met for the construction of error bounds in section 4.2.3. In the case of kinematically admissible condition, it refers to the Dirichlet boundary condition.

3.2   Capacitor

Capacitors of any shape consist of two conductors which carry a charge (which is of course static for electrostatics); the charges are of equal value, but opposite signs

$$\Gamma_N$$

$$\Gamma_D$$

$$\Omega$$
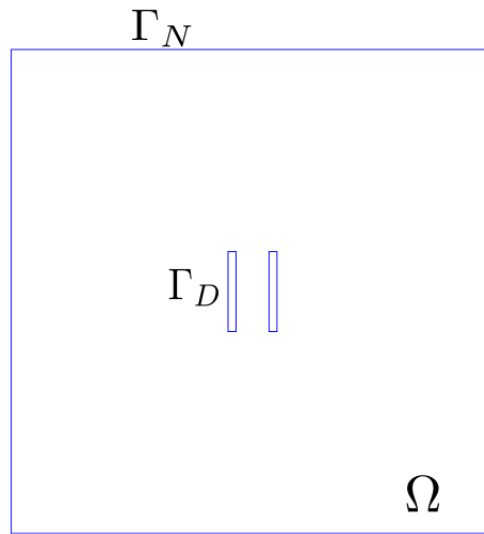
Figure 3.1: Configuration of a parallel plate capacitor inside a box

(e.g. see Fig. 3.1). Gauss' law describes how these charges create an electrostatic potential. Therefore, a capacitor stores the energy required to carry out the work for moving charges between the conductors. In other words, the amount of energy relates to the density of charges stored in the capacitor. This gives rise to the capacitance of a capacitor of any shape and configuration.

The capacitance C describes the amount of charge q that can be stored in a capacitor. The unit of capacitance is farad (F). A 1 farad capacitor, when charged with 1 coloumb has a potential difference of 1 volt. What plays a significant role in the determination of capacitance are the geometry of the conductors and the permittivity of the medium separating them. For parallel plate capacitors, the capacitance is relative to the applied voltage V. It is given by the ratio q/V, which depends only on the size and shape of the conductor [11]. For the example capacitor in Fig. 3.1, the conductor plates are rectangular.

The capacitor is the choice for numerical experiments in this dissertation because they are clear examples for electrostatic partial differential equation. Capacitors are also of high demand in industry and their lines of manufacturing are developing constantly. As high tech products are becoming more popular among consumers, capacitors are one of the primary element of electrical products. Efforts are being made to get the most capacitance for each capacitor model. However, some common faults occuring in the manufacturing processes such as an impurification of dielectric materials or dents in the capacitor geometries or conductor plates. These kinds of faults cause a distortion to the distribution of electrostatic potential or even sometimes malfunctioning of the models by deteriorating the capacitance. The interest is to find out the range of the errors these manufacturing mistakes make in the functionality of the capacitors and whether we are able to ignore these mistakes or not. These errors can be estimated from the simplification error proposed in this dissertation and put to the test in finite element simulations of capacitors.

The capacitor for the numerical simulation is opted to be formed by two parallel rectangular plates of area S and separation d. It is accepted that the conditions between two parallel plates provide a stable and uniform field between them. The potential difference between the plates is simply $V = Et$, and thus the capacitance is

$$C = q/V = \varepsilon_r S/d. \tag{3.29}$$

As it can be seen from the capacitance equation, the capacity value increases by increasing the relative permittivity, ε_r, of the material between the two conductors. Later, in the first numerical experiment, the space between the conductor plates is filled with an *insulator*, and the effect of dielectric materials on the flux and capacitance is studied. The insulator is made of dielectric materials which may contain contaminations, which makes it hard to determine a constant relative permittivity for its whole domain to calculate the capacitance. The interest is to estimate the error induced in the capacitance by eliminating the contamination for the simulations. Later on I also study the effect of simplifying the boundaries in the capacitor model, in particular removing

dents and extrusions.

The solution of finite element simulation is electrostatic potential which is taken for the computation of the modeling simplification error estimation. For electrostatics problems, two additional conditions should be met: (1) Inside a conductor the voltage is constant, hence E, D, and ρ vanish inside the conductor. (2) There are no charges inside a dielectric domain. This indicates that charges are allowed only on the boundary of conductors. The charges on the conductors are equally distributed, giving rise to a constant potential on the conductor boundaries. The total potential of work stored in the capacitor is

$$W = \int_0^Q V \, \mathrm{d}q = \int_0^Q \frac{q}{C} \, \mathrm{d}q = \frac{1}{2}\frac{Q^2}{C} = \frac{1}{2}CV^2 = \frac{1}{2}VQ \qquad (3.30)$$

where Q is the total charge of a capacitor, V the potential difference between capacitor plates, and C is the capacitance.

Chapter 4

Goal-Oriented Simplification Error Estimation

A goal-oriented approach is developed for estimating the simplification error. Initially it is explained the different possibilities for the feature locations and related defeaturing techniques. The solution of the boundary value problem for the simplified model is used to construct the bounds for the simplification error in terms of the difference between a quantity of interest for fully-featured and simplified model. The adopted method is an *a posteriori* goal-oriented simplification error estimation method [66, 68, 57] with a quantity of interest that is linear in the solution of the electrostatics problem. To bound the simplification error, constitutive relation error (CRE) techniques [44, 48, 46] are employed. These construct the bound in the energy norm. They will later on be applied to estimate the simplification error for specific feature types: internal features, negative and positive boundary features for electrostatics problems.

4.1 Defeaturing and Model Simplification

A feature is defined in general as a subset of a CAD model or even it could be a missing part related to the CAD model, typically associated with some semantic context. For example, holes, pockets, slots, etc. are referred to as features. For the purpose of this work, it is not considered specific semantic feature types, but only refer to them as
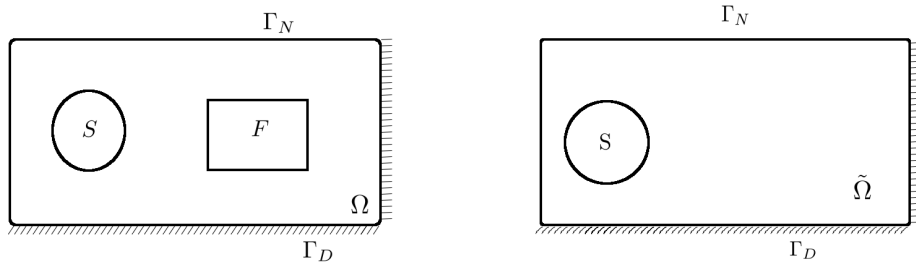
Figure 4.1: Model with internal feature, before and after defeaturing. F: **Domain of internal feature;** Γ_D: **Part of boundary with Dirichlet boundary conditions;** Γ_N: **Part of boundary with Neumann boundary conditions;** S: **Domain of quantity of interest;** Ω: **Domain of original model;** $\tilde{\Omega}$: **Domain of simplified model.**

subsets of the boundary value problem domain Ω and its boundary $\partial\Omega$. Note that the the feature domain F cannot overlap with the area of interest S used for calculating the quantity of interest. This leaves the feature with three general types:

- An *internal feature* F, lies inside the domain, i.e. $F \subset \Omega$. In this case, the feature can be in the form of a domain with material properties different from those of the surrounding domain. By simplifying the internal feature, the domain becomes more uniform as there are no discontinuities in the domain; see Fig. 4.1.

- A *negative boundary feature* F is an intrusion into the boundary of the geometry. In the original problem the negative feature can take the form of a void without material, and it changes the boundary conditions by removing it, $F \subset \partial\Omega$; see Fig. 4.2.

- A *positive feature* F is a protrusion on the boundary of the domain Ω. It can contain a material with properties different from the surrounding domain. If it is removed, the boundary conditions will change after removing the subset from the domain, $F \subset \partial\Omega$; see Fig. 4.3.
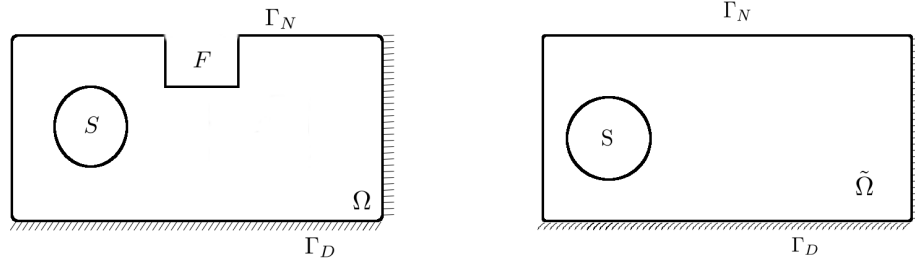
Figure 4.2: Model with negative boundary feature, before and after defeaturing.
F**: Domain of negative boundary feature;** Γ_D**: Part of boundary with Dirichlet boundary conditions;** Γ_N**: Part of boundary with Neumann boundary conditions;** S**: Domain of quantity of interest;** Ω**: Domain of original model;** $\tilde{\Omega}$**: Domain of simplified model. Note that the negative feature may occur on either the Neumann or Dirichlet part of the boundary.**

Positive and negative features generally make the boundary more complex, meaning meshing is more expensive. The internal feature can also disturb the uniform mesh inside Ω. To simplify the boundary, the feature can be either filled with the same material as the rest of the domain if it is a negative feature, or cut out of the boundary if it is a positive feature. An internal feature can be simplified by changing its material properties to match those of the surrounding domain. The internal feature can also lie adjacent to the boundaries, meaning the intersection between the feature boundary and the domain boundary is not empty. As long as the boundary of the domain Ω and the boundary conditions do not change, it can be handled like other internal features for simplification error estimation.

4.2 *A Posteriori* Error Estimation

The approach is based on a posteriori goal-oriented error estimation, which was devised for estimating and subsequently reducing the simulation error for a particular
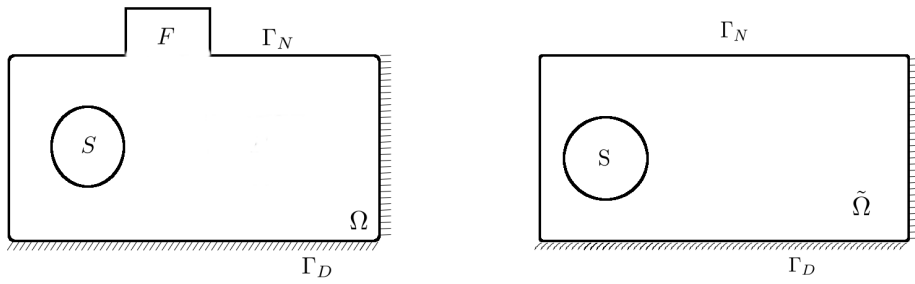
Figure 4.3: Model with positive boundary feature, before and after defeaturing.
F**: Domain of positive boundary feature;** Γ_D**: Part of boundary with Dirichlet boundary conditions;** Γ_N**: Part of boundary with Neumann boundary conditions;** S**: Domain of quantity of interest;** Ω**: Domain of original model;** $\tilde{\Omega}$**: Domain of simplified model. Note that the positive feature may occur on either the Neumann or Dirichlet part of the boundary.**

QoI [57, 66, 68]. Goal-oriented error estimation provides a framework for relating the residual error (the main source of computational error) to the estimated QoI value. When considering simplification, the residual error becomes the difference between the finite element solutions for the original and simplified problems. To bound the error measures in the energy norm, a strategy is utilized based on constitutive relation error (CRE) which leads to guaranteed bounds for the error in the QoI, providing a robust error estimator for the simplification error. The benefit of these bounds is to estimate the simplification error in a particular subset of the original model without expensive solving of the original problem.

4.2.1   Quantity of Interest (QoI) Error Estimation

Let Δ be a second order linear partial differential operator and f be a sufficiently smooth function over $\Omega \subset \mathbb{R}^d$. The smoothness of the function should be adequate so it meets the conditions for the discretized solver. I wish to solve the equation $\Delta u = f$

in Ω with homogeneous or inhomogeneous boundary conditions; it is called this the original problem. Similarly let $\Delta \tilde{u} = \tilde{f}$ be the simplified version of the problem over another domain $\tilde{\Omega}$. Note that $\tilde{\Omega}$ may consist of sub-domains with different material constants from those in Ω and may have additional areas or removed areas depending on the defeaturing operation. In order for the differences between various functionals and the integrals employed by the suggested estimation to be well defined, there is a need to define a *simplified domain* $\widehat{\Omega}$. This domain must be compatible with Ω. It is based on a feature area F and represents a modification of the defeatured domain $\tilde{\Omega}$ in order to make the computation of the bound possible. For the three different feature types it yields the following cases:

(i) $\widehat{\Omega} = \tilde{\Omega}$ for an **inner feature**: the defeatured domain $\tilde{\Omega}$ and the simplified domain $\widehat{\Omega}$ are the same (but the functionals defined on them differ, e.g., due to different material properties).

(ii) $\widehat{\Omega} = \tilde{\Omega} \setminus F$ for a **negative boundary feature**: the simplified domain $\widehat{\Omega}$ is constructed from the defeatured domain $\tilde{\Omega}$ by removing the negative feature area to enable the evaluation of the energy norm integrals.

(iii) $\widehat{\Omega} = \tilde{\Omega}$ for a **positive boundary feature**: this follows the same idea in the construction of $\widehat{\Omega}$ with the difference of adding the feature domain F, again to make the integrals over differences well defined.

In the following Φ and other notations are used to refer to the fields, functionals and sets relating to the original problem and its domain Ω; $\tilde{\Phi}$ and related notations using the symbols with "tilde" refer to the corresponding entities of the defeatured problem and its domain $\tilde{\Omega}$; and $\widehat{\Phi}$ and similar notations using symbols with "hats" refer to the corresponding entities of the simplified problem and its domain $\widehat{\Omega}$. $\tilde{\Phi}$ and $\widehat{\Phi}$ both represent the simplified problem, but $\widehat{\Phi}$ is defined on the same domain as Φ to enable the comparison for the error bound calculation. The construction of $\widehat{\Omega}$ also includes the addition of a new boundary condition between F and $\tilde{\Omega}$ that facilitates $\widehat{\Omega}$ to become

compatible to the original domain Ω. Details of their construction will be explained later when it is discussed the different feature types. For the general derivation of the error bounds it will be always referred to $\widehat{\Omega}$, $\widehat{\Phi}$ and related here.

Let $\widehat{\Phi}$ be the solution of the discretized boundary value problem Eqs. (3.18)–(3.16) over the simplified domain $\widehat{\Omega}$ and Φ be the solution of the original problem over Ω, for the a posteriori goal-oriented error estimation [2, 66]. Let Q be the QoI for the problem, which must be linear in the solution. It is often an integral involving the solution over a subset of Ω, e.g. $Q(\Phi) = \frac{1}{|S|} \int_S \ell(\Phi) \, d\Omega$ where $S \subset \Omega$ is the area of interest, and ℓ is the linear functional for the original problem. The goal is to approximate

$$Q(\Phi) - Q(\widehat{\Phi}) = Q(\Phi - \widehat{\Phi}) = Q(e) \text{ for } e = \Phi - \widehat{\Phi}. \tag{4.1}$$

The linearity of the QoI plays a significant role in the derivation of the simplification error estimate as it enables to compare the solutions for the simplified and original models according to a specific criterion. Note that in case the desired Q is not linear, it can be linearized in certain cases, introducing further errors. The following construction of the error bounds is considered under the assumption that the QoI is linear; approximation errors caused by any linearisation of the QoI are assumed to be sufficiently small compared to the simplification error. The computation of bounds for nonlinear QoIs is out of scope for this dissertation. Moreover, defeaturing must not affect the area of interest S, i.e. $F \cap S = \emptyset$. This is justified as any features overlapping with S are very likely to have a large effect on the QoI and so should not be considered for defeaturing.

The solution of the simplified primal and dual boundary value problems are used to construct an upper and lower bound for the error in the QoI as explained now. The general weak form of the electrostatic PDE, given in Eq. (3.23), yields the weak forms of the original and simplified electrostatic problems,

$$B(\Phi, \Psi) = \ell(\Psi), \quad \Phi \in U, \quad \forall \Psi \in V, \tag{4.2}$$

$$\widehat{B}(\widehat{\Phi}, \Psi) = \widehat{\ell}(\Psi), \quad \widehat{\Phi} \in U, \quad \forall \Psi \in V, \tag{4.3}$$

respectively, where U and V are suitable function spaces for the trial and test functions, $\ell : V \to \mathbb{R}$ and $\widehat{\ell} : V \to \mathbb{R}$ are linear forms, and bilinear forms $B : U \times V \to \mathbb{R}$ and $\widehat{B} : U \times V \to \mathbb{R}$ are symmetric and positive definite, which define an inner product on U and V. The *energy norm* is defined as

$$\|\Phi\|_{\varepsilon_r} := \sqrt{B(\Phi, \Phi)} = \sqrt{\int_\Omega \varepsilon_r \nabla \Phi \cdot \nabla \Psi \, \mathrm{d}\Omega}. \tag{4.4}$$

The test functions Ψ for the primal and dual model are taken from

$$V = \{\Psi \in H^1(\Omega) \mid \Psi = 0 \text{ on } \Gamma_D\}. \tag{4.5}$$

For the dual model, $\Psi = 0$ on Γ_N where Γ_N is the boundary of Ω with Neumann boundary conditions and Γ_D the boundary of Ω with Dirichlet boundary conditions such that $\Gamma_N \cap \Gamma_D = 0$, $\Gamma_D \cup \Gamma_N = \partial\Omega$. As B and $\widehat{B}$ are defined on the same domain, we can define the *residual*

$$R(\Psi) = B(\Phi - \widehat{\Phi}, \Psi) = B(e, \Psi), \quad \forall \Psi \in V. \tag{4.6}$$

The choice of QoI depends on the engineering problem to be studied, the physics and governing equation. Here the electric energy stored in the area of interest S is chosen. It is the sum of all potential work that can be done in this area by the electric field,

$$q(\Phi) = \int_S D \cdot E \, \mathrm{d}\Omega = \int_S \varepsilon_r \nabla^2 \Phi \, \mathrm{d}\Omega. \tag{4.7}$$

This is a quadratic function, so it must be linearized $q(\Phi)$ by replacing it with the first term of its Taylor expansion. Due to the linearity requirement this approximation is necessary, and it is assumed the nonlinear component is negligible. Of course this reduces the accuracy of the bound. The study of a nonlinear function for QoI is out of the scope of this dissertation. The primal solution Φ is replaced by Ψ (the test function) due to the equality of the function spaces for test and trial functions. Thus, the linearized QoI is

$$q'(\Psi) = \int_S \varepsilon_r \nabla \Phi \cdot \nabla \Psi \, \mathrm{d}\Omega. \tag{4.8}$$

However, Φ, the solution of the original primal model, is unknown and it should be substituted by the solution of the simplified model $\widehat{\Phi}$, giving the linearized QoI of the simplified model

$$Q(\Psi) = \int_S \varepsilon_r \nabla \widehat{\Phi} \cdot \nabla \Psi \, \mathrm{d}\Omega \approx q(\Phi). \tag{4.9}$$

With this approximation Eq. (4.1) can now be used to estimate the simplification error from the finite element solution of the simplified problem (solving the primal and dual simplified problems only). The benefit of this is to estimate the simplification error in a particular subset of the original model without expensive solving of the original problem.

4.2.2 Dual (adjoint) Model

Goal-oriented a posteriori error estimation requires to define an adjoint problem, which seeks a generalized Green's function associated with the QoI. It enables to localize the error to the area of interest associated with the QoI. As Δ is a self-adjoint operator, the original and simplified dual problems to the primal problems are introduced in Eqs. (4.2) and (4.3):

$$B(\Psi, \Phi^*) = Q(\Psi), \quad \Phi^* \in U, \quad \forall \Psi \in V, \tag{4.10}$$

$$\widehat{B}(\Psi, \widehat{\Phi}^*) = Q(\Psi), \quad \widehat{\Phi}^* \in U, \quad \forall \Psi \in V, \tag{4.11}$$

where the respective bilinear forms are the same as in the primal problems with suitable boundary conditions. The choice of linear forms on the right hand side is the QoI, Q. This is quite often the suitable choice for many goal-oriented a posteriori error estimation problems.

The role of the dual model in goal-oriented error estimation is to relate the error in the QoI to the source of the error via setting the right hand side to the QoI over the area of interest S. The dual boundary value problem should always be homogeneous, so it has a dual solution, Φ^*, for the non-zero right hand side for the governing equation. It is

derived similarly to Eq. (3.16), except for the fact that the right hand side is given by the QoI and Dirichlet and Neumann boundary conditions are set to zero:

$$
\begin{aligned}
D^* - \widehat{D}_s &= -\varepsilon_r \nabla \Phi^* && \text{in } S, \\
D^* &= -\varepsilon_r \nabla \Phi^* && \text{in } \Omega/S, \\
\nabla \cdot (-\varepsilon_r \nabla \Phi^*) &= Q(\Psi) && \text{in } \Omega, \\
\Phi^* &= 0 && \text{on } \Gamma_D, \\
\mathbf{n} \cdot (\varepsilon_r \nabla \Phi^*) &= 0 && \text{on } \Gamma_N,
\end{aligned}
\tag{4.12}
$$

where D^* is the dual electric displacement and $\widehat{D}_s$ is the flux of the solution of the simplified primal model in the region of interest S. Like in the primal case, the original and simplified models give dual solutions Φ^* and $\widehat{\Phi}^*$ respectively. For the dual problem, the Neumann and Dirichlet boundary conditions are equal to zero while the right hand side of the PDE is no longer zero. Note that the solution of the dual problem satisfies the kinematic admissibility condition on the Dirichlet boundary due to the homogeneous boundary condition. However, it is difficult to target the equilibrium constitutive equation to satisfy the static admissibility condition for the flux.

The bilinear form derived from the original dual problem for Eq. (4.12) is

$$
B(\Phi^*, \Psi) = \int_{\Omega} \varepsilon_r \nabla \Phi^* \cdot \nabla \Psi \, \mathrm{d}\Omega = -\int_S \widehat{D}_s \cdot \nabla \Psi \, \mathrm{d}\Omega = \int_S \varepsilon_r \nabla \widehat{\Phi}^* \cdot \nabla \Psi \, \mathrm{d}\Omega. \tag{4.13}
$$

The function space V of the test function Ψ is the same than for the primal model, $V = \{\Psi \in H^1 \mid \Psi = 0 \text{ on } \Gamma_D \text{ and } \Gamma_N\}$. Similarly, the bilinear form of the weak form for the simplified dual problem is

$$
B(\widehat{\Phi}^*, \Psi) = \int_{\widehat{\Omega}} \varepsilon_r \nabla \widehat{\Phi}^* \cdot \nabla \Psi \, \mathrm{d}\Omega = \int_S \varepsilon_r \nabla \widehat{\Phi}^* \cdot \nabla \Psi \, \mathrm{d}\Omega. \tag{4.14}
$$

As it has been chosen the same functional spaces for primal and dual models, $e = \Phi - \widehat{\Phi}$ and $e^* = \Phi^* - \widehat{\Phi}^*$ can be considered particular test functions. Hence, it calls

$$
Q(e) = B(e, \Phi^* - \widehat{\Phi}^*) + B(e, \widehat{\Phi}^*) = B(e, e^*) + R(\widehat{\Phi}^*). \tag{4.15}
$$

Here $R(\widehat{\Phi}^*)$ is the residual for the simplified dual problem, similar to Eq. (4.6). Hence,

$$Q(e) - R(\widehat{\Phi}^*) = B(e, e^*). \tag{4.16}$$

The Cauchy-Schwarz inequality then gives the bound,

$$|Q(e) - R(\widehat{\Phi}^*)| \leq \sqrt{B(e^*, e^*)}\sqrt{B(e, e)} = \| \bigtriangledown e^* \|_{\varepsilon_r} \| \bigtriangledown e \|_{\varepsilon_r} \leq \nu^* \nu, \tag{4.17}$$

where $\|.\|_{\varepsilon_r}$ denotes the energy norm of the error over the domain Ω, and ν and ν^* are global estimates for the norms of the error of primal and dual simplified solutions. The bounds in Eq. (4.17) are not computable as the energy norm of the exact error fields is not available. Instead, bounds, ν and ν^*, for these quantities are calculated. This is elaborated in Section 4.2.3 where the CRE is employed to bound the energy norms. Provided that the bounds are sufficiently sharp and can be computed with reasonable effort, they bound the simplification error in the energy norm from the finite element solution of the primal and dual simplified model. Hence, the construction of the bound components must always satisfy the principle of virtual work and the constitutive equation. Thus, the admissibility conditions must be satisfied.

4.2.3   Bounding Error in Constitutive Relation Error

I take advantage of the *constitutive relation error* (CRE) to bound the the energy norms ν and ν^* for primal and dual models. It only requires to employ the admissibility conditions. CRE provides a bound that is conceptually simple to understand, implement and control. It constructs a recovered electrostatic displacement that is statically admissible, or equilibrated. CRE applies the kinematic admissibility condition on the field which must be verified for the finite element model and its boundary conditions. The distance calculated in the energy norm between the recovered flux (electrostatic displacement) and simplified finite element electrostatic displacement is a bound for the simplification error.

The solution $\widehat{\Phi}$ of the simplified model is kinematically admissible, in other words the field $\widehat{\Phi}$ meets the Dirichlet boundary conditions. It will be sought in

$$U = \{\widehat{\Phi} \in H^1(\Omega) \mid \widehat{\Phi} = \Phi_D \text{ on } \Gamma_D\}. \tag{4.18}$$

The flux, $\widehat{D}$, must be statically admissible, i.e.

$$\int_{\widehat{\Omega}} \widehat{D} \cdot \nabla\Psi \, \mathrm{d}\Omega = \int_{\widehat{\Omega}} \rho\Psi \, \mathrm{d}\Omega + \int_{\Gamma_N} \mathbf{n} \cdot (\varepsilon_r \nabla\Phi)\Psi \, \mathrm{d}\Gamma, \tag{4.19}$$

which means that the constitutive equation must be always satisfied.

The relative permittivity ε_r in Eq. (3.18) is assumed to be a piecewise constant and scalar, naturally giving rise to a partition of the domain into areas of constant permittivity. For the original model, this means in the simplest case,

$$\varepsilon_r(x) = \begin{cases} \epsilon_R & \text{for } x \in \Omega \setminus F, \\[2mm] \epsilon_F & \text{for } x \in F \end{cases} \tag{4.20}$$

where $\epsilon_R, \epsilon_F \in \mathbb{R}_0^+$. The error bounds are derived for these constants, enabling us to construct the CRE error bounds for all concerned feature types. This is used later in the computation and evaluation of the error bounds for different feature types.

To make Eq. (4.17) practically useful, the error energy norm bounds ν^2 and $(\nu^*)^2$ for $B(e, e)$ and $B(e^*, e^*)$ respectively must be found (in addition to the residual error $R(\widehat{\Phi}^*)$). For $B(\Phi - \widehat{\Phi}, \Phi - \widehat{\Phi}) = B(e, e) \leq \nu^2$, noting that $\widehat{D} = -\widehat{\varepsilon}_R \nabla\widehat{\Phi}$, let

$$\begin{aligned} \nu^2 &= \|\widehat{D} + \epsilon_R \nabla\widehat{\Phi}\|^2_{\epsilon_R^{-1}} + \|\widehat{D} + \epsilon_F \nabla\widehat{\Phi}\|^2_{\epsilon_F^{-1}} \\ &= \int_{\widehat{\Omega}/F} (\widehat{D} + \epsilon_R \nabla\widehat{\Phi})\epsilon_R^{-1}(\widehat{D} + \epsilon_R \nabla\widehat{\Phi}) \, \mathrm{d}\Omega \\ &\quad + \int_F (\widehat{D} + \epsilon_F \nabla\widehat{\Phi})\epsilon_F^{-1}(\widehat{D} + \epsilon_F \nabla\widehat{\Phi}) \, \mathrm{d}\Omega. \end{aligned} \tag{4.21}$$

This definition requires to calculate two norms, one over the feature domain F with relative permittivity ϵ_F, and the other one covering the error measure in the energy norm for the remainder, $\Omega \setminus F$, with relative permittivity ϵ_R. Note that in order to eliminate additional numerical approximations and return the exact value of the integration in the

feature domain, the mesh is kept in the feature area unchanged from the original to the simplified model. This assumption enables to avoid more approximation in the proof of the tightness of bounds for numerical simulations. The integration can instead be approximated for the geometry belonging to the feature area in the simplified domain with the approach of [93]. This assumption is not considerable in the manufacturing problem when the contamination (specific material property) is removed from the feature domain as are not concerned with meshing rather considering different material properties. The numerical experimentations are illustrative examples to prove the bound theory with all assumptions made. It is chosen to compute the energy norms in terms of electric displacement, which is a linear function related to the electrostatic potential. The electric displacement of the simplified problem, $\widehat{D}$, follows the same formula as the electric displacement D defined in Eq. (3.9) with a different finite element solution for the simplified model in the domain $\widehat{\Omega}$. $\widehat{D}$ helps to construct the flux to distinguish the feature domain F from other parts of the original domain Ω for the computation of the error bounds.

By subtracting $0 = D + \varepsilon_r \nabla \Phi$ in the definition of ν^2 it yields

$$
\begin{aligned}
\nu^2 &= \|\widehat{D} - D - \epsilon_R \nabla \Phi + \epsilon_R \nabla \widehat{\Phi}\|_{\epsilon_R^{-1}}^2 + \|\widehat{D} - D - \epsilon_F \nabla \Phi + \epsilon_F \nabla \widehat{\Phi}\|_{\epsilon_F^{-1}}^2 \\
&= \|(\widehat{D} - D) + \epsilon_R (\nabla \widehat{\Phi} - \nabla \Phi)\|_{\epsilon_R^{-1}}^2 + \|(\widehat{D} - D) + \epsilon_F (\nabla \widehat{\Phi} - \nabla \Phi)\|_{\epsilon_F^{-1}}^2 \\
&= \int_{\widehat{\Omega}/F} (\widehat{D} - D) \epsilon_R^{-1} (\widehat{D} - D) \, \mathrm{d}\Omega + \int_F (\widehat{D} - D) \epsilon_F^{-1} (\widehat{D} - D) \, \mathrm{d}\Omega \\
&\quad + \int_{\widehat{\Omega}/F} (\nabla \widehat{\Phi} - \nabla \Phi) \epsilon_R^{-1} (\nabla \widehat{\Phi} - \nabla \Phi) \, \mathrm{d}\Omega \\
&\quad + \int_F (\nabla \widehat{\Phi} - \nabla \Phi) \epsilon_F^{-1} (\nabla \widehat{\Phi} - \nabla \Phi) \, \mathrm{d}\Omega + 2 \underbrace{\int_{\widehat{\Omega}} (\widehat{D} - D)(\nabla \widehat{\Phi} - \nabla \Phi) \, \mathrm{d}\Omega}_{=0} \, .
\end{aligned}
$$
(4.22)

Eq. (3.18) follows from Eq. (3.9) by taking the gradient under the divergence free condition. In combination with the weak form in Eq. (3.21), it returns for D and $\widehat{D}$

respectively:

$$\int_{\Omega} D \cdot \nabla \Psi \, \mathrm{d}\Omega = \ell(\Psi), \tag{4.23}$$

$$\int_{\widehat{\Omega}} \widehat{D} \cdot \nabla \Psi \, \mathrm{d}\Omega = \ell(\Psi), \tag{4.24}$$

where Ψ is substituted for the test function in the bilinear and linear forms. Subtracting Eq. (4.23) from Eq. (4.24) gives

$$\int_{\widehat{\Omega}} (\widehat{D} - D) \cdot \nabla \Psi \, \mathrm{d}\Omega = \ell(\Psi) - \ell(\Psi) = 0. \tag{4.25}$$

This means the divergence free electric displacements D and $\widehat{D}$ satisfy the static admissibility condition. $\widehat{\Phi}$ is kinematically admissible because it is equal to Φ on Γ_D. The divergence free condition for D gives Eq. (4.25), leading to an orthogonality condition between statically and kinematically admissible variables by setting $\Psi = \Phi - \widehat{\Phi}$:

$$\int_{\widehat{\Omega}} (D - \widehat{D}) \cdot (\nabla \Phi - \nabla \widehat{\Phi}) \, \mathrm{d}\Omega = 0 \ \text{ as } \Phi - \widehat{\Phi} = 0 \text{ on } \Gamma_D. \tag{4.26}$$

So the last term of the expanded Eq. (4.22) is indeed zero and Eq. (4.22) yields

$$\nu^2 = \underbrace{\|\widehat{D} - D\|^2_{\epsilon_R^{-1}} + \|\widehat{D} - D\|^2_{\epsilon_F^{-1}}}_{\geq 0} + \|\nabla \widehat{\Phi} - \nabla \Phi\|^2_{\varepsilon_r}, \tag{4.27}$$

which implies

$$\|e\|^2_{\varepsilon_r} = B(e, e) = \|\nabla \Phi - \nabla \widehat{\Phi}\|^2_{\varepsilon_r} \leq \nu^2. \tag{4.28}$$

Note that the closeness of the bound depends on the value of $\|\widehat{D} - D\|^2_{\epsilon_R^{-1}} + \|\widehat{D} - D\|^2_{\epsilon_F^{-1}}$. If the simplification only has a minor effect on the finite element solution, ν is nearly equal to the energy norm and hence provides a good estimate. If the effect is larger, it is overestimated more strongly.

Similarly, the CRE ν^* is derived from the simplified dual model solution $\widehat{\Phi}^*$:

$$\begin{aligned}(\nu^*)^2 &= \|\widehat{D}^* + \epsilon_R \nabla \widehat{\Phi}^*\|^2_{\epsilon_R^{-1}} + \|\widehat{D}^* + \epsilon_F \nabla \widehat{\Phi}^*\|^2_{\epsilon_F^{-1}} \\ &= \int_{\widehat{\Omega}/F} (\widehat{D}^* + \epsilon_R \nabla \widehat{\Phi}^*) \epsilon_R^{-1} (\widehat{D}^* + \epsilon_R \nabla \widehat{\Phi}^*) \, \mathrm{d}\Omega \\ &\quad + \int_F (\widehat{D}^* + \epsilon_F \nabla \widehat{\Phi}^*) \epsilon_F^{-1} (\widehat{D}^* + \epsilon_F \nabla \widehat{\Phi}^*) \, \mathrm{d}\Omega,\end{aligned} \tag{4.29}$$

where $\widehat{D}^*$ is the flux of the solution of the simplified dual model. As before, similar to Eq. (4.28), the energy norm of the error, this time of the dual problem, is bounded,

$$\|e^*\|_{\varepsilon_r}^2 = B(e^*, e^*) = \|\nabla\Phi^* - \nabla\widehat{\Phi}^*\|_{\varepsilon_r}^2 \leq (\nu^*)^2. \tag{4.30}$$

After the computation of the distance error norms for primal and dual models, ν and ν^*, the CRE error norm constructions are linked to the QoI by the computation of the residual. Eq. (4.6) gives

$$\begin{aligned} R(\widehat{\Phi}^*) &= B(e, \widehat{\Phi}^*) = B(\Phi, \widehat{\Phi}^*) - B(\widehat{\Phi}, \widehat{\Phi}^*) = \ell(\widehat{\Phi}^*) - B(\widehat{\Phi}, \widehat{\Phi}^*) \\ &= \int_{\Gamma_N} (\mathbf{n} \cdot (\varepsilon_r \nabla\Phi))\widehat{\Phi}^* \, d\Gamma + \int_\Omega \rho\widehat{\Phi}^* \, d\Omega - \int_\Omega \varepsilon_r \nabla\widehat{\Phi} \cdot \nabla\widehat{\Phi}^* \, d\Omega. \end{aligned} \tag{4.31}$$

This is the residual error of original versus simplified model. This residual equation is valid if and only if the bilinear form B is self-adjoint, positive-definite and symmetric. These are the basic requirements that every bilinear form should hold. With these assumptions the error bounds are constructed.

Finally, $R(\widehat{\Phi}^*)$, ν and ν^* in combination give the general form of the upper and lower bounds for the simplification error,

$$R(\widehat{\Phi}^*) - \nu\nu^* \leq Q(e) \leq R(\widehat{\Phi}^*) + \nu\nu^*, \tag{4.32}$$

$$Q(\widehat{\Phi}) + R(\widehat{\Phi}^*) - \nu\nu^* \leq Q(\Phi) \leq Q(\widehat{\Phi}) + R(\widehat{\Phi}^*) + \nu\nu^*. \tag{4.33}$$

In the following sections these error bounds are applied to various numerical problems for different feature types. The error bounds must be adapted to internal, negative and positive features for electrostatics problems and it is shown their performance in practical settings.

Chapter 5

Simplification Error Estimation for Different Feature Types of a Capacitor

In this chapter the simplification error analysis is applied to various feature types of a parallel plate capacitor model. It is first shown how to adapt the theory and bounds to internal features and then how to deal with bounding the modeling simplification error for the features on the boundaries.

5.1 Quantity of Interest (QoI) for Electrostatics Problems

The electric energy stored in the area of interest S is used as QoI. It is the sum of all potential work that can be done in this area by the electric field,

$$q(\Phi) = \int_S D \cdot E \, \mathrm{d}\Omega = \int_S \varepsilon_r \nabla^2 \Phi \, \mathrm{d}\Omega. \tag{5.1}$$

This is a quadratic function, so it must be linearized $q(\Phi)$ by replacing it with the first term of its Taylor expansion. Due to the linearity requirement this approximation is necessary and it is assumed the nonlinear component is negligible. The proof for viability of this approximation is out of scope for this work and strongly depends on the estimation problem. Nevertheless, a simple justification that the linearization is generally suitable for electrostatic PDEs can be given based on the properties of the

field. The electrostatic is linear and divergence free, and therefore, the elimination of higher order terms in Taylor expansion will typically have a small effect on the PDE solution in the comparison to the linear term. Of course this means our bound is only valid for the linearization. A rigorous mathematical proof for the linearization of nonlinear QoI is fully elaborated in the work of [13]. The primal solution Φ is replaced by Ψ (the test function) due to the equality of the function spaces for test and trial functions. Thus, the linearized QoI is

$$Q(\Phi) = \int_S \varepsilon_r \nabla \Phi \cdot \nabla \Psi \, \mathrm{d}\Omega. \tag{5.2}$$

As the aim is to estimate the simplification error according to Eq. (4.1), Eq. (4.33) is now used to obtain this estimate from the finite element solution of the simplified model (solving the primal and dual simplified problems only).

5.2 Internal Feature Simplification Error Estimation

Eq. (4.33) with Eqs. (4.21), (4.29) and (4.31) provide the bound for the simplification error of the QoI given by Eq. (4.9). The residual Eq. (4.31) must be adapted to the specific linear form $\ell(\Psi)$ of the governing Eqs. (3.18) and (3.16). In this problem, Fig. 5.1, there is no charge density in the domain $\tilde{\Omega}$, $\rho = 0$, so $\ell(\Psi) = 0$ in Eqs. (4.31) and (3.23). The relative permittivity in F is constant, i.e. $\varepsilon_r(x) = \epsilon_F$ for $x \in F$, but different from the surrounding permittivity in $\Omega \setminus F$. For the simplified problem, $\tilde{\varepsilon}_r$ is constant on the whole domain $\tilde{\Omega}$. Because the Dirichlet boundary condition is not zero, it needs to be shifted to the right hand side via lifting the boundary condition. This results in the lifted weak form,

$$B(\Phi_0, \Psi) = \int_\Omega \varepsilon_r \nabla \Phi_0 \nabla \Psi \, d\Omega = -\int_{\Gamma_D} \varepsilon_r \nabla \Phi_D \nabla \Psi \, d\Omega = -B(\Phi_D, \Psi), \tag{5.3}$$

where Φ_0 is the solution. The simplified problem given by $\tilde{B}$, $\tilde{\ell}$ has a constant relative permittivity $\tilde{\varepsilon}_r \equiv \epsilon_R$ and $\Phi, \tilde{\Phi} \in H^1(\Omega)$ and $\Psi, \tilde{\Psi} \in H_0^1(\Omega)$.
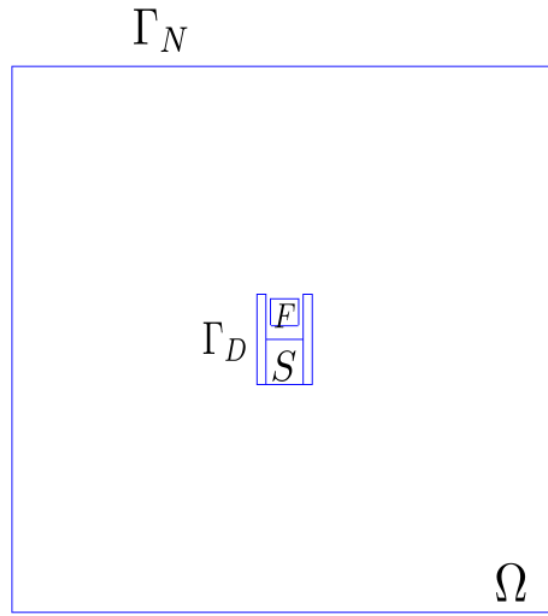
Figure 5.1: Parallel plate capacitor model for electrostatics simulation with area of interest S and feature F in domain Ω with Dirichlet boundary Γ_D and Neumann boundary Γ_N.

To bound $Q(e)$, the solution $\tilde{\Phi}$ of the simplified problem is substituted into Eq. (4.21) to determine ν and for $\tilde{D}$ it yields to

$$\int_{\tilde{\Omega}} (\nabla \cdot \tilde{D}) \Psi \, \mathrm{d}\Omega = 0. \tag{5.4}$$

By noting that the Neumann boundary condition is zero and the test function Ψ vanishes on Γ_D, integrating the above by parts gives

$$\underbrace{\int_{\tilde{\Omega}} \nabla(\tilde{D}\Psi) \, \mathrm{d}\Omega}_{=\int_{\partial\tilde{\Omega}} (\mathbf{n} \cdot \tilde{D}) \Psi \, \mathrm{d}\Gamma = 0} - \int_{\tilde{\Omega}} \tilde{D} \nabla\Psi \, \mathrm{d}\Omega = 0. \tag{5.5}$$

Using Eq. (4.25), subtracting the fluxes of the original and simplified models, means the static admissibility condition is fulfilled:

$$\int_{\hat{\Omega}} (D - \tilde{D}) \cdot \nabla\Psi \, \mathrm{d}\Omega = 0 \quad \forall \Psi \in H_0^1. \tag{5.6}$$

Eq. (4.27) now ν is computed from the solution of the simplified model:

$$
\begin{aligned}
\nu^2 &= \parallel \tilde{D} + \epsilon_R \nabla \tilde{\Phi} \parallel_{\epsilon_R^{-1}}^2 + \parallel \tilde{D} + \epsilon_F \nabla \tilde{\Phi} \parallel_{\epsilon_F^{-1}}^2 \\
&= \underbrace{\int_{\tilde{\Omega}/F} (\tilde{D} + \epsilon_R \nabla \tilde{\Phi}) \epsilon_R^{-1} (\tilde{D} + \epsilon_R \nabla \tilde{\Phi}) \, \mathrm{d}\Omega}_{=0} \\
&\quad + \int_F (\tilde{D} + \epsilon_F \nabla \tilde{\Phi}) \epsilon_F^{-1} (\tilde{D} + \epsilon_F \nabla \tilde{\Phi}) \, \mathrm{d}\Omega.
\end{aligned}
\tag{5.7}
$$

ν depends on the integration over two separate domains, F and $\Omega \setminus F$. The term for $\Omega \setminus F$ is zero due to the construction of $\tilde{D}$: field and flux only differ by the material property of the domain that they belong to. Technically, $\tilde{D}$ ensures that the solution of the simplified model, $\tilde{\Phi}$, and flux in $\Omega \setminus F$ are identical with the recovered flux and field in ν. Therefore, it is only needed to consider the feature domain F with the different relative permittivities. Hence, from Eqs. (4.22) and (4.27),

$$
\begin{aligned}
\nu^2 &= \int_F (\epsilon_R \nabla \tilde{\Phi} - \epsilon_F \nabla \tilde{\Phi}) \epsilon_F^{-1} (\epsilon_R \nabla \tilde{\Phi} - \epsilon_F \nabla \tilde{\Phi}) \, \mathrm{d}\Omega \\
&= \int_F \frac{(\epsilon_R - \epsilon_F)^2}{\epsilon_F} \nabla \tilde{\Phi} \nabla \tilde{\Phi} \, \mathrm{d}\Omega.
\end{aligned}
\tag{5.8}
$$

Similarly, ν^* is calculated via Eq. (4.29) for the dual model, except that it now depends on the solution $\tilde{\Phi}^*$ of the dual simplified model:

$$
\begin{aligned}
(\nu^*)^2 &= \parallel \tilde{D} + \epsilon_R \nabla \tilde{\Phi}^* \parallel_{\epsilon_R^{-1}}^2 + \parallel \tilde{D} + \epsilon_F \nabla \tilde{\Phi}^* \parallel_{\epsilon_F^{-1}}^2 \\
&= \underbrace{\int_{\widehat{\Omega}/F} (\widehat{D} + \epsilon_R \nabla \widehat{\Phi}^*) \epsilon_R^{-1} (\widehat{D} + \epsilon_R \nabla \widehat{\Phi}^*) \, \mathrm{d}\Omega}_{=0} \\
&\quad + \int_F (\widehat{D} + \epsilon_F \nabla \widehat{\Phi}^*) \epsilon_F^{-1} (\widehat{D} + \epsilon_F \nabla \widehat{\Phi}^*) \, \mathrm{d}\Omega.
\end{aligned}
\tag{5.9}
$$

The integration over $\widehat{\Omega} \setminus F$ is zero because the flux remains the same between the two models in this domain, and the remaining equation construction follows the same steps that lead to Eq. (5.8), so:

$$
(\nu^*)^2 = \int_F \frac{(\epsilon_R - \epsilon_F)^2}{\epsilon_F} \nabla \tilde{\Phi}^* \nabla \tilde{\Phi}^* \, \mathrm{d}\Omega.
\tag{5.10}
$$

As for the capacitor, $\ell(\Psi) = 0$, the residual error $R(\tilde{\Phi}^*)$ given by Eq. (4.31) simplifies to $R(\tilde{\Phi}^*) = -B(\tilde{\Phi}, \tilde{\Phi}^*)$. As $\tilde{\Phi}^*$ vanishes on the Dirichlet boundary, it ends up to:

$$
\begin{aligned}
B(\tilde{\Phi}^*, \tilde{\Phi}) &= \int_F \epsilon_F \nabla\tilde{\Phi}\nabla\tilde{\Phi}^* \mathrm{d}\Omega + \int_{\tilde{\Omega}/F} \epsilon_R \nabla\tilde{\Phi}\nabla\tilde{\Phi}^* \mathrm{d}\Omega \\
&= \int_F (\epsilon_F + \epsilon_R - \epsilon_R)\nabla\tilde{\Phi}\nabla\tilde{\Phi}^* \mathrm{d}\Omega + \int_{\tilde{\Omega}/F} \epsilon_R \nabla\tilde{\Phi}\nabla\tilde{\Phi}^* \mathrm{d}\Omega \\
&= \underbrace{\int_{\tilde{\Omega}} \epsilon_R \nabla\tilde{\Phi}\nabla\tilde{\Phi}^* \mathrm{d}\Omega}_{=0} + \int_F (\epsilon_F - \epsilon_R)\nabla\tilde{\Phi}\nabla\tilde{\Phi}^* \mathrm{d}\Omega. \quad (5.11)
\end{aligned}
$$

The first term in the last line above is zero because the bilinear form of the simplified model satisfies the general boundary value problem and its boundary conditions. Hence,

$$
R(\tilde{\Phi}^*) = \int_F (\epsilon_R - \epsilon_F)\nabla\tilde{\Phi}\nabla\tilde{\Phi}^* \mathrm{d}\Omega. \tag{5.12}
$$

With this, all components help to calculate the bounds for Eq. (4.33). The integrals are evaluated on the same mesh before and after defeaturing. This is to avoid additional numerical errors from approximating the integrals over the various domains by keeping the meshing in the feature domain consistent between original and simplified models.

5.3 Simplification Error Estimation for Boundary Features of a Capacitor

In this section, it is considered features on the boundary of the domain Ω. Positive features are distinguished, that are subtracted from Ω by the simplification, and negative features, that are added to Ω by the simplification. As in all these cases the simplification implies a change of the domain, it must be suitably expanded or reduced the defeatured domains $\tilde{\Omega}$ such that it remain compatible over the original domain, i.e. construct $\hat{\Omega} = \Omega$, which was not necessary for internal features. It further requires to distinguish between features located on the Neumann and Dirichlet boundaries. It

is first considered the case of Neumann boundary conditions for positive and negative features and then also discuss the Dirichlet boundary condition case.

5.3.1   Positive Features with Neumann Boundary Conditions

It is first considered the case of a positive feature being simplified on the Neumann boundary. The domain Ω is partitioned into a feature area F and the remaining defeatured domain $\tilde{\Omega}$ such that $\Omega = \tilde{\Omega} \cup F$. Here defeaturing removes the positive feature by setting the electric permittivity in the feature domain, $\varepsilon_r|_F \equiv 0$, which means the simplified domain $\widehat{\Omega}$ remains equal to Ω, but with different relative permittivity.

Note, in order to calculate the error bound, it is required to set up a new boundary value problem on the feature domain and to calculate ν, ν^* and $R(\widehat{\Phi}^*)$ from the finite element solution of the model. For this it is especially defined a Dirichlet boundary condition on the interface between $\tilde{\Omega}$ and F, determined by the solution of the defeatured model. So an electrostatic potential $\tilde{\Phi}$ is assigned to the interface boundary. This is obtained from the finite element solution of the defeatured model at the interface between $\tilde{\Omega}$ and F, yielding the following problem:

$$
\begin{aligned}
\nabla \cdot (\epsilon_F \nabla \Phi_F) &= 0 \quad \text{in } F, \\
\Phi_F &= \tilde{\Phi} \quad \text{on } \partial F \cap \partial \tilde{\Omega}, \\
\mathbf{n} \cdot (\epsilon_F \nabla \Phi_F) &= 0 \quad \text{on } \partial F \cap \Gamma_N,
\end{aligned}
\tag{5.13}
$$

where Φ_F is the solution for this *feature problem*; also see Fig. 5.2. At the interface between the feature and defeatured domain, the fluxes should be equal in length, but point in opposite directions across the interface for the defeatured problem and the feature problem. This means the electrostatic potential remains continuous across the interface for the defeatured problem solution and the feature problem solution which gives an overall simplified solution on $\widehat{\Omega}$. Nevertheless, it is assumed $D_F = \epsilon_F \nabla \Phi_F$ is null in F, which enables to calculate the bounds from the simplified model. The rationale for this assumption lies in the construction of the bound based on a posteriori
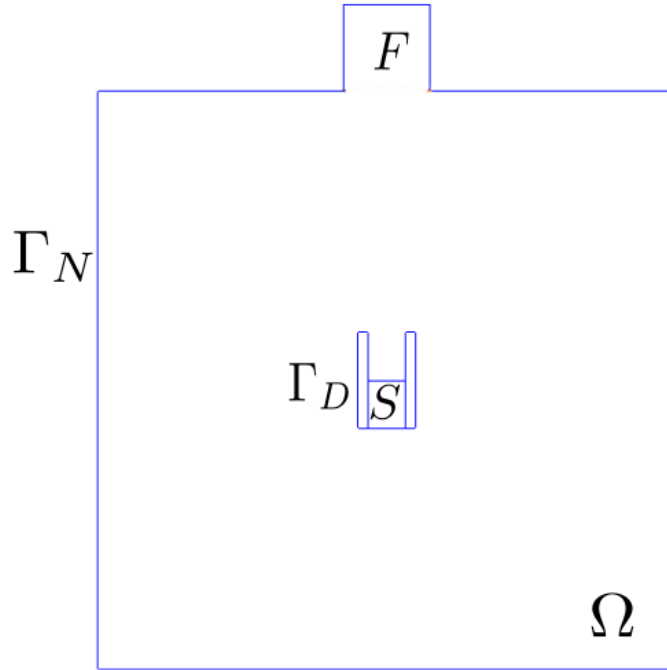
Figure 5.2: Capacitor model with positive feature F on the Neumann boundary Γ_N and domain $\Omega = \tilde{\Omega} \cup F$.

error estimation from the solution of the simplified model and the CRE. To calculate the terms needed for the bound, it is required a field over the feature domain and this approach represents effectively the removal of an area from the problem domain. Consequently, ν, ν^* and $R(\widehat{\Phi}^*)$ are computed over the feature domain, where the simplification error bounds are calculated based on the assumption of eliminating the flux. As explained in Section 4, the calculation of the error bounds follows Eq. (4.33). The calculation of the terms for this feature type is described below.

ν is related to the CRE Eq. (4.22) based on the separation of the energy norm computation for F from $\tilde{\Omega}$. The solution $\widehat{\Phi}$ is used over the simplified domain $\widehat{\Omega}$ which combines the solution of the defeatured problem and the feature problem. Based on

Eqs. (4.22) and (4.21), with the specific relation between F and $\tilde{\Omega}$ in this case, it calls

$$
\begin{aligned}
\nu^2 =& \|\widehat{D} - \epsilon_R \nabla \widehat{\Phi}\|^2_{\epsilon_R{}^{-1}} + \|\widehat{D} - \epsilon_F \nabla \widehat{\Phi}\|^2_{\epsilon_F{}^{-1}} \\
=& \int_{\tilde{\Omega}} (\widehat{D} - D)\epsilon_R{}^{-1}(\widehat{D} - D) \, \mathrm{d}\Omega \\
& + \int_F (\widehat{D} - D)\epsilon_F{}^{-1}(\widehat{D} - D) \, \mathrm{d}\Omega + \int_{\tilde{\Omega}} (\nabla \widehat{\Phi} - \nabla\Phi)\epsilon_R{}^{-1}(\nabla\widehat{\Phi} - \nabla\Phi) \, \mathrm{d}\Omega \\
& + \int_F (\nabla\widehat{\Phi} - \nabla\Phi)\epsilon_F{}^{-1}(\nabla\widehat{\Phi} - \nabla\Phi) \, \mathrm{d}\Omega - 2 \underbrace{\int_\Omega (\widehat{D} - D)(\nabla\widehat{\Phi} - \nabla\Phi) \, \mathrm{d}\Omega}_{=0}.
\end{aligned}
$$

$$(5.14)$$

The last term above is zero because of the orthogonality between static and kinematic admissibility conditions. For this to be fulfilled, the following must be true for the flux, though:

$$
\int_\Omega \widehat{D} \cdot \nabla\Phi \, \mathrm{d}\Omega = 0 \; \forall \Phi \in H^1_0(\Omega). \tag{5.15}
$$

This condition is fulfilled, if $\widehat{D}$ is divergence free and the Neumann boundary condition is fulfilled for the original model. The construction of $\widehat{D}$ means $\widehat{D}|_F \equiv 0$, so it is sufficient that $\widehat{D}|_{\tilde{\Omega}} \equiv \tilde{D}|_{\tilde{\Omega}}$. Hence, it returns overall

$$
\begin{aligned}
\nu^2 &= \int_F (\widehat{D} - \epsilon_F \nabla\widehat{\Phi})\epsilon_F{}^{-1}(\widehat{D} - \epsilon_F \nabla\widehat{\Phi}) \, \mathrm{d}\Omega + \int_{\tilde{\Omega}} (\widehat{D} - \epsilon_R \nabla\widehat{\Phi})\epsilon_R{}^{-1}(\widehat{D} - \epsilon_R \nabla\widehat{\Phi}) \, \mathrm{d}\Omega \\
&= \int_F \epsilon_F \nabla\widehat{\Phi}\nabla\widehat{\Phi} \, \mathrm{d}\Omega + \int_{\tilde{\Omega}} \underbrace{(\widehat{D} - \epsilon_R \nabla\widehat{\Phi})\epsilon_R{}^{-1}(\widehat{D} - \epsilon_R \nabla\widehat{\Phi})}_{=0} \, \mathrm{d}\Omega.
\end{aligned}
$$

$$(5.16)$$

ν^* follows the methodology for ν. For the dual problem, $\widehat{\Phi}$ is replaced by $\widehat{\Phi}^*$ in Eq. (4.12):

$$
\begin{aligned}
D^* - \tilde{D}_s &= -\varepsilon\nabla\widehat{\Phi}^* &&\text{in } S, \\
D^* &= -\varepsilon\nabla\widehat{\Phi}^* &&\text{in } \widehat{\Omega} \setminus S, \\
\nabla \cdot (-\varepsilon\nabla\widehat{\Phi}^*) &= Q(\Psi) &&\text{in } \widehat{\Omega}, \\
\widehat{\Phi}^* &= 0 &&\text{on } \Gamma_D, \\
\mathbf{n} \cdot (\varepsilon\nabla\widehat{\Phi}^*) &= 0 &&\text{on } \Gamma_N.
\end{aligned}
$$

$$(5.17)$$

The above dual model has the solution $\widehat{\Phi}^*$ from which ν^* is calculated as

$$
(\nu^*)^2 = \int_F \epsilon_F \nabla\widehat{\Phi}^* \nabla\widehat{\Phi}^* \, \mathrm{d}\Omega. \tag{5.18}
$$

The residual given by Eq. (4.6) must be adapted to the positive feature due to the separate feature problem in Eq. (5.13). It becomes

$$R(\widehat{\Phi}^*) = -\int_\Omega \varepsilon_r \nabla\widehat{\Phi}\nabla\widehat{\Phi}^* \, \mathrm{d}\Omega = -\int_{\tilde{\Omega}} \epsilon_R \nabla\tilde{\Phi}\nabla\widehat{\Phi}^* \, \mathrm{d}\Omega - \int_F \epsilon_F \nabla\widehat{\Phi}\nabla\widehat{\Phi}^* \, \mathrm{d}\Omega \quad (5.19)$$

as $\widehat{\Phi} \equiv \tilde{\Phi}$ in $\tilde{\Omega}$. The bilinear form for the defeatured problem subjected to the prescribed boundary conditions vanishes on $\tilde{\Omega}$, $\int_{\tilde{\Omega}} \epsilon_R \nabla\tilde{\Phi}\nabla\widehat{\Phi}^* \, \mathrm{d}\Omega = 0$. Hence,

$$R(\widehat{\Phi}^*) = -\int_F \epsilon_F \nabla\widehat{\Phi}\nabla\widehat{\Phi}^* \, \mathrm{d}\Omega. \quad (5.20)$$

5.3.2 Negative Features with Neumann Boundary Conditions

In the case of a negative feature on the Neumann boundary, the simplified domain $\tilde{\Omega} = \Omega \cup F$ contains F, while F is not a subset of Ω. It must be extended ε_r to $\widehat{\Omega} = \tilde{\Omega} = \Omega \cup F$ and set the relative permittivity ϵ_F of the feature domain close to 0; see Fig. 5.3. With this, it is made the negative feature part of the domain $\widehat{\Omega}$ and set a permittivity that indicates the original void. This is related to using a penalty factor for the relative permittivity in the feature area,

$$\widehat{\varepsilon}_r(x) = \alpha \cdot \epsilon_R \text{ for } x \in F, \quad (5.21)$$

where it has been chosen $\alpha = 10^{-5}$ for the numerical results and ϵ_R is the permittivity of the surrounding area.

The same approach is followed as Section 4 to bound the simplification error with Eq. (4.33). The only difference is that it is set a small relative permittivity on F. According to Eqs. (4.22) and (4.21) this gives:

$$\begin{aligned}
\nu^2 &= \|\widehat{D} - \epsilon_R\nabla\widehat{\Phi}\|^2_{\epsilon_R^{-1}} + \|\widehat{D} - \alpha\epsilon_R\nabla\widehat{\Phi}\|^2_{\epsilon_F^{-1}} \\
&= \int_{\tilde{\Omega}} (\widehat{D} - \epsilon_R\nabla\widehat{\Phi})\epsilon_R^{-1}(\widehat{D} - \epsilon_R\nabla\widehat{\Phi}) \, \mathrm{d}\Omega \\
&\quad + \int_F (\widehat{D} - \alpha\epsilon_R\nabla\widehat{\Phi})(\alpha\epsilon_R)^{-1}(\widehat{D} - \alpha\epsilon_R\nabla\widehat{\Phi}) \, \mathrm{d}\Omega \\
&= \int_F \alpha\epsilon_R\nabla\widehat{\Phi}\nabla\widehat{\Phi} \, \mathrm{d}\Omega,
\end{aligned} \quad (5.22)$$
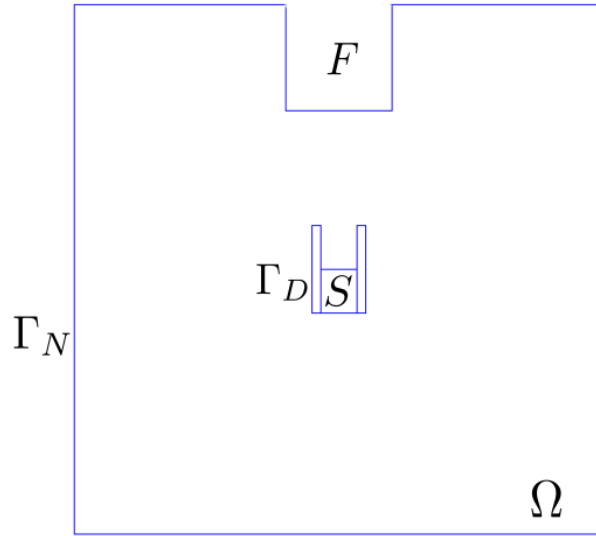
Figure 5.3: The geometry configuration of the capacitor model with the negative feature F on the Neumann boundary Γ_N.

and similarly, based on Eq. (4.29),

$$(\nu^*)^2 = \int_F \alpha\epsilon_R \nabla\widehat{\Phi}^* \nabla\widehat{\Phi}^* \, \mathrm{d}\Omega. \tag{5.23}$$

The residual in Eq. (4.31) is derived similarly to Eq. (5.19), yielding

$$R(\widehat{\Phi}^*) = -\int_F \alpha\epsilon_R \nabla\widehat{\Phi} \nabla\widehat{\Phi}^* \, \mathrm{d}\Omega. \tag{5.24}$$

5.3.3   Features with Dirichlet Boundary Condition

In the capacitor model, the conductors are described by Dirichlet boundary conditions. So for simplifying features on the capacitor plates, this work has to consider these cases. Again, the feature can be positive or negative, but as the boundary condition type is different, the general equations in Chapter 4 must be adapted differently from the Neumann boundary cases. Here it is dealt with the simplification error by removing only the negative feature on the Dirichlet boundary; the positive feature case follows

the same approach for the simplification of a positive Neumann feature. The condition requires assigning zero to the electrostatic potential in the feature domain. The feature is placed on the Dirichlet boundary; therefore the potential in the whole domain equals the potential value of the Dirichlet condition. This ensures the continuity of the field at the boundary of feature and simplified capacitor domain. In either case, the following main conditions must be fulfilled:

1. The electrostatic potential (field) must be continuous across the interface between the feature and the rest of the domain.

2. The electrostatic displacement (flux) must be divergence free.

For an example of a negative feature on a capactior plate see Fig. 5.4 (left). The position of the feature is the dominant factor determining the simplification error. As for the negative feature on the Neumann boundary, the negative feature must be added to the domain and with this actually mesh the feature area. Again, a penalty factor is introduced as in Eq. 5.21 to extend the relative permittivity to the feature domain. The assumption for calculating the energy norms on the feature domain is that all vertices in the feature domain are assigned with the Dirichlet electrostatic potential values Φ_D, i.e. the whole feature domain contains a uniform electrostatic potentia such that $\Phi_F = \Phi_D$. The simplified domain is $\widehat{\Omega} = \tilde{\Omega} \setminus F = \Omega$. The breakup of the simplified domain ensures all integrals are well defined.

The electric displacement (flux) should be divergence free in the feature and equal to the flux in the capacitor domain at the interface, though in opposite directions. So overall it returns

$$\widehat{\Omega} = \tilde{\Omega} \setminus F, \tag{5.25}$$

$$\widehat{\Phi} = \Phi_D \qquad \text{in } F, \tag{5.26}$$

$$\widehat{D} = \tilde{D} \qquad \text{in } \partial F \cap \Gamma_D. \tag{5.27}$$

The derivation of the error bounds is otherwise equivalent to the negative boundary feature case in Section 5.3.2, following Eq. (4.33). The new assumption and conditions
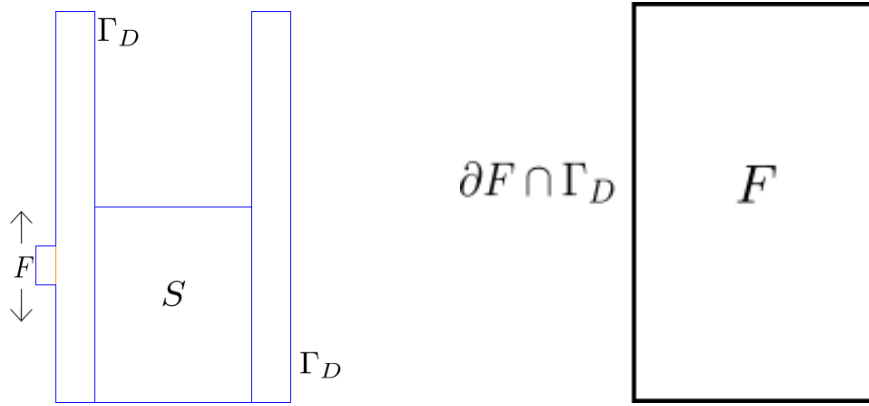
Figure 5.4: Left: a negative feature on a capacitor plate for a parallel plate capacitor (Dirichlet Boundary; with its direction of the motion, relevant later for Experiment 3). For clarity only the capacitor plates without the surrounding domain are shown. Right: the standalone negative feature and its associated boundary conditions.

change the results of the integrations, still restricted to the feature domain F. The relative permittivity ϵ_F of the feature domain is adjusted to simulate the closest conditions with respect to the original model ($\widehat{\varepsilon}_r(x) = \alpha \cdot \epsilon_R$ for $x \in F$). Fig. 5.4(right) depicts the boundary of the feature and its intersection with the Dirichlet boundary condition.

Hence, from Eqs. (4.22) and (4.21) and it yields

$$
\begin{aligned}
\nu^2 &= \|\widehat{D} - \epsilon_R \nabla\widehat{\Phi}\|^2_{\epsilon_R{}^{-1}} + \|\widehat{D} - \alpha\epsilon_R\nabla\widehat{\Phi}\|^2_{\epsilon_F{}^{-1}} \\
&= \int_{\tilde{\Omega}} (\widehat{D} - \epsilon_R\nabla\widehat{\Phi})\epsilon_R{}^{-1}(\widehat{D} - \epsilon_R\nabla\widehat{\Phi})\ \mathrm{d}\Omega \\
&\quad + \int_F (\widehat{D} - \alpha\epsilon_R\nabla\widehat{\Phi})(\alpha\epsilon_R)^{-1}(\widehat{D} - \alpha\epsilon_R\nabla\widehat{\Phi})\ \mathrm{d}\Omega \\
&= \int_F \alpha\epsilon_R\nabla\widehat{\Phi}\nabla\widehat{\Phi}\ \mathrm{d}\Omega,
\end{aligned}
\tag{5.28}
$$

under consideration of the field being equal to the Dirichlet value in the feature domain. The calculation of ν^* requires the solution $\widehat{\Phi}^*$ of the simplified dual model (5.17),

$$
(\nu^*)^2 = \int_F \alpha\epsilon_R\nabla\widehat{\Phi}^*\nabla\widehat{\Phi}^*\ \mathrm{d}\Omega.
\tag{5.29}
$$

The residual is given by Eq. (4.6) adapted to the negative feature on the Dirichlet boundary and its new conditions. It gives the same result as Eq. (5.24), except that the

Modelling simplification error bound
$Q(\widehat{\Phi}) + R(\widehat{\Phi}^*) - \nu\nu^* \leq Q(\Phi) \leq Q(\widehat{\Phi}) + R(\widehat{\Phi}^*) + \nu\nu^*$

Feature Type	Bounds Components
Internal Feature	$\nu^2 = \int_F \dfrac{(\epsilon_R - \epsilon_F)^2}{\epsilon_F} \nabla\tilde{\Phi}\nabla\tilde{\Phi} \ \mathrm{d}\Omega$ $(\nu^*)^2 = \int_F \dfrac{(\epsilon_R - \epsilon_F)^2}{\epsilon_F} \nabla\tilde{\Phi}^*\nabla\tilde{\Phi}^* \ \mathrm{d}\Omega$ $R(\widehat{\Phi}^*) = \int_F (\epsilon_R - \epsilon_F)\nabla\tilde{\Phi}\nabla\tilde{\Phi}^*\mathrm{d}\Omega$
Negative Feature (Neumann boundary)	$\nu^2 = \int_F \alpha\epsilon_R \nabla\widehat{\Phi}\nabla\widehat{\Phi} \ \mathrm{d}\Omega$ $(\nu^*)^2 = \int_F \alpha\epsilon_R \nabla\widehat{\Phi}^*\nabla\widehat{\Phi}^* \ \mathrm{d}\Omega$ $R(\widehat{\Phi}^*) = -\int_F \alpha\epsilon_R \nabla\widehat{\Phi}\nabla\widehat{\Phi}^* \ \mathrm{d}\Omega$
Negative Feature (Dirichlet boundary)	$\nu^2 = \int_F \alpha\epsilon_R \nabla\widehat{\Phi}\nabla\widehat{\Phi} \ \mathrm{d}\Omega$ $(\nu^*)^2 = \int_F \alpha\epsilon_R \nabla\widehat{\Phi}^*\nabla\widehat{\Phi}^* \ \mathrm{d}\Omega$ $R(\widehat{\Phi}^*) = -\int_F \alpha\epsilon_R \nabla\widehat{\Phi}\nabla\widehat{\Phi}^* \ \mathrm{d}\Omega$
Positive Feature (Neumann boundary)	$\nu^2 = \int_F \epsilon_F \nabla\widehat{\Phi}\nabla\widehat{\Phi} \ \mathrm{d}\Omega$ $(\nu^*)^2 = \int_F \epsilon_F \nabla\widehat{\Phi}^*\nabla\widehat{\Phi}^* \ \mathrm{d}\Omega$ $R(\widehat{\Phi}^*) = -\int_F \epsilon_F \nabla\widehat{\Phi}\nabla\widehat{\Phi}^* \ \mathrm{d}\Omega$

Table 5.1: The components of the modeling simplification error bound for different feature types.

field in the feature domain is replaced with the Dirichlet boundary value, $\Phi_F = \Phi_D$:

$$R(\widehat{\Phi}^*) = -\int_F \alpha\epsilon_R \nabla\widehat{\Phi}\nabla\widehat{\Phi}^* \ \mathrm{d}\Omega. \tag{5.30}$$

The final bound equations for the simplification modeling error are shown in the Table. 5.1 for each considered defeaturing case.

Chapter 6

Numerical Experiments to Estimate the Simplification Error for Different Feature Types of a Capacitor

In this chapter it is presented numerical results to demonstrate and evaluate the quality and tightness of the simplification error bounds for a quantity of interest. The effectivity index is first introduced. Then it is discussed internal and boundary feature simplification cases for the capacitor to demonstrate the tightness properties of the bound numerically. To further show the practical relevance of the bounds, it is shown the speedup that can be achieved when simplifying the model and estimating the simplification error for positive features on the Neumann boundary. In another practical example it is shown how the bounds can be used to estimate the effect of a manufacturing defect in a glass capacitor towards estimating uncertainties arising from manufacturing errors.

6.1 Numerical Results for Feature Simplifications

Numerical results are given to illustrate the effectivity of the bounds using a simple capacitor model and simplifying different features. [44, 48] have already proven that the CRE bounds are guaranteed and tight bounds can be achieved for elasticity problems, but no numerical results have been provided for electrostatic problems and the

simplification error. The CRE method is applied in goal-oriented error estimation, which consequently makes the error bounds in the energy norm more accurate by localising the error computation to a sub-set of Ω. The error estimation is implemented as C++ plugin for the finite element solver NGSsolve [77] within the Netgen mesh generator [76] to calculate and render the solutions. It is shown how well our method is able to estimate the simplification error. For this the accuracy of the error is studied using an effectivity index comparing the bounds with the actual simplification error:

$$\mathfrak{I} = \frac{|Q(\Phi)| + |U - L|}{|Q(\Phi)|} = 1 + \frac{|U - L|}{|Q(\Phi)|}, \tag{6.1}$$

where U is the upper and L the lower bound. The closer the effectivity index is to one, the better the bounds are. The effectivity index indicates the ratio between the exact value and its bounds. When it equals to one, there is no error in the approximated value with respect to the exact value. Values larger than one indicate the ratio of deviation between the bounds and the exact value.

As the QoI is calculated to represent electrostatic energy by approximating Eq. (4.7) using relative permittivities on centimeter scales, all QoI values in this Chapter are in $c * \text{Joules}$ with $c = 2 * 10^4/\epsilon_0 \approx 2.26 * 10^{15}$ and ϵ_0 is the (dimensionless) electric constant (permittivity of vacuum).

Numerical results are first provided for simplification of a capacitor model with internal features. The simplification error in terms of the stored electrostatic energy in the area of interest S is investigated for two different simplifications: (i) removal of a fixed feature area with different dielectric material properties, different from the surrounding domain; (ii) removal of a feature that grows in size with fixed dielectric constant, different from the surrounding domain. In both cases the feature is removed by setting the dielectric constant inside its area to the dielectric constant of the surrounding area. The numerical results are then provided for negative and positive feature on the Neumann and Dirichlet boundaries. The error bounds can be calculated from this according to Eq. (4.33). Note that for the calculation of the integrals is assumed the meshes between simplified and original modal remain compatible, which specifically means that they

are compatible across the boundary between F and $\tilde{\Omega}$, to minimise effects from numerical approximations of the integrals. Together these results demonstrate the tightness properties of the bounds numerically.

A further section is devoted to demonstrate the speedup in analysis time it can be achieved via simplifying positive features on the Neumann boundary. As practical example toward estimating the effect of manufacturing uncerrtainties, the results are then presented for a parallel plate capacitor with pyrex dielectric and a sodium contamination.

6.2 Experiment 1: Internal Features with Different Material Properties

This experiment is used to demonstrate the viability of the method and tightness of error bounds, rather than being a practically useful problem. It is considered the example of a parallel plate capacitor shown in Fig. 5.1 where the feature F and the area of interest S lie between the two capacitor plates with Dirichlet boundary conditions on Γ_D and Neumann boundary conditions on the far boundary Γ_N surrounding the capacitor. F is an internal feature, i.e. $F \subset \Omega$ with $F \cap d\Omega = \emptyset$ where the simplification consists of a change of the material properties in F, usually setting it to the material properties of the surrounding domain. This means the boundary conditions of the original versus simplified model remain intact and $\Omega = \tilde{\Omega} = \widehat{\Omega}$. The governing equations for the finite element simulation are given by Eq. (3.18). Each conductor plate has width of 0.001m and length of 0.01m, at a potential of 220 volt with opposite signs. The outer box of model capacitor used in our experiments has a shape of square, its length is 0.06m.

Note that, as the capacitor plates are conductors, the potential is constant (but different) on each plate boundary and it is set to $+220V$ and $-220V$ respectively. This produces a symmetric distribution of the field inside the capacitor. For the Neumann boundary,

the far boundary has zero charge density, $\rho|_{\Gamma_N} = 0$, and the normal component of the electric displacement on the boundary is zero, $\mathbf{n} \cdot (\varepsilon_r \nabla \Phi) = 0$. Using the linear QoI approximating the electrostatic energy in the capacitor can be utilised to show the effect that a dielectric material has on the capacitance. An upper and lower bound is provided for the difference between the QoI of the original and simplified model.

The experiment is run for several dielectric materials with different relative permittivities. Here it is chosen the relative permittivities from $\epsilon_F = 3\epsilon_R$ to $13\epsilon_R$, where ϵ_R is the relative permittivity of air (1.0005). The purpose of this experiment is to test the method to bound the simplification error for different permittivity values in the feature area where the simplification replaces the material of the feature area with the relative permittivity of the surrounding domain. It is demonstrated how the QoI can be estimated by bounding the simplification error.

Fig. 6.1 shows the distribution of the electric potential before and after defeaturing. It can be seen by a simple comparison of the two solutions that the dielectric material in the feature domain pushes away the electric field. Removing of dielectric material makes changes in the stored value of electric energy in the area of interest, S. In order to estimate the simplification error the dual problem represented by Eq. (4.12) must be solved. Its solution is shown in Fig. 6.2.

Fig. 6.3 shows the upper and lower energy norm bounds compared to the exact QoI value. The larger the relative permittivity value, the less tight the estimation of the QoI is. It can even become negative, which is meaningless. So the simplification error estimation becomes less useful when the influence of the suppressed feature on the QoI becomes stronger. While this is not ideal, the overestimation of the error can still prevent us from making an inappropriate simplification. In some instances, the distance between upper and lower bounds is significantly larger than the error in the QoI, resulting in a very large overestimation of modeling simplification error. This occurs when removing dielectric materials thjt have a huge impact on the physical property of the capacitor. Therefore, it can be concluded from those examples that

whenever the role and effect of dielectric material supersedes a thershold specific to the investigated capacitor, the changes caused by simplifying the material cannot be ignored in the analysis. Another factor worthwhile to mention is the distance between the location of dielectric material to the domain of interest S for the computation of the QoI. When the dielectric material gets close to the domain of interest S, the suppression of the dielectric domain has a large effect on the field in S and so on the QoI.
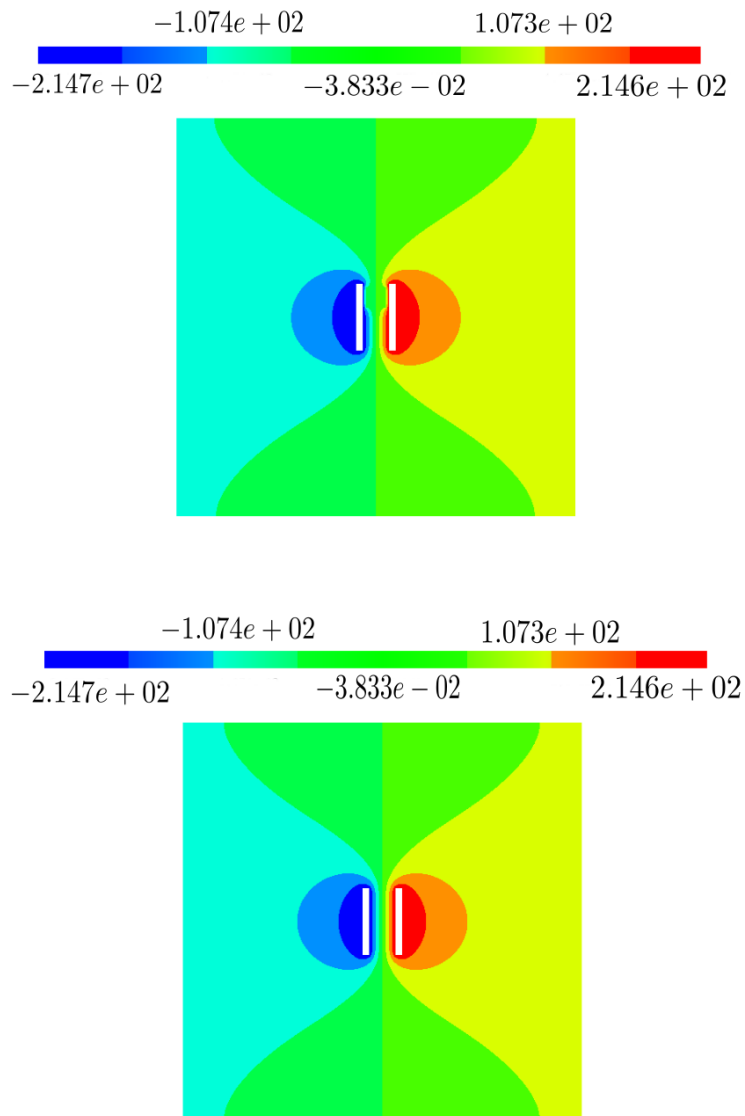
Figure 6.1: **Top: Finite element solution for the original capacitor model for Experiment 1. The feature affects the distribution of the electrostatic potential nearby. Bottom: Finite element solution for the simplified capacitor model. The field is not distorted in the feature domain and its surrounding area.**
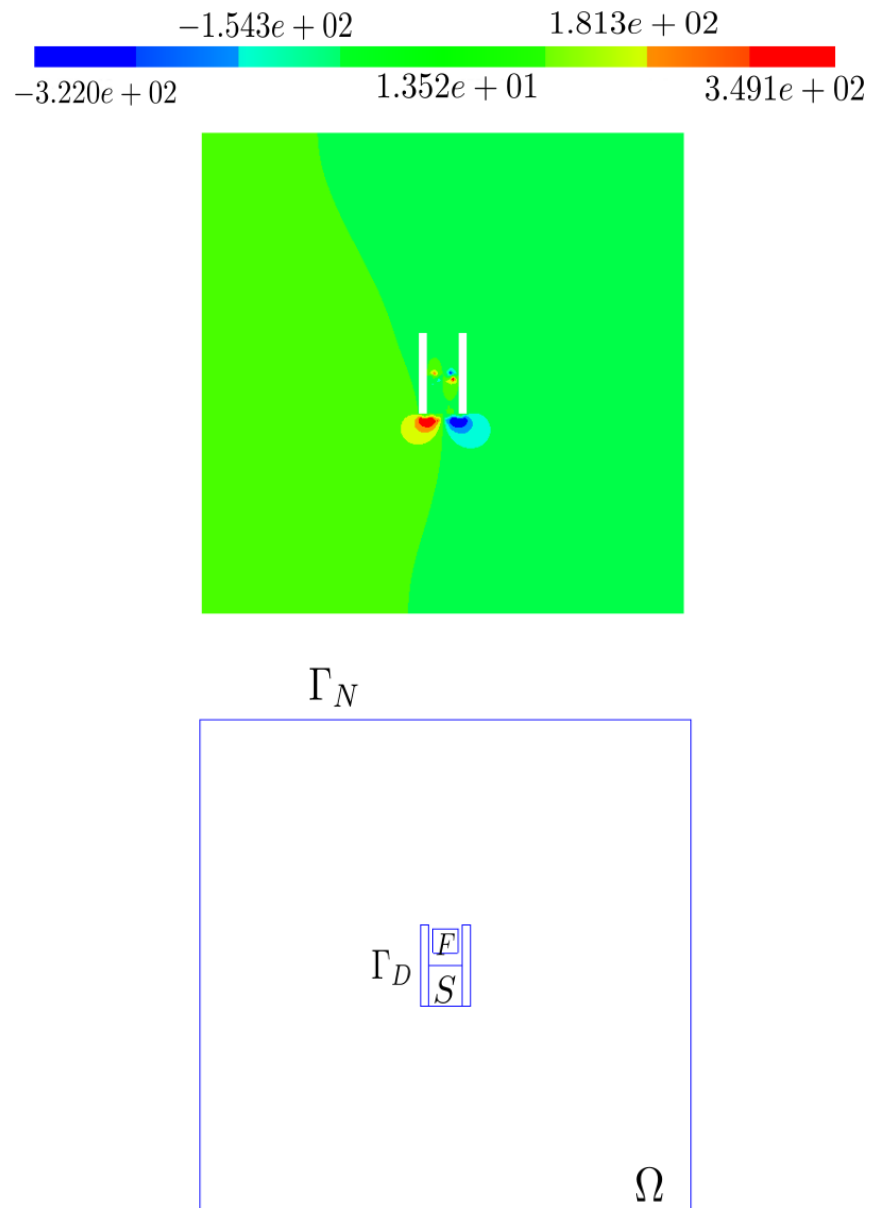
Figure 6.2: The finite element solution of the dual model for Experiment 1 (top) and a representation of the geometry of the model (bottom).
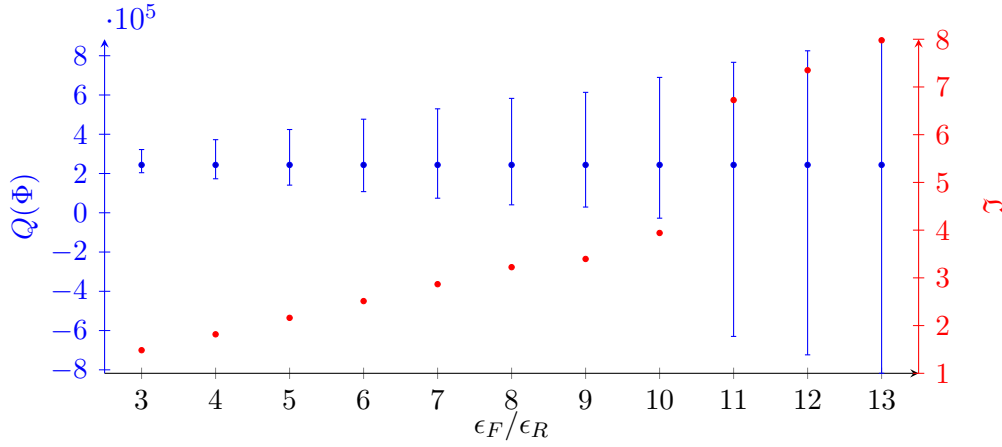
ϵ_F/ϵ_R	$\mathfrak{I}$	$Q(\tilde{\Phi})$	$Q(\Phi)$	U	L
3	1.48420	243706	243729	322114	204100
4	1.81723	243706	243748	372406	173208
5	2.16218	243706	243769	424159	140855
6	2.51326	243706	243789	476665	107749
7	2.86756	243706	243807	529569	74246
8	3.22398	243706	243825	582738	40477
9	3.39615	243706	243841	613448	29168
10	3.94073	243706	243856	689565	-27549
11	6.72556	243706	243869	766425	-629861
12	7.35087	243706	243882	825171	-723693
13	7.97833	243706	243893	884180	-817786

Figure 6.3: Bounds of the simplification error for the QoI for different dielectric values in an internal feature for Experiment 1. The table lists the relative permittivity ϵ_F in the feature area, the effectivity index $\mathfrak{I}$, the exact QoI $Q(\Phi)$ and approximate QoI $Q(\tilde{\Phi})$, and the upper U and lower L bounds..

6.3   Experiment 2: Internal Features of Different Sizes

The aim of this experiment is to test the performance of the simplification error for different feature geometries, in particular for a feature increasing in size, under constant relative permittivity in the feature. The capacitor and its components are kept the same as among all of the experiments. Each conductor plate has width of 0.001m and length of 0.01m, at a potential of 220 volt with opposite signs. The outer box of model capacitor used in our experiments has a shape of square, its length is 0.06m. In this case, the internal feature F lies outside the conductor plates, while S, the capacitor geometry and boundary conditions are the same as in Experiment 1; see Fig. 6.4. The location of the dielectric material is at the top of conductors between the outside boundary of capacitor. The center of dielectric material(F) sits on the vertical axis. The relative permittivity of the dielectric material inside F is set to $5\epsilon_R$ for all simulations, where ϵ_R is the relative permittivity of air (1.0005). The capacitor is filled with air. Defeaturing replaces the relative permittivity in the feature domain F with the relative permittivity of the material surrounding it. The size of F is increased from a width and height of 0.5cm, 0.4cm to a width and height of 1.6cm, 1.5cm in 0.1cm steps added to both at the same time. The center of F is kept fixed at its location. It has also been added two larger rectangular feature areas. In each step, the simplification error is bounded as before.

As the feature increases in size, it repels the electrostatic potential more, which changes the energy in the area of interest. The simulation analysis result for the largest feature is shown in Fig. 6.5.

The upper and lower bounds for the QoI with their effectivity indices are shown in the Fig. 6.6. The effectivity indices in this case are close to one, indicating that the error can be well characterised. As the feature F moves further away from the area of interest S, the influence it has on the QoI is reduced. The error bounds become less tight as the size of the feature expands, though. It indicates that whenever the feature is farther away from the domain of interest S, the effect of the simplification on the
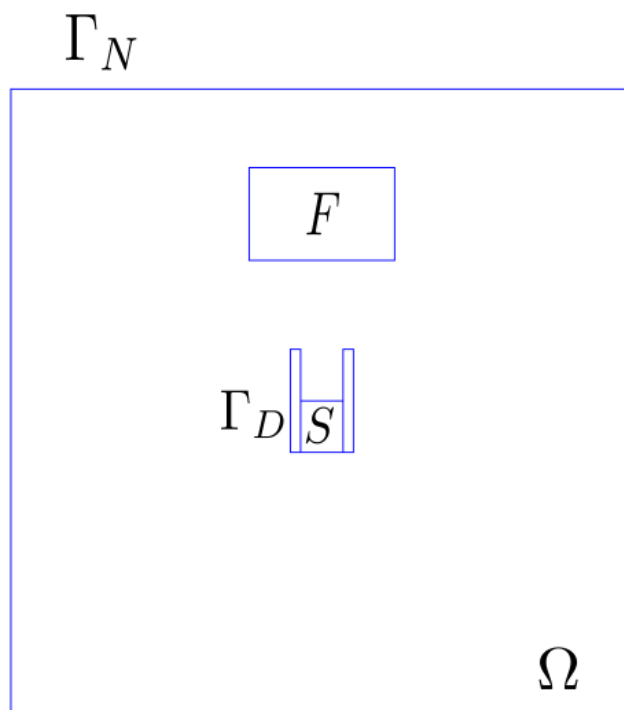
Figure 6.4: Capacitor with an internal feature of variable size used in Experiment 2.

quantity of interest is small and can be estimated well. It can be concluded that the bounds are accurate enough for all the defeaturing experiments and estimate the QoIs well.
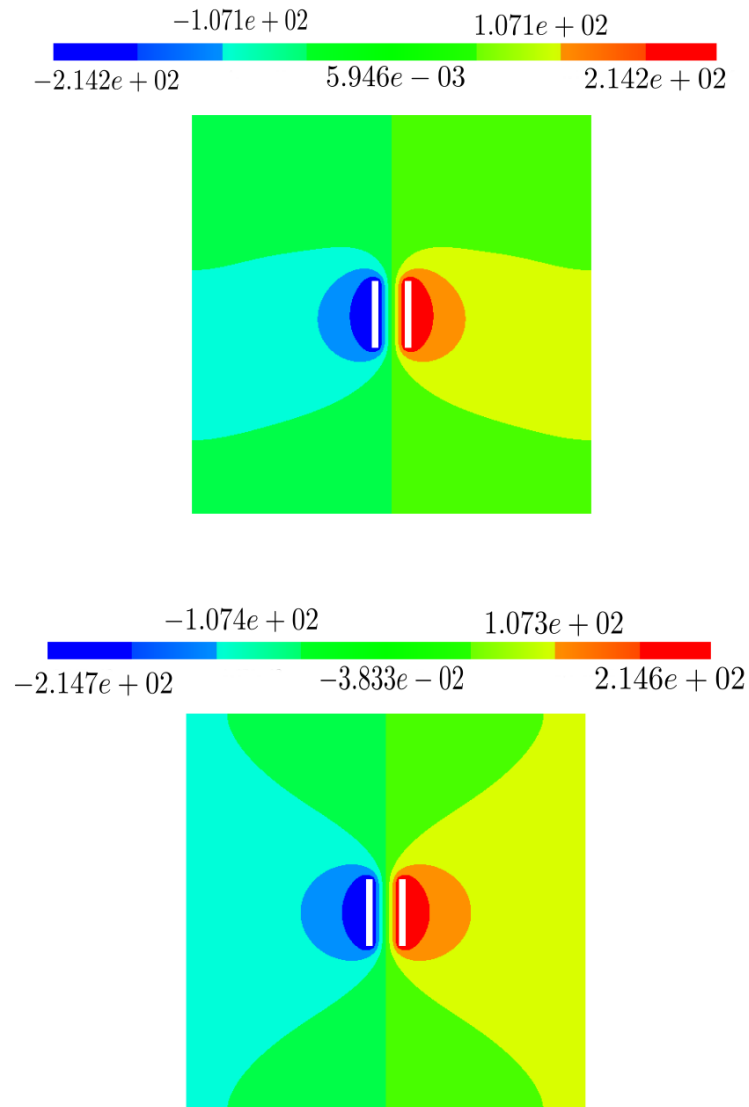
Figure 6.5: Top: The finite element solution for the field Φ for the original capacitor model for Experiment 2. Bottom: The finite element solution of the simplified capacitor model.
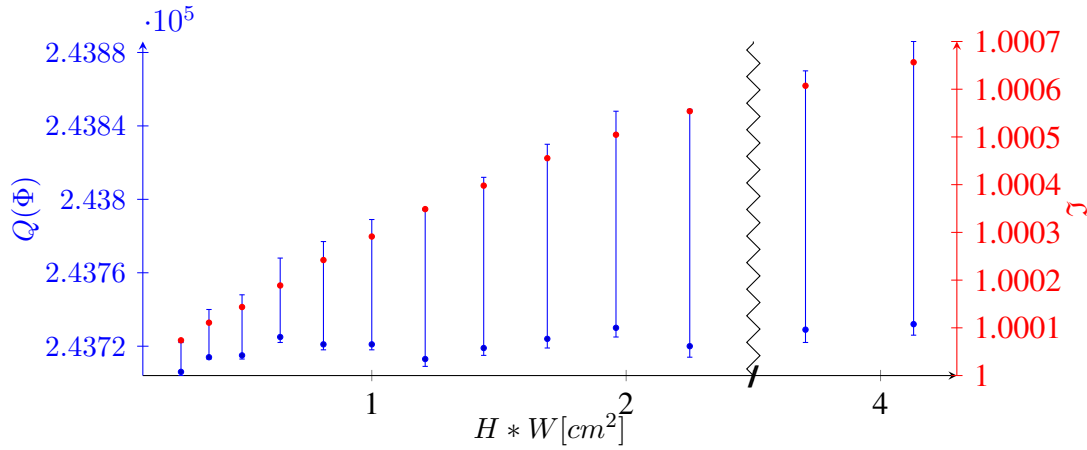
(H, W)	$\mathfrak{I}$	$Q(\tilde{\Phi})$	$Q(\Phi)$	U	L
(0.5,0.4)	1.00007	243704	243706	243722	243704
(0.6,0.5)	1.00011	243704	243714	243740	243713
(0.7,0.6)	1.00014	243704	243715	243748	243713
(0.8,0.7)	1.00019	243704	243725	243768	243722
(0.9,0.8)	1.00024	243704	243721	243777	243718
(1.0,0.9)	1.00029	243704	243721	243789	243718
(1.1,1.0)	1.00035	243704	243713	243794	243709
(1.2,1.1)	1.00040	243704	243719	243812	243715
(1.3,1.2)	1.00046	243704	243724	243830	243719
(1.4,1.3)	1.00050	243704	243730	243848	243725
(1.5,1.4)	1.00055	243704	243720	243849	243714
(1.3,2.85)	1.00061	243704	243729	243870	243722
(1.4,2.95)	1.00066	243704	243732	243886	243726

Figure 6.6: Bounds on the simplification error in Experiment 2 for varying internal feature dimensions. The table lists the height H and width W of the feature area, the effectivity index $\mathfrak{I}$, the exact QoI $Q(\Phi)$ and approximate QoI $Q(\tilde{\Phi})$, and the upper U and lower L bounds..

6.4 Experiment 3: Negative Features with Neumann Boundary Conditions

The tightness of the error bounds for negative features on the Neumann boundary with increasing size is tested with the same QoI and a similar capacitor model as before; see Fig. 5.3. Each conductor plate has a width of 0.001m and length of 0.01m, at a potential of 220 volt with opposite signs. The outer box of model capacitor used in our experiments has a square shape, its length is 0.06m. The length of the initial square feature is 0.3cm, increased in steps of 0.3cm to 2.4cm. Fig. 6.7 shows the finite element solutions for the simplified and original model. Fig. 6.8 shows the results. It can be seen that by making the slot size bigger, the deviation of the value of the QoI of the simplified model from the exact one increases. The values of the effectivity indices also clearly indicate that increasing the size of the negative feature drastically reduces the tightness of the bound. The effectivity index for the largest two features indicate that the simplification error estimation is not suitable for such large features. However, the effectivity indices for smaller sized features are in an acceptable range to bound the error. It appears that if the size of the negative feature exceeds a threshold, the bounds become very quickly quite inaccurate, in particular when the lower bounds become negative for two last feature sizes.
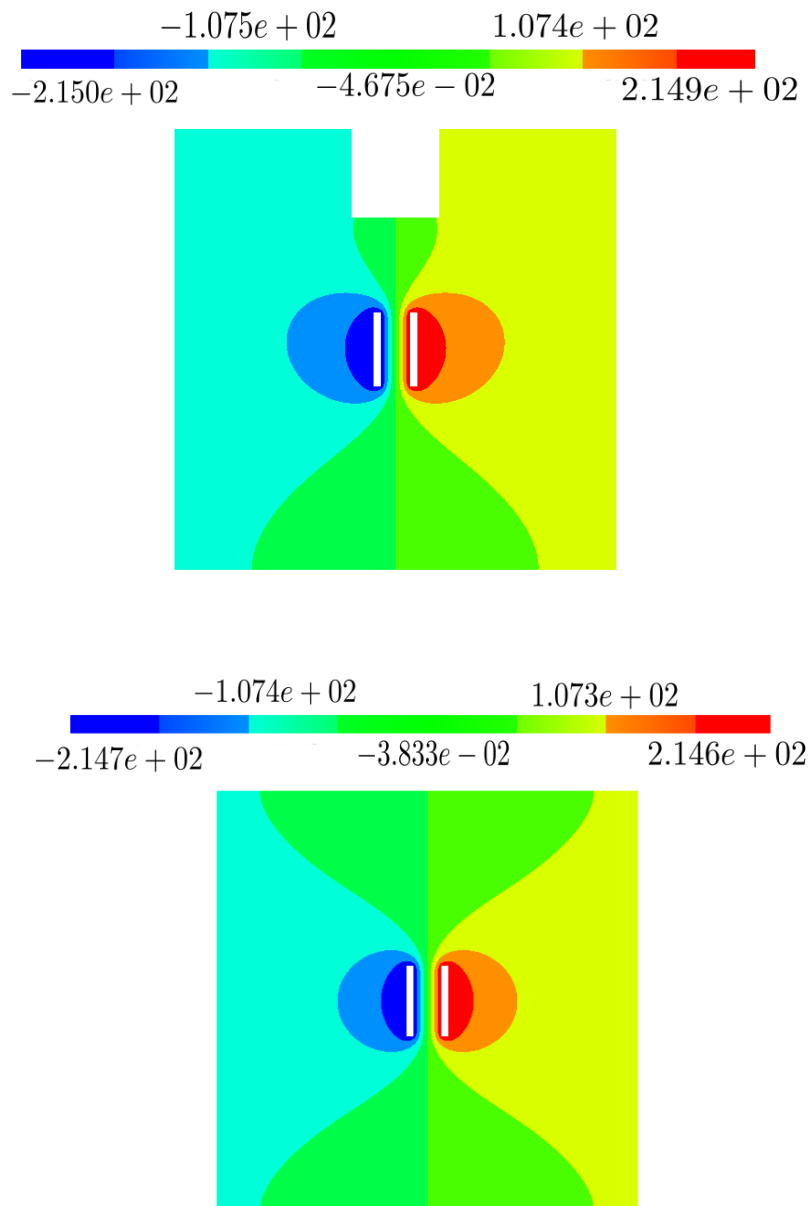
Figure 6.7: Top: The finite element solution for the capacitor model with a negative feature on the Neumann boundary for Experiment 3. Bottom: The finite element solution for the simplified model.
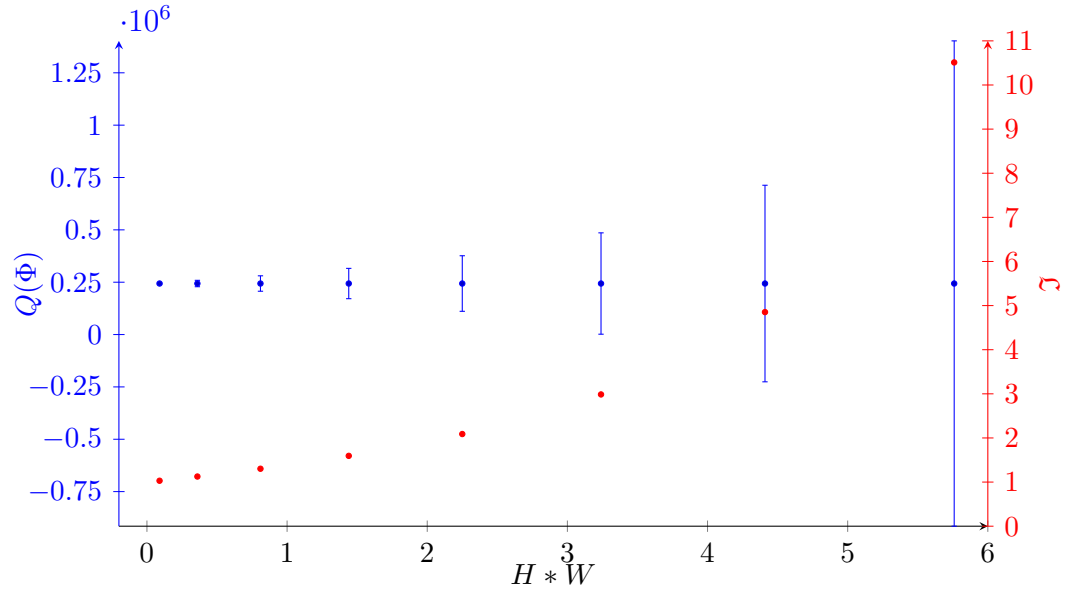
(W,H)	$\Im$	$Q(\tilde{\Phi})$	$Q(\Phi)$	U	L
(0.3,0.3)	1.03022	243704	243719	247400	240034
(0.6,0.6)	1.12558	243704	243715	259020	228414
(0.9,0.9)	1.30225	243704	243713	280545	206883
(1.2,1.2)	1.59428	243704	243709	316112	171281
(1.5,1.5)	2.08878	243704	243702	376369	111031
(1.8,1.8)	2.98621	243704	243693	485712	1686
(2.1,2.1)	4.85242	243704	243681	713065	-225697
(2.4,2.4)	10.51136	243704	243680	1402538	-915189

Figure 6.8: Bounds on the simplification error in Experiment 3 for varying boundary feature dimensions. The table lists the height H and width W of the feature area, the effectivity index $\Im$, the exact QoI $Q(\Phi)$ and approximate QoI $Q(\tilde{\Phi})$, and the upper U and lower L bounds.

6.5 Experiment 4: Features with Dirichlet Boundary Condition

As shown in Fig. 5.4, the feature moves along the outer side of the left conductor blade. Each conductor plate has width of 0.001m and length of 0.01m, at a potential of 220 volt with opposite signs. The outer box of model capacitor used in our experiments has a shape of square, its length is 0.06m. The feature takes the shape of a negative feature on the conductor which is described by Dirichlet boundary condition. With the same choice of QoI as before, the interest is in the effect of removing the negative feature, e.g. representing a manufacturing deficiency at different locations, and specifically the performance of the error bounds. The feature is moved along side the conductor plate by a step size of 0.1cm. All of the measurements are taken from the origin at the center of the capacitor. Fig. 6.9 shows the solution for the simplified and original problem, squeezed in due to the feature.

Results for the error bounds, shown in Fig. 6.10, emphasize that the position of the feature plays a significant role in how the simplification affects the QoI. As the feature moves upwards from the bottom of the conductor plate to the middle of the plate, where it is next to the area of interest S, the simplification error spikes. After it passed that location, the simplification error and the bound widths are significantly reduced. The effectivity indices indicate that when the feature is next to the area of interest S, the estimation of the simplification error is worse. The error bound effectivity becomes better when the feature moves further upwards from S. It also shows that when the feature is at the bottom of the conductor plate, next to S, the bound is less tight. This is still in line with the general estimation results earlier that small effects of the feature are quite well estimated, but larger effects are overestimated. Hence, the bounds are a useful practical indicator of when a feature has a small effect on the QoI, but not vice versa. The experiment is conducted for the negative feature on Dirichlet boundary and the corresponding equations are derived for this feature type. The positive feature on

this boundary follows the same formulations for the bounds constructions. In order to avoid repetition of experiments, tests for positive features on the Dirichlet boundary are omitted. With this experiment we only show that the modeling simplification error bounds are guaranteed for negative features on the Dirichlet boundary.
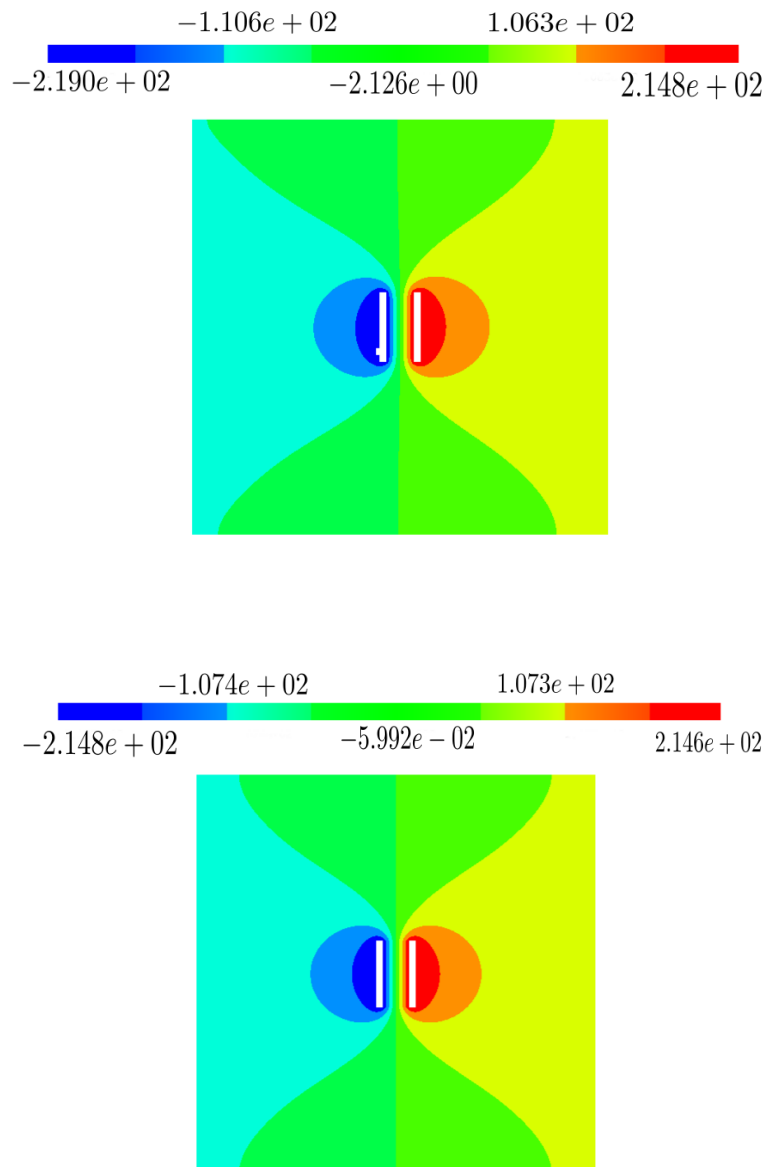
Figure 6.9: Top: Finite element solution for the capacitor model with a negative feature on the conductor plate (Dirichlet Boundary) for Experiment 4. Bottom: Finite element solution of the simplified model.
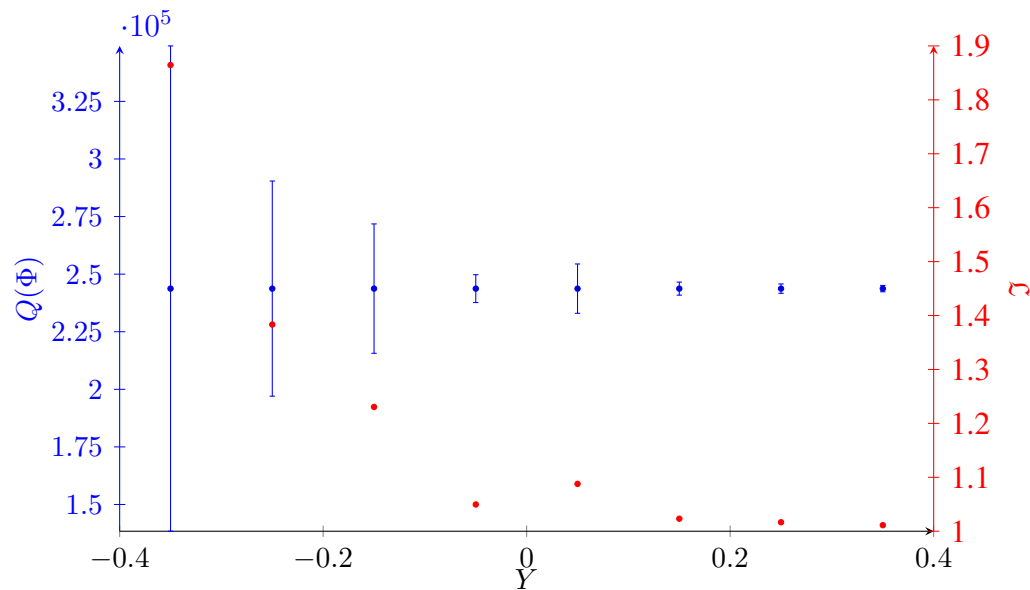
(X,Y)	$\mathfrak{I}$	$Q(\tilde{\Phi})$	$Q(\Phi)$	U	L
(-0.325,-0.35)	1.86450	243712	243723	349083	138385
(-0.325,-0.25)	1.38331	243712	243713	290430	197012
(-0.325,-0.15)	1.23048	243712	243716	271806	215635
(-0.325,-0.05)	1.04962	243712	243711	249765	237671
(-0.325,0.05)	1.08788	243712	243708	254421	233004
(-0.325,0.15)	1.02327	243712	243716	246556	240884
(-0.325,0.25)	1.01665	243712	243716	245746	241688
(-0.325,0.35)	1.01123	243712	243718	245085	242349

Figure 6.10: **Bounds on the simplification error in Experiment 4 for varying boundary feature location. The table lists the feature location (X,Y), the effectivity index $\mathfrak{I}$, the exact QoI $Q(\Phi)$ and approximate QoI $Q(\tilde{\Phi})$, and the upper U and lower L bounds.**

6.6   Experiment 5: Positive Features with Neumann Boundary Conditions

To test the bound for a positive feature on the Neumann boundary, we use the QoI from Section 4.2.1 for a capacitor model; see Fig 5.2. Each conductor plate has width of 0.001m and length of 0.01m, at a potential of 220 volt with opposite signs. The outer box of model capacitor used in our experiments has a shape of square, its length is 0.06m. The positive feature is a square of length 0.3cm initially. The length is increased by 0.3cm up to 2.4cm. The solution of electrostatic potential for the original and simplified model is shown in Fig. 6.11. The results for the simplification error bounds are shown in Fig. 6.12. Overall the effectivity index still indicates good performance and is in line with the conclusions for the internal feature results, Section 6.1.
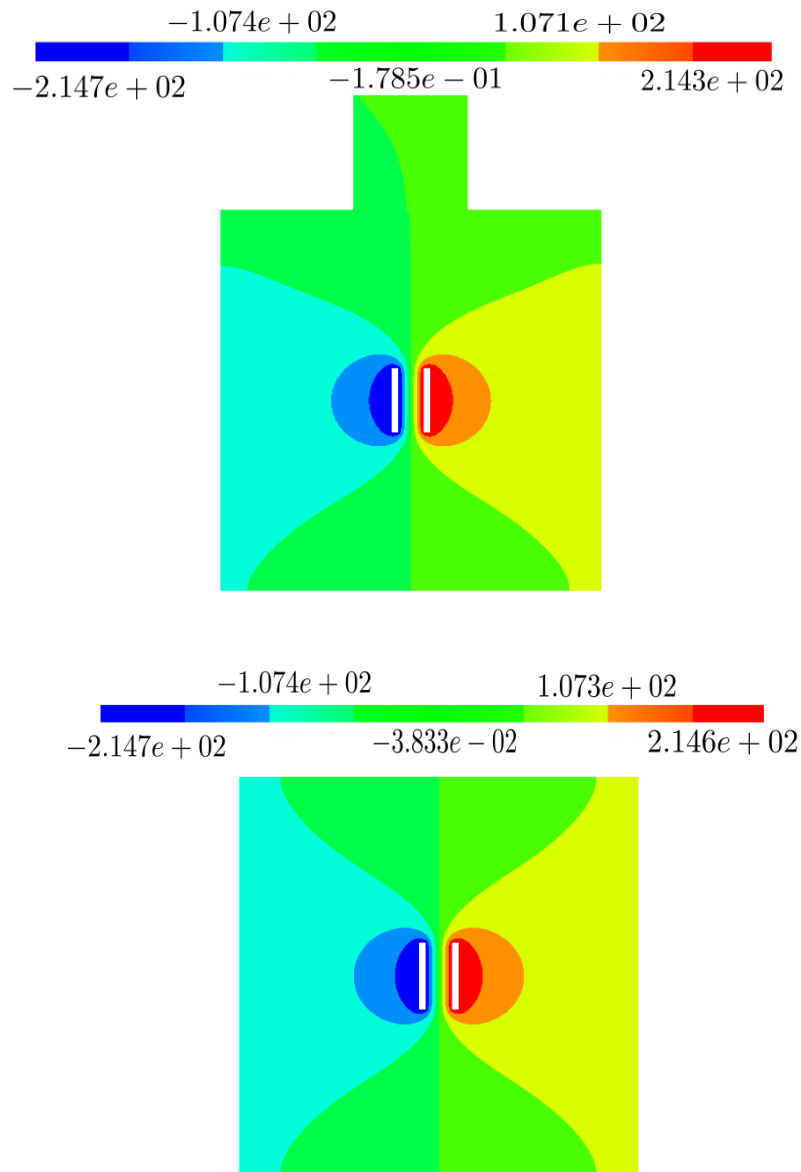
Figure 6.11: Top: The finite element solution Φ for the capacitor model with the positive feature on the Neumann boundary for Speedup Experiment. Bottom: The finite element solution for the simplified model.
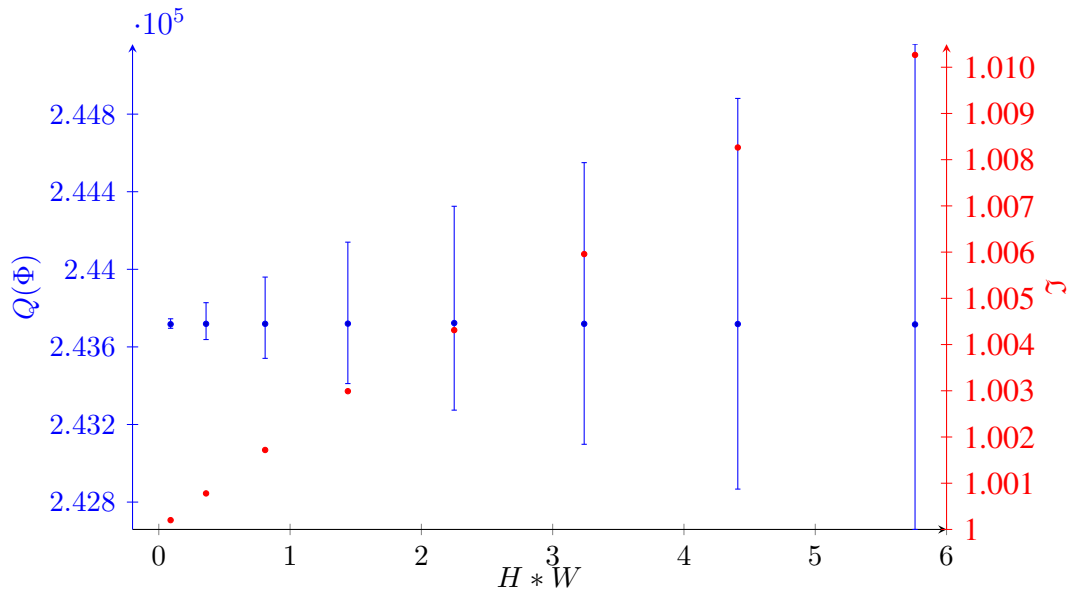
(H,W)	$\mathfrak{I}$	$Q(\tilde{\Phi})$	$Q(\Phi)$	U	L
(0.3,0.3)	1.00020	243715	243717	243745	243696
(0.6,0.6)	1.00078	243715	243719	243828	243638
(0.9,0.9)	1.00172	243715	243719	243960	243541
(1.2,1.2)	1.00299	243715	243720	244140	243411
(1.5,1.5)	1.00431	243715	243723	244325	243274
(1.8,1.8)	1.00596	243715	243719	244550	243098
(2.1,2.1)	1.00826	243715	243718	244881	242867
(2.4,2.4)	1.01027	243715	243716	245161	242659

Figure 6.12: Bounds on the simplification error in Speedup Experiment for varying boundary feature dimensions. The table lists the height H and width W of the feature area, the effectivity index $\mathfrak{I}$, the exact QoI $Q(\Phi)$ and approximate QoI $Q(\tilde{\Phi})$, and the upper U and lower L bounds.

6.7 Analysis Speedup for Simplifying Positive Features with Neumann Boundary Conditions

The capacitor dimension and its conductor has width of 0.001m and length of 0.01m, at a potential of 220 volt with opposite signs. The outer box of model capacitor used in our experiments has a shape of square, its length is 0.06m. The advantages gained from the simplification of positive features are mainly related to the potential speedup of the analysis. Tables 6.2 and 6.1 show the time spent on meshing and analyzing the capacitor before and after defeaturing for the model used for Experiment 5 in Section 6.6.

The analysis computation time of the simplified model always remains the same between all of experiments because it has the same mesh structure and coarseness. Fig. 6.13 shows the comparison of mesh sizes between the simplified and original model. The original model discretized with triangular mesh type to 8517 mesh elements. The simplified model, on the other hand, reduces to 321 mesh elements with the same triangular mesh type and geometry. The analysis computation times of the simplified model are listed in Table 6.1.

Table 6.2 lists the times required for meshing and analyzing the original models from Experiment 5 for the different feature sizes. This table needs to be compared with Table 6.1 to demonstrate the computational time saving provided by the simplification. The time required for the computation of bounds and dual model is included in the analysis of the simplified model. The time for the analysis of the feature domain is negligible in comparison to the total time of original model, and therefore it is not mentioned in the table. Its range values varies approximately between 0.003 and 0.010 seconds. The speedup factor is defined to indicate the ratio between the computation time of the original model versus the simplified model.
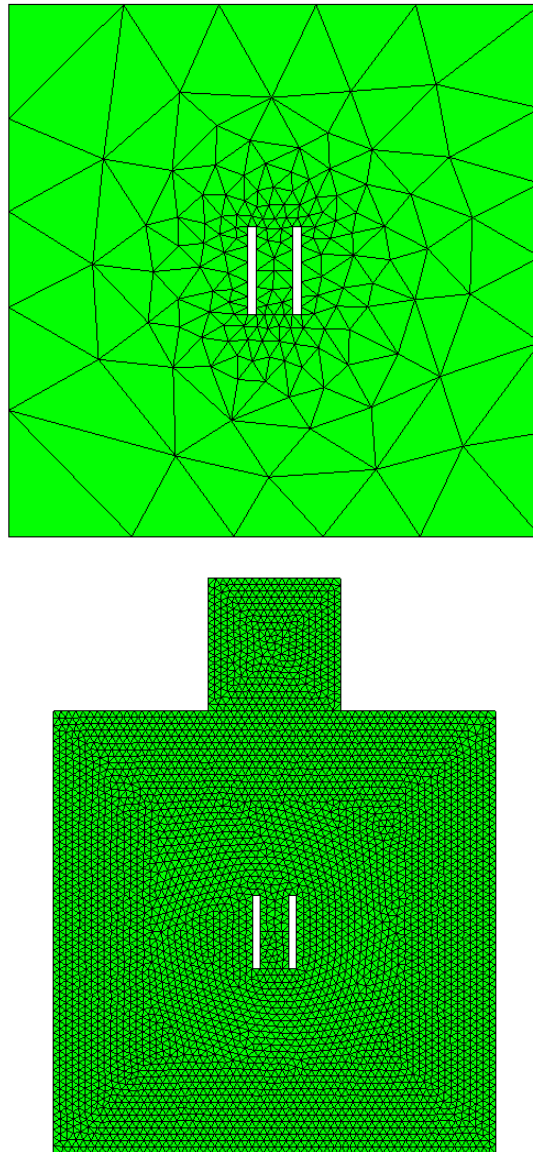
Figure 6.13: Top: The generated mesh for a capacitor model after simplification, 321 mesh elements. Bottom: The generated mesh for a capacitor model with positive feature with 8517 mesh elements.

Table 6.1: The analysis computation time for the simplified model for a positive feature on the Nuemann boundary. This time is independent of the problem, as the mesh remains the same..

$MeshingTime(s)$	$AnalyzingTime(s)$	$TotalTime(s)$
0.48	0.36	0.84

Table 6.2: The time required for meshing and analyzing the original model with a positive feature of different sizes on the Neumann boundary.

(H, W)	$MeshingTime(s)$	$AnalyzingTime(s)$	$TotalTime(s)$	$SpeedupFactor$
(0.3,0.3)	0.5107	0.879	1.3897	1.65
(0.6,0.6)	0.5174	0.905	1.4224	1.69
(0.9,0.9)	0.4932	0.918	1.4112	1.68
(1.2,1.2)	0.5115	0.9787	1.4902	1.77
(1.5,1.5)	0.5162	0.988	1.5042	1.79
(1.8,1.8)	0.5296	0.993	1.5226	1.81
(2.1,2.1)	0.5406	1.025	1.5656	1.86
(2.4,2.4)	0.5588	1.039	1.5978	1.90

6.8   Parallel Plate Capacitor with Glass Dielectric Material

The glass capacitor model is the parallel plate capacitor shown in Fig. 6.15 with the area of interest S and the feature area F being simplified lying between the two capacitor plates. There are many shapes for practical capacitors. However, they all consist of at least two electrical plates separated by a dielectric. The whole model domain for the capacitor is a square of 6cm length. The conductor plates have a rectangular shape, each of the same width and length of 0.1cm and 1cm respectively, and they are placed in the centre of the domain. The conductor plates are 0.4cm apart from each other. They are given a voltage of $+220$V and -220V. The right plate is the positive conductor. The capacitor is surrounded by air. The dielectric material between the capacitor plates stores the electric energy by becoming polarized, determining the capacitance. In order to maximise the capacitance, the dielectric material should have the highest possible permittivity. The dielectric material in our model is Corning 7740 (pyrex), a glass wafer. Glass provides reliable and stable performance and operates in a wide range of temperatures. The relative permittivity of pyrex is 4.6 [65]. When manufacturing this material, there is a probability of it being contaminated by sodium. Sodium contamination can be deleterious to the electrical properties of pyrex structures. The permittivity of sodium, higher than pyrex, can cause damage to the capacitor [79]. The relative permittivity of sodium is 8.4 [65]. The full 3D capacitor model is illustrated in Figs. 6.14 and 6.15. The domain F is allocated to the area containing the sodium contamination, surrounded by the pyrex dielectric material.

In this experiment, the simplification error is investigated after replacing the sodium domain with pyrex and the area of interest S is the lower half of the space between the conductor plates. The QoI represents the capacity in this area and is interesting for several engineering applications [75]. e.g., it is a characteristic that can be used in the design of capacitors or to analyze the properties of a molecular system. Here a simpli-
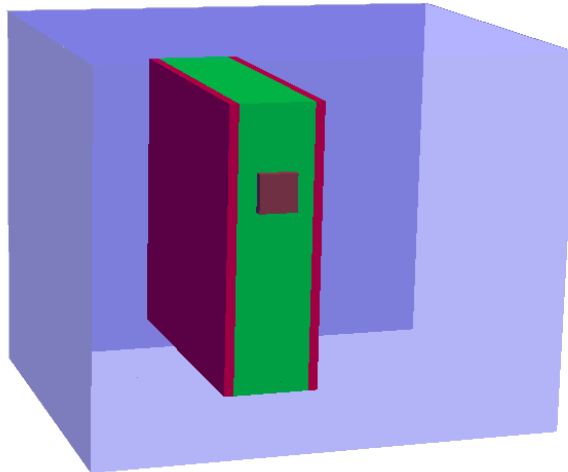
Figure 6.14: 3D glass capacitor model with two metal conductor plates in red. The whole box of the capacitor is filled with air (only partially shown to have a larger view of the capacitor itself). The dielectric material is in green (glass - Corning 7740) with a sodium contamination in brown.

fication error bound is calculated for a specific contamination to give an estimation of the effect of a specific, known contamination on the performance of the capacitor. This is to demonstrate that the bounds are relevant to practical problems and may be used in future work to estimate the effect on manufacturing uncertainties.

The sodium contamination is a square of length 0.2cm. In 3D it is in the form of a cube, but in the simulation its projected onto a 2D domain. The contamination cannot be embedded in or interfaced to the area of interest S because of the assumptions made in the simplification error estimation. The location of the contamination F in the dielectric material is shown in the Fig. 6.14, showing a cut plane through the middle of the capacitor. It can be seen that the dielectric material is placed between the capacitor plates. The area of interest S is in the lower half of the dielectric material where there is no contamination in that region. Fig. 6.16 shows the same model after removing the contamination from dielectric material.
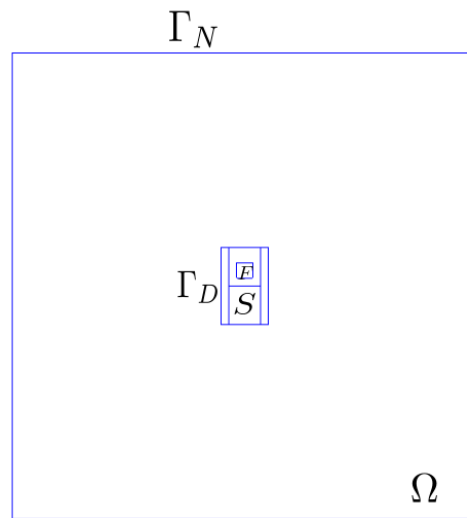
Figure 6.15: 2D model of the glass capacitor, where Ω is the whole domain. The Dirichlet boundary Γ_D is at the conductor plates. The outer box of the capacitor is the Neumann boundary Γ_N. The area of interest S is the lower half between the capacitor plates. The sodium contamination is the domain F.
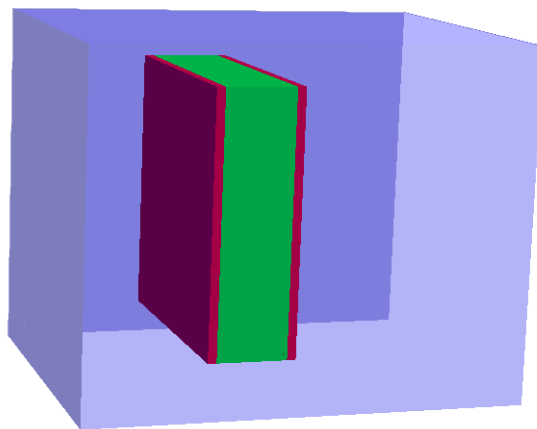
Figure 6.16: The geometry model of glass capacitor in Fig. 6.14 after simplification (the sodium contamination is removed from the pyrex material).

Finite element analysis is run for both, the original and simplified problems for the 2D model in Fig. 6.15 and its simplification. Fig. 6.17 shows the solution of both. It can be seen that the sodium contamination disturbs the electric field in the pyrex material.

The error bound is computed according to Eq. (4.33). It requires the finite element solution of primal and dual simplified models, shown in Figs. 6.17, 6.18, to calculate ν, ν^*, and $R(\tilde{\Phi}^*)$. The exact and simplified QoI are obtained from the solutions of the original and simplified models. The results of this gives $L = 293032.95 \leq Q(\Phi) = 293213 \leq U = 293408.05$ resulting in $\Im = 1.0012793$, indicating good quality bounds.

This is just one sample of the modeling simplification for manufacturing uncertainties. In order to develop a general pattern for the estimation of the modeling simplification error for manufacturing uncertainties, it requires to estimate the statistical variation of modeling simplification error for several manufacturing uncertainties. This is left as future work.
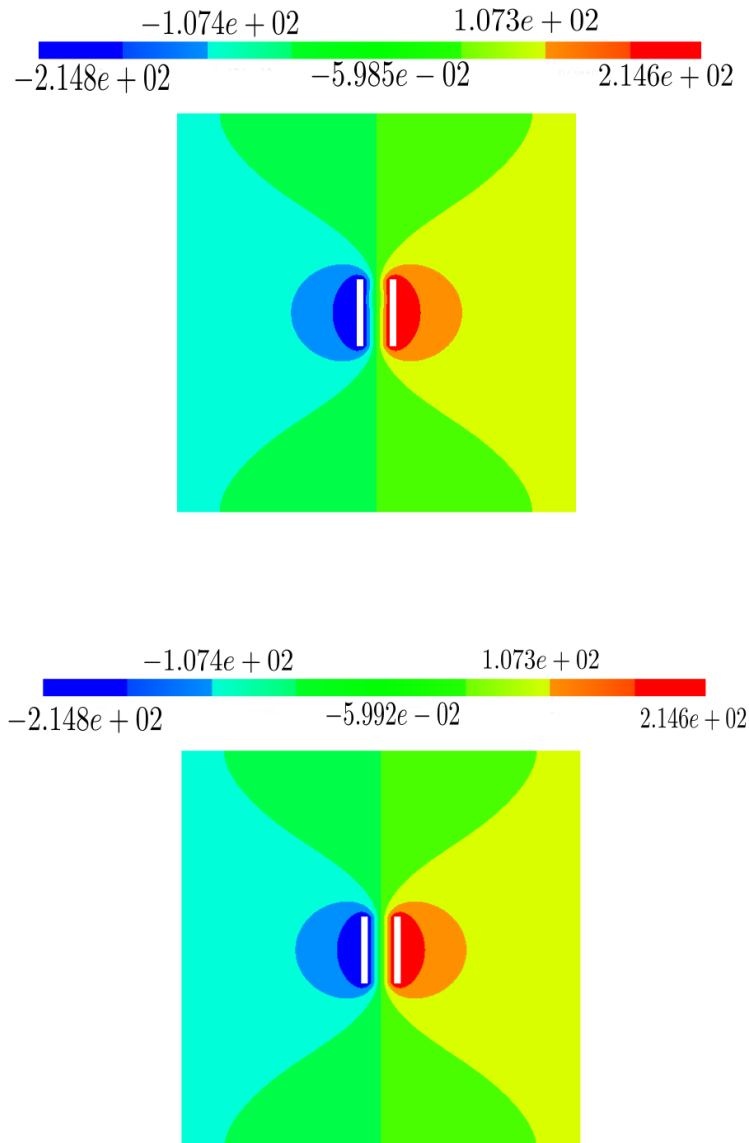
Figure 6.17: Top: Finite element solution for the original glass capacitor model. The feature affects the distribution of the electrostatic potential nearby. Bottom: Finite element solution for the capacitor model after defeaturing. The electric field is symmetric between the capacitor plates.
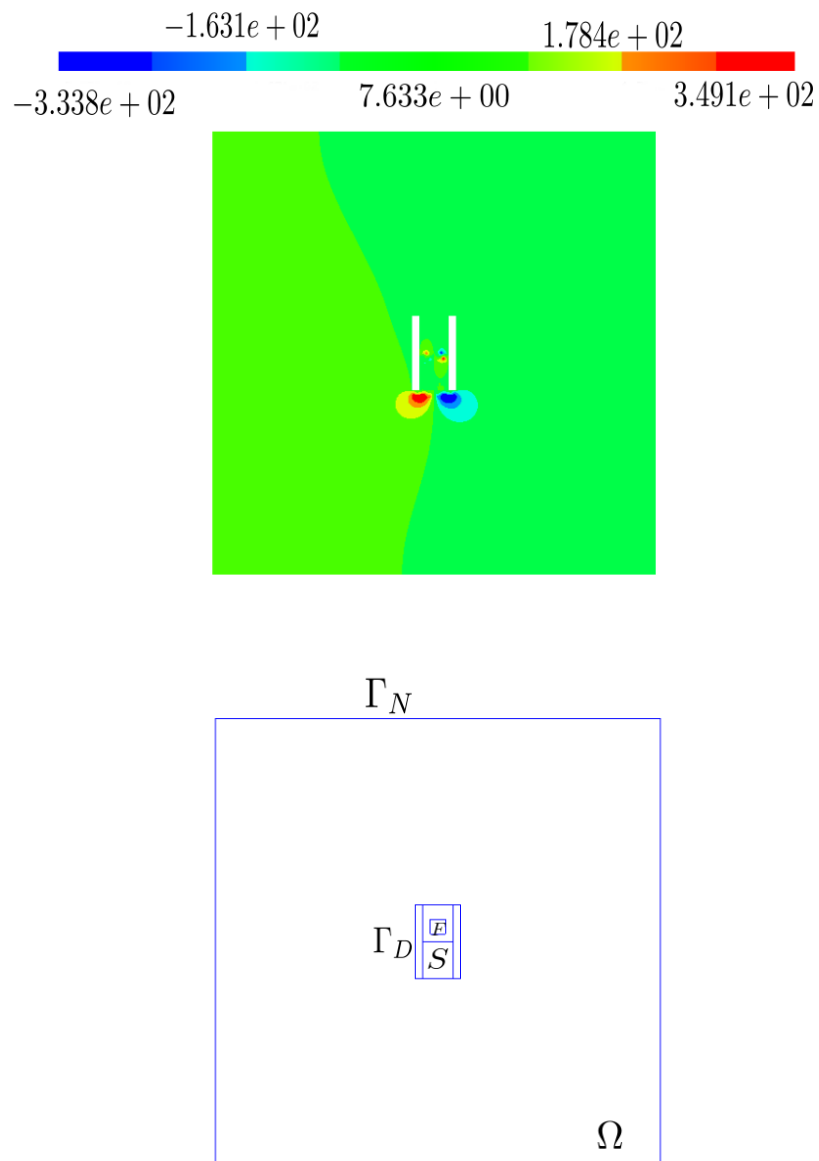
Figure 6.18: The finite element solution of the dual simplified model for the glass capacitor (top). The distribution of the solution is compared to the referential geometry setup at the bottom.

Chapter 7

Conclusions and Future Work

This chapter discusses future work arising from the results presented and conclude with a brief summary.

7.1   Future Work

The strategy to estimate the simplification error can be applied to a much wider range of electrostatic and similar problems. All these types of problem have similar functional operators with divergence free properties of the solution of the governing PDE. The effectiveness of the approach for the case of Laplacian PDEs in other elasticity problems can be explored. For each PDE the bound calculation needs to be changed due to a change in the operators, but follows similar approaches to those presented for the features for the capacitor.

The suggested method in this dissertation has the potential to be utilized for quantification of uncertainties arising from manufacturing processes as well as uncertainties in material properties, as already indicated by the glass capacitor example. Typically, a statistical PDE over the variation must be solved to find the uncertainties in the performance caused by the uncertainties in the model. The proposed bounds may help to simplify solving this problem by estimating the effect of simplifying uncertain features such as removing material contaminations or small boundary defects.

The computation of the bounds in the discretized system currently is carried out on

the same mesh structure between simplified and original models for different feature types, apart from the test case of positive feature on Neumann boundary condition used for demonstrating the speedup achieved by simplification. In order to achieve the speedup for all bound computations, a method is required that can compute the integrals involved in the bounds calculation sufficient accuracy without having the feature structure being preserved in the mesh. This requires a method to calculate integrals of fields over a mesh where the integration domain is not aligned with the mesh. A potential approach to calculate these integrals efficiently could be based on Whitney integration [93] in combination with techniques from discrete differential geometry [12].

The bounds could be made tighter for the estimation of the simplification error for a quantity of interest. This may be achieved by taking advantage of machine learning methods. It may lead to more accurate learned estimations for the residual and the ν and ν^*, and it can make the bounds tighter, at the cost of potentially loosing the guarantee that the bounds always hold (for linear QoIs). Furthermore, the involved integrations can be studied more carefully for complex geometries and non-linear approximations may be considered. The type of physical problem and operators matter in terms of different options for the quantity of interest, and the tightness of the bounds calculations need to be adjusted in accordance with the choice of the quantity of interest. One approach to improve the bounds may be to learn correction factors for the bounds based on the ν or ν^* values using machine learning techniques, e.g. by learning a Gaussian Process or another Bayesian method where ν and/or ν^* are the variables indicating the correction. This would of course lead to uncertain bounds, but with explicit uncertainty that may be improved by increasing the learning data or adjusting the variables.

The computational costs calculating the bounds may be reduced by spending less computational effort for solving the adjoint model in the case of more complex features. It may further be approximated with cheaper, less accurate techniques as long as the error bounds are still sufficiently tight and accurate for specific simplification cases,

which makes this highly problem dependent.

The goal-oriented error estimation algorithms may furthermore be generalized, so that it can operate on linear and nonlinear problems. There is a restriction in the general approach of goal-oriented error estimation for operating with linear quantities of interest. In order to make the simplification error more accurate, the quantity of interest that can be handled must be extended to nonlinear functions. This can be done by following the methodology proposed in the Ph.D dissertation of [13]. The method supports the nonlinearity in QoI for the goal oriented error estimation, and it can be utilized in the modeling simplification error. The choice of non-linear functions for the quantity of interest would enable it to cover a wider range of models and effects of simplification methods.

Simplification in this work has only been considered for a single feature. The usefulness of the proposed strategy may be extended to study simplification of several features, considering the interaction between the features. In this case, each feature involved in the simplification might induce different effects on the quantity of interest and complex interactions between the features can create complex scenarios. Treating it as a sequential simplification error estimation problem by removing each feature at a time is not an appropriate strategy due to feature interactions and dependence on the order in which the features are simplified.

7.2   Conclusions

In this dissertation, it has been devised a novel strategy, to construct lower and upper bounds for the simplification error for Laplacian PDEs with Dirichlet and Neumann boundary conditions in a bounded domain. The particular choice of PDE that numerical experiments have been carried out with is the electrostatic PDE. The methodology has been proven that it can bound the modeling simplification error for the divergence-free elliptic PDEs such as the electrostatic equation. The choice for electrostatic PDE

is that it has a variety of practical applications in industry. The finite element simulations are computed for a capacitor model, designed to be representative of the kind of capacitors which are frequently implemented in industry.

The simplification error is derived within a goal-oriented a posteriori error estimation context, which is based on the residual error, localized on a subdomain, and utilizes the adjoint method. The bounds are constructed in the energy norm, based upon the constitutive relation error equation, which implies the wide applicability of the bounds. The residual error comes out of the modeling simplification in finite element solution of the capacitor model constructed for a quantity of interest. The proposed approach bounds the simplification error in the energy norm in terms of difference between a quantity of interest between the simplified and original model. The solution for the original model does not have to be computed for this. The computation of the simplification error in the energy norm makes it a computationally affordable approach.

The bounds have been implemented to demonstrate the effectiveness (numerically) of the approach for different simplification error estimation problems for electrostatic problems. The specific applications of the electrostatic models are capacitors. Different defeaturing operations for simplification have been chosen for internal features and positive and negative boundary features with different boundary conditions. The general approach presented can be adapted easily to these specific cases. The results are promising; the performance of the bounds for all simplification types is appropriate to determine whether the geometry simplification of the model has only a small effect on a quantity of interest, defined by the user. For larger effects of the geometry simplification on the quantity of interest, the effectiveness of the bounds is considerably less accurate. However, even if the effect is overestimated in these cases, the bounds are still practically useful to decide whether the effect is small and hence the simplification can be applied. The bounds are universally applicable to a wide range of problems and not constructed for very specific cases. In the capacitor context, their performance is determined by the electrical capacitance properties. They also indicate the effect of

manufacturing uncertainties. The bounds, on a quantity of interest representing the electric energy over a region of interest, indicate whether the features have a noticeable impact on the functionality of the capacitor. The conclusion can be drawn for the bounds quality with respect to the location of the feature, its functionality whether it can be as a dielectric material, or whether in the form of positive and negative geometry figure on the boundaries of the capacitor, and last but not least its distance to the interested domain. It can be easily perceived that as far as the feature gets closer to the proximity of the interested domain, the simplification affects QoI more noticeably, and subsequently it deteriorates the quality of bounds and they grow larger. Another factor that plays an important role in the computation of the good quality bounds is as if the presence of the feature makes a significant distortion in the flux of the capacitor around the interested domain. Therefore, by removing the feature, the computations of the energy norm error bounds witness the big distance between upper and lower bounds. This effect sometimes turns that much significant that it returns to the negative lower bounds. The judgment on the quality of the bounds are reflected in the effectivity index. As if this index moves further away from one, it indicates that the bounds quality exacerbates more.

Bibliography

[1] A Abdulle and G Vilmart. A priori error estimates for finite element methods with numerical quadrature for nonmonotone nonlinear elliptic problems. *Numerische Mathematik*, 121(3):397–431, 2012.

[2] M Ainsworth and JT Oden. *A Posteriori Error Estimation in Finite Element Analysis.* John Wiley & Sons, 2011.

[3] C Andújar, P Brunet, and D Ayala. Topology-reducing surface simplification using a discrete solid representation. *ACM Transactions on Graphics (TOG)*, 21(2):88–105, 2002.

[4] T Ansaldi, C Airiau, CP Arroyo, and G Puigt. Pse-based sensitivity analysis of turbulent and supersonic single stream jet. In *Proceedings of the 22nd AIAA/CEAS Aeroacoustics Conference*, page 3052, 2016.

[5] I Babuška and WC Rheinboldt. A-posteriori error estimates for the finite element method. *International Journal for Numerical Methods in Engineering*, 12(10):1597–1615, 1978.

[6] I Babuška and A Miller. A feedback finite element method with a posteriori error estimation: Part i. the finite element method and some basic properties of the a posteriori error estimator. *Computer Methods in Applied Mechanics and Engineering*, 61(1):1–40, 1987.

[7] I Babuška and T Strouboulis. *The finite element method and its reliability.* Oxford University Press, 2001.

[8] RE Bank and A Weiser. Some a posteriori error estimators for elliptic partial differential equations. *Mathematics of Computation*, 44(170):283–301, 1985.

[9] Y Bazilevs, VM Calo, JA Cottrell, JA Evans, TJrR Hughes, S Lipton, MA Scott, and TW Sederberg. Isogeometric analysis using t-splines. *Computer Methods in Applied Mechanics and Engineering*, 199(5):229–263, 2010.

[10] R Becker and R Rannacher. An optimal control approach to a posteriori error estimation in finite element methods. *Acta Numerica 2001*, 10:1–102, 2001.

[11] BI Bleaney, and B Bleaney. *Electricity and Magnetism*, volume 2. Oxford University Press, 2013.

[12] AI Bobenko, and JM Sullivan, and P Schröder, and G Ziegler. *Discrete Differential Geometry.* Springer, 2008.

[13] C Bryant. On goal-oriented error estimation and adaptivity for nonlinear systems with uncertain data and application to flow problems. , *The University of Texas at Austin, Institute for Computational Engineering and Sciences*, Ph.D Dissertation, 2014.

[14] KK Choi and NH Kim. *Structural Sensitivity Analysis and Optimization 1: Linear Systems.* Springer Science & Business Media, 2006.

[15] JA Cottrell, TJR Hughes, and Y Bazilevs. *Isogeometric Analysis: Toward Integration of CAD and FEA.* John Wiley & Sons, 2009.

[16] P Dabke, V Prabhakar, and S Sheppard. Using features to support finite element idealizations. *Computers in Engineering*, 1:183–183, 1994.

[17] F Danglade, JP Pernot, and P Véron. On the use of machine learning to de-feature CAD models for simulation. *Computer-Aided Design and Applications*, 11(3):358–368, 2014.

[18] H Date, S Kanai, T Kishinami, I Nishigaki, and T Dohi. High-quality and prop-erty controlled finite element mesh generation from triangular meshes using the multiresolution technique. *Journal of Computing and Information Science in En-gineering*, 5(4):266–276, 2005.

[19] H Date, S Kanai, T Kishinami, and I Nishigaki. Flexible feature and resolution control of triangular meshes. In *Proceedings of the sixth IASTED International Conference on Visualization, Imaging and Image Processing, Palma De Mal-lorca, Spain*, pages 319–324, 2006.

[20] S Dey, MS Shephard, and MK Georges. Elimination of the adverse effects of small model features by the local modification of automatically generated meshes. *Engineering with Computers*, 13(3):134–152, 1997.

[21] L Demkowicz. *Computing with hp-Adaptive Finite Elements: Volume 1 One and Two Dimensional Elliptic and Maxwell problems*. CRC Press, 2006.

[22] RJ Donaghy, CG Armstrong, and MA Price. Dimensional reduction of surface models for analysis. *Engineering with Computers*, 16(1):24–35, 2000.

[23] RM Errico. What is an adjoint model? *Bulletin of the American Meteorological Society*, 78(11):2577–2591, 1997.

[24] RA Feijóo, AA Novotny, E Taroco, and C Padra. The topological derivative for the poisson's problem. *Mathematical Models and Methods in Applied Sciences*, 13(12):1825–1844, 2003.

[25] R Ferrandes, PM Marin, JC Léon, and F Giannini. A posteriori evaluation of sim-plification details for finite element model preparation. *Computers & Structures*, 87(1):73–80, 2009.

[26] L Fine, L Remondini, and JC Leon. Automated generation of fea models through idealization operators. *International Journal for Numerical Methods in Engineering*, 49(1-2):83–108, 2000.

[27] G Foucault, JC Cuillière, V François, Jean-Claude Léon, and Roland Maranzana. Adaptation of cad model topology for finite element analysis. *Computer-Aided Design*, 40(2):176–196, 2008.

[28] JF Hiller and KJ Bathe. On higher-order-accuracy points in isoparametric finite element analysis and an application to error assessment. *Computers & Structures*, 79(13):1275–1285, 2001.

[29] DSR Gago, DW Kelly, OC Zienkiewicz, I Babuska, et al. A posteriori error analysis and adaptive processes in the finite element method. Part II: adaptive mesh refinement. *International Journal For Numerical Methods In Engineering*, 19(11):1621–1656, 1983.

[30] Y Garden, C Minich Feature-based models for CAD/CAM and their limits. *Computer in Industry*, Elsevier, 23:3–13, 1993.

[31] SH Gopalakrishnan and K Suresh. A formal theory for estimating defeaturing-induced engineering analysis errors. *Computer-Aided Design*, 39(1):60–68, 2007.

[32] SH Gopalakrishnan and K Suresh. Feature sensitivity: A generalization of topological sensitivity. *Finite Elements in Analysis and Design*, 44(11):696–704, 2008.

[33] MB Giles and E Süli. Adjoint methods for pdes: a posteriori error analysis and postprocessing by duality. *Acta Numerica*, 11:145–236, 2002.

[34] MB Giles and NA Pierce. An introduction to the adjoint approach to design. *Flow, Turbulence and Combustion*, 65(3-4):393–415, 2000.

[35] T Grätsch and KJ Bathe. A posteriori error estimation techniques in practical finite element analysis. *Computers & Structures*, 83(4):235–265, 2005.

[36] T Grätsch and KJ Bathe. Goal-oriented error estimation in the analysis of fluid flows with structural interactions. *Computer Methods in Applied Mechanics and Engineering*, 195(41):5673–5684, 2006.

[37] P Houston, B Senior, and E Süli. hp-discontinuous galerkin finite element methods for hyperbolic problems: error analysis and adaptivity. *International Journal for Numerical Methods in Fluids*, 40(1-2):153–169, 2002.

[38] A Ibrahimbegovic, I Grešovnik, D Markovic, S Melnyk, and T Rodic. Shape optimization of two-phase inelastic material with microstructure. *Engineering Computations*, 22(5/6):605–645, 2005.

[39] K Inoue, T Itoh, A Yamada, T Furuhata, and K Shimada. Face clustering of a large-scale cad model for surface mesh generation. *Computer-Aided Design*, 33(3):251–261, 2001.

[40] Jd Jackson. *Classical Electrodynamics*, 3rd edition. John Wiley & Sons, 1998.

[41] A Jameson, L Martinelli, and NA Pierce. Optimum aerodynamic design using the Navier–Stokes equations. *Theoretical and Computational Fluid Dynamics*, 10(1-4):213–237, 1998.

[42] DW Kelly. Bounds on discretization error by special reduced integration of the lagrange family of finite elements. *International Journal for Numerical Methods in Engineering*, 15(10):1489–1506, 1980.

[43] DW Kelly, De SR Gago, OC Zienkiewicz, I Babuska, et al. A posteriori error analysis and adaptive processes in the finite element method: Part i-error analysis. *International Journal for Numerical Methods in Engineering*, 19(11):1593–1619, 1983.

[44] P Kerfriden, JJ Ródenas, and SPA Bordas. Certification of projection-based reduced order modelling in computational homogenisation by the constitutive

relation error. *International Journal for Numerical Methods in Engineering*, 97(6):395–422, 2014.

[45] J Kim. Control of turbulent boundary layers. *Physics of Fluids (1994-present)*, 15(5):1093–1105, 2003.

[46] P Ladevèze, JP Pelle, FF Ling, EF Gloyna, and WH Hart. *Mastering Calculations in Linear and Nonlinear Mechanics*. Springer, 2005.

[47] P Ladeveze, JP Pelle, and Ph Rougeot. Error estimation and mesh optimization for classical finite elements. *Engineering Computations*, 8(1):69–80, 1991.

[48] P Ladevèze and L Chamoin. On the verification of model reduction methods based on the proper generalized decomposition. *Computer Methods in Applied Mechanics and Engineering*, 200(23):2032–2047, 2011.

[49] K Lee. *Principles of CAD/CAM/CAE systems.* Addison-Wesley Longman Publishing Co., Inc., 1999.

[50] YG Lee and K Lee. Geometric detail suppression by the fourier transform. *Computer-Aided Design*, 30(9):677–693, 1998.

[51] JY Lee, JH Lee, H Kim, and HS Kim. A cellular topology-based approach to generating progressive solid models from feature-centric models. *Computer-Aided Design*, 36(3):217–229, 2004.

[52] SHun Lee and K Lee. Partial entity structure: a compact boundary representation for non-manifold geometric modeling. *Journal of Computing and Information Science in Engineering*, 1(4):356–365, 2001.

[53] SH Lee. Feature-based multiresolution modeling of solids. *ACM Transactions on Graphics (TOG)*, 24(4):1417–1441, 2005.

[54] M Li and S Gao. Estimating defeaturing-induced engineering analysis errors for arbitrary 3d features. *Computer-Aided Design*, 43(12):1587–1597, 2011.

[55] L Linardakis and N Chrisochoides. Algorithm 870: A static geometric medial axis domain decomposition in 2d Euclidean space. *ACM Transactions on Mathematical Software (TOMS)*, 34(1):4, 2008.

[56] M Li, J Zheng, and RR Martin. Quantitative control of idealized analysis models of thin designs. *Computers & Structures*, 106:144–153, 2012.

[57] M Li, S Gao, and K Zhang. A goal-oriented error estimator for the analysis of simplified designs. *Computer Methods in Applied Mechanics and Engineering*, 255:89–103, 2013.

[58] M Li, B Zhang, and RR Martin. Second-order defeaturing error estimation for multiple boundary features. *International Journal for Numerical Methods in Engineering*, 100(5):321–346, 2014.

[59] M Li, S Gao, and RR Martin. Engineering analysis error estimation when removing finite-sized features in nonlinear elliptic problems. *Computer-Aided Design*, 45(2):361–372, 2013.

[60] M Mäntylä. *An Introduction to Solid Modeling.* Computer Science Press, 1988.

[61] A Mielke. *Analysis, Modeling and Simulation of Multiscale Problems.* Springer, 2006.

[62] AV Mobley, MP Carroll, and SA Canann. An object oriented approach to geometry defeaturing for finite element meshing. *Proceesings ofd the 7th International Meshing Roundtable*, pages 547–563, 1998.

[63] P Monk. *Finite element methods for Maxwell's equations.* Oxford University Press, 2003.

[64] Z Niu. *Declarative CAD Feature Recognition — An Efficient Approach.* Cardiff University, School of Computer Science and Informatics, Ph.D Dissertation, 2016.

[65] HS Nalwa. *Handbook of Low and High Dielectric Constant Materials and their Applications, two-volume set.* Academic Press, 1999.

[66] JT Oden and S Prudhomme. Goal-oriented error estimation and adaptivity for the finite element method. *Computers & Mathematics with Applications*, 41(5):735–756, 2001.

[67] J Peddie. 2015 CAD report. `http://jonpeddie.com/publications/cad_report`, 2015. [Online, accessed 7-May-2016].

[68] S Prudhomme and JT Oden. On goal-oriented error estimation for elliptic problems: application to the control of pointwise errors. *Computer Methods in Applied Mechanics and Engineering*, 176(1):313–331, 1999.

[69] RE Plessix. A review of the adjoint-state method for computing the gradient of a functional with geophysical applications. *Geophysical Journal International*, 167(2):495–503, 2006.

[70] O Pironneau. On optimum design in fluid mechanics. *Journal of Fluid Mechanics*, 64(01):97–110, 1974.

[71] WR Quadros and SJ Owen. Defeaturing cad models using a geometry-based size field and facet-based reduction operators. *Engineering with Computers*, 28(3):211–224, 2012.

[72] M Rezayat. Midsurface abstraction from 3D solid models: general theory and applications. *Computer-Aided Design*, 28(11):905–915, 1996.

[73] Y Saad. *Iterative Methods for Sparse Linear Systems.* SIAM, 2003.

[74] AMS Budge, J Bonet, A Huerta, and J Peraire. Computing bounds for linear functionals of exact weak solutions to Poisson's equation. *SIAM Journal on Numerical Analysis*, 42(4):1610–1630, 2004.

[75] I Sakalli, J Schoberl, and EW Knapp. MFES: A robust molecular finite element solver for electrostatic energy computations. *Journal of Chemical Theory and Computation*, 10(11):5095–5112, 2014.

[76] J Schoeberl. Mesh generator. `https://sourceforge.net/projects/netgen-mesher/`, September 2016.

[77] J Schoeberl. FEM Library. `https://sourceforge.net/projects/ngsolve/`, September, 2016.

[78] J Sokolowski and A Zochowski. On the topological derivative in shape optimization. *SIAM Journal on Control and Optimization*, 37(4):1251–1272, 1999.

[79] KS Henriksen, GU Jensen, A Hanneborg, and H Jakobsen. Sodium contamination of SiO2 caused by anodic bonding. *Journal of Micromechanics and Microengineering*, 13(6):845, 2003.

[80] TW Sederberg, J Zheng, A Bakenov, and A Nasri. T-splines and T-NURCCs. *ACM Transactions on Graphics (TOG)*, 22, 477–484. ACM, 2003.

[81] A Sheffer. Model simplification for meshing using face clustering. *Computer-Aided Design*, 33(13):925–934, 2001.

[82] K Shimada. Current issues and trends in meshing and geometric processing for computational engineering analyses. *Journal of Computing and Information Science in Engineering*, 11(2):021008, 2011.

[83] MS Shephard, MW Beall, and RM O'Bara. Revisiting the elimination of the adverse effects of small model features in automatically generated meshes. In *Proceedings of the 7ths International Meshing Roundtable*, pages 119–131. , 1998.

[84] E Stein, R De Borst, and TJR Hughes. *Encyclopedia of Computational Mechanics*. Wiley, 2004.

[85] BA Szabo and I Babuška. *Finite Element Analysis*. John Wiley & Sons, 1991.

[86] S Tornincasa, F Di Monaco, et al. The future and the evolution of CAD. In *Proceedings of the 14th International Research/Expert Conference: Trends in the Development of Machinery and Associated Technology*, pages 11–18, 2010.

[87] A Thakur, AG Banerjee, and SK Gupta. A survey of cad model simplification techniques for physics-based simulation applications. *Computer-Aided Design*, 41(2):65–80, 2009.

[88] I Turevsky, SH Gopalakrishnan, and K Suresh. Defeaturing: A posteriori error analysis via feature sensitivity. *International Journal for Numerical Methods in Engineering*, 76(9):1379–1401, 2008.

[89] I Turevsky, SH Gopalakrishnan, and K Suresh. An efficient numerical method for computing the topological sensitivity of arbitrary-shaped features in plate bending. *International Journal for Numerical Methods in Engineering*, 79(13):1683–1702, 2009.

[90] T Varady, RR Martin, and J Cox. Reverse engineering of geometric models. *Computer-Aided Design*, 29(4):255–268, 1997.

[91] WA Wall, MA Frenzel, and C Cyron. Isogeometric structural shape optimization. *Computer Methods in Applied Mechanics and Engineering*, 197(33):2976–2988, 2008.

[92] DR White, S Saigal, and SJ Owen. Meshing complexity: predicting meshing difficulty for single part cad models. *Engineering with Computers*, 21(1):76–90, 2005.

[93] H Whitney *Geometric Integration Theory*. Courier Corporation, 2012.

[94] G Xu, B Mourrain, R Duvigneau, and A Galligo. Analysis-suitable volume parameterization of multi-block computational domain in isogeometric applications. *Computer-Aided Design*, 45(2):395–404, 2013.

[95] K Vemaganti and N Billade. Local error estimation for dimensional reduction: application to special geometries. *Communications in Numerical Methods in Engineering*, 20(4):323–333, 2004.

[96] S Venkataraman and M Sohoni. Reconstruction of feature volumes and feature suppression. *Proceedings of the 7th ACM Symposium on Solid Modeling and Applications*, pages 60–71. ACM, 2002.

[97] Y Zhang, W Wang, and TJR Hughes. Conformal solid T-spline construction from boundary T-spline representations. *Computational Mechanics*, 51(6):1051–1059, 2013.

[98] OC Zienkiewicz and RL Taylor. *The Finite Element Method*, Volume 3. McGraw-Hill London, 1977.

[99] OC Zienkiewicz and JZ Zhu. A simple error estimator and adaptive procedure for practical engineerng analysis. *International Journal for Numerical Methods in Engineering*, 24(2):337–357, 1987.

[100] OC Zienkiewicz and JZ Zhu. The superconvergent patch recovery and a posteriori error estimates. Part 1: The recovery technique. *International Journal for Numerical Methods in Engineering*, 33(7):1331–1364, 1992.

[101] OC Zienkiewicz and JZ Zhu. The superconvergent patch recovery and a posteriori error estimates. part 2: Error estimates and adaptivity. *International Journal for Numerical Methods in Engineering*, 33(7):1365–1382, 1992.

[102] J Sokolowski and JP Zolésio. *Introduction to shape optimization: Shape sensitivity analysis*. Springer Series Computational Mathematics, Springer, 1992.

[103] H Zhu and CH Menq. B-rep model simplification by automatic fillet/round suppressing for efficient automatic feature recognition. *Computer-Aided Design*, 34(2):109–123, 2002.